NUMERICAL SIMULATION OF INTERFACE DELAMINATION — WITH APPLICATION TO IC PACKAGING

CHEONG WEE GEE

(B. Eng. (Hons.), NUS)

A THESIS SUBMITTED

FOR THE DEGREE OF MASTER OF ENGINEERING

DEPARTMENT OF MECHANICAL ENGINEERING

NATIONAL UNIVERSITY OF SINGAPORE

2004

Acknowledgements

The author would, first of all, like to express his thanks to his research supervisor, Associate Professor Cheng Li, for her patience, guidance and moral support throughout the course of the project. Through her enthusiasm and expertise, she has imparted much knowledge and shared valuable insights to the research process.

The author would also like to express his gratitude to Dr Guo Tian Fu, visiting researcher from Tsinghua University, for his invaluable guidance and assistance in the theoretical and computational aspects of the project. His patience and willingness to share his knowledge have been a constant help in completing the research.

The author is also grateful to Chong Chee Wei, Thong Chee Meng, Leo Chin Kin and Chew Huck Beng, fellow postgraduate students of A/Prof. Cheng Li, for the assistance in the clarification of ideas crucial to the project and for the constant encouragements.

Sincere gratitude also goes to the technical officers and peers in the Strength of Materials Laboratory 2, and many others who have contributed to the completion of this thesis.

Table of contents

Summary

The study of interface delamination of integrated circuits (IC) packages, which often are intricate multilayer structures, forms the basis of the present research. Numerical simulation is employed to gain a deeper understanding on the initiation of cracks in IC packages during reflow soldering. Using the vapor pressure incorporated cell element model, the research concentrates on identifying the possible mechanisms that cause the initiation of interface delamination, and also the position of crack initiation along interfaces in common IC package geometries, explicitly a thin quad flat pack (TQFP) and a plastic ball grid array (PBGA) package. The cell element model is also used to identify critical interfaces in an IC package that will undergo extensive damage.

For TQFP, the focus is on the die pad/molding compound interface (Type I popcorn failure) and the die/die attach interface (Type II popcorn failure). For both interfaces, increased initial porosity and initial vapor pressure levels cause rises in the void growth and fall in stress carrying capacity of the cell elements, resulting in weakened interfaces. High initial porosity and vapor pressure favor formation of a continuous damage zone along the die/die attach interface. The regions of intense void growth for both interfaces appear to concentrate near the interface corners. For each of the interfaces considered, crack initiates close to the interface corner and propagates in both directions towards the interface center and corner. Furthermore, by replacing the material of the copper die pad with alloy42, the die/die attach interface experiences more damage while the die pad/molding compound interface undergoes less void growth, suggesting that different die pad materials will increase the factor of risk for different popcorn failure types in TQFP. Since the die attach is sandwiched between two moisture impermeable substrates and only allows moisture diffusion from the interface corner, a further

investigation is made by modeling the die/die attach interface with non uniform vapor pressure levels. It is found that, even with the limited amount of moisture diffused into the die attach, the die/die attach interface undergoes significant void damage.

A parametric study of the effects of vapor pressure and thermal mismatch stress on a plastic ball grid array (PBGA) package is also performed. The vapor pressure incorporated cell element model, with the additional feature of modeling the coalescence effect, is adapted to model void damage and crack initiation at the die/die attach interface in the PBGA. With higher initial porosity distribution and initial vapor pressure, the integrity of the interface is largely compromised. For the analyses with temperature independent and temperature dependent material properties, the interface corner is identified as the most possible initiation site for interface delamination during moisture sensitivity tests. As the initial vapor pressure increases, two competing sites of interface crack initiation arises, which accounts for the fast and complete delamination of the whole interface during the short period of reflow soldering. The phenomenon is confirmed when investigating the behavior of the interface under Pb-free reflow soldering, where the peak reflow temperature is raised further.

The final part of this thesis involves a full field analysis of the PBGA package when all elements of the overmold are governed by the modified Gurson flow potential. It is found that the zones of intense void growth and damage occur only at the interfaces, and limited void growth occurs within the bulk material. In the event of the complete delamination of the die/die attach interface, the critically damaged region in the overmold closest to the die attach will undergo cracking, and lead to popcorn failure.

List of Figures

List of Tables

Chapter 1

Introduction

Driven by the ongoing trend of miniaturization and function integration, the electronics industry requires increased power dissipation, junction temperature, and reliability requirements on electronic packages. Packaging engineers and analysts need to understand the important physical locations in the package where delamination will pose real risks to package reliability. The ability to fully and accurately qualify the materials and interface performance will be necessary for future development.

To completely understand and to characterize the basic failure mechanisms is the key in strengthening interfaces whether they are between metal/polymer or polymer/polymer in the assembled packages. Fundamental work will be needed to characterize material behavior due to environment factors such as temperature and moisture as well as interface physical characteristics such as void composition and filler content. As such, modeling and simulation capabilities that account for the complex interface geometries (sharp corners and voids) and the realistic materials behavior are needed. The ultimate goal would be to simulate and optimize the design of a virtual product and also the manufacturing process entirely based on numerical analysis before a physical product is built.

Moisture-induced failure continues to be a major package reliability issue for plastic integrated circuits (IC) packages. Due to the hygroscopic nature of the polymeric

package materials, the plastic packages tend to absorb moisture during storage, causing them to be susceptible to moisture-induced delamination and package cracking. Confirmed by studies of moisture diffusion in various IC package types [Shook and Sastry, 1997; Wong et al., 1998; Liu et al., 2002], the absorbed moisture condenses in micropores and defects that are present in the substrate, solder mask, die attach and other package materials, and along interfaces, particularly at the die pad/molding compound and die/die attach interfaces. In dealing with popcorn failure in IC packages, it is crucial to understand the entire cracking process: crack initiation, crack growth and final fracture. The very question of dependence of growth of micro voids on stress, temperature and moisture-induced conditions are of paramount practical importance.

High thermal mismatch stresses are often generated within the IC package, which primarily consists of multilayered thin films with different coefficients of thermal expansion. Furthermore, the absorbed moisture vaporizes rapidly during reflow soldering, causing high internal vapor pressure within the micropores. The pressure generated can reach 3-6 MPa [Liu and Mei, 1995], which is comparable to the yield strengths of the overmold and die attach near glass transition temperatures. The voids, especially those along the interfaces, are thus triggered to grow and further coalescence at an alarming rate to cause interface delamination. Moisture in the surrounding subsequently diffuses into the delaminated interface, adding on to the vapor pressure on the crack surface, and increasing the crack size, ultimately leading to popcorn failure.

Vapor pressure effects on void growth in hygroscopic polymeric materials have been studied by Guo and Cheng (2002). They showed that high porosity and high moisture

content are exceedingly detrimental to fracture toughness. In fact, popcorn cracking could be treated as unstable growth of a voided cell when the combined thermal loading and vapor pressure reach the critical traction or intrinsic cavitation stress.

The above studies affirm evidence of vapor pressure assisted void growth and coalescence as a key mechanism of popcorn failure. In Chapter 4, the combined effect of thermal mismatch stress and internal vapor pressure on a thin quad flat pack (TQFP) while undergoing the moisture sensitivity test (MST) is investigated. A mechanism based approach, the vapor pressure incorporated cell element model is adapted to model damage and predict the onset of delamination at critical interfaces, namely the die pad/molding compound interface (Type I popcorn failure) and the die/die attach interface (Type II popcorn failure). Each interface is modeled by a narrow strip of porous material of initial thickness D. The exceedingly detrimental combination of thermal mismatch stress and vapor pressure to the interfaces is studied. The effects of different die pad materials on damage across the interfaces are also discussed. Other factors, such as strain hardening exponent, initial void volume fraction, the progress of each moisture sensitivity tests loading cycle, individual cell element behaviors, crack initiation and propagation along the interfaces are detailed. A study is also made involving the modeling of the die/die attach interface with non uniform vapor pressure levels.

A parametric study on the effects of vapor pressure and thermal mismatch stress on a plastic ball grid array (PBGA) package is performed. The cell element model, without assuming any pre-existing crack, is adapted to model void damage and crack initiation,

a precursor to interface delamination and popcorn failure, at the die/die attach interface in the PBGA. The key difference with the analysis of TQFP lies in the additional modeling of the coalescence effect through the complete loss of material stress carrying capacity at a realistic void volume fraction. The effects of porosity distribution and void vapor pressure on the integrity of the interface are discussed. The model is also extended to consider the effects of Pb-free reflow soldering. Interface damage analysis of the die/die attach interface using temperature dependent material properties is further discussed. A full field analysis is subsequently performed by implementing the Gurson constitutive law throughout the polymeric overmold to predict the likely popcorn failure mode from identifying the severely damaged regions within the package.

The main purpose of the current thesis is to numerically simulate interface delamination of typical IC packages described above and gain insights into the possible mechanisms of popcorn failure. The background literature and methodology are reviewed respectively in Chapter 2 and Chapter 3. The report concludes with a summary of all the important findings. Where possible, relevance will be drawn between the results from the present investigations and the documented literature to ensure consistency and relevance, and the implications of the findings will be discussed.

Chapter 2

Literature Review

2.1 Introduction to IC packaging

2.1.1 Integrated circuits (IC) package

An IC package is utilized to protect, power and cool microelectronic devices or integrated circuits and to provide electrical and mechanical connection between the device and the outside world. Different packaging process is used for different chips, and many types of IC package technologies have been developed that vary in their structures, materials, fabrication methodology, bonding technologies, size, thickness, number of input-output (I/O) connections, heat removal capability, electrical performances, reliability and costs [Morris and Tummala, 2001].

IC packages can be classified generally into two categories: through-hole and surface mount. The two categories refer to the methodology used in assembling the packages to the printed wiring board (PWB). Through-hole packages have pins that can be inserted into holes in the PWB. Surface mount packages, on the other hand, are not inserted into the PWB, but are mounted on the surface of the PWB. The advantage of the surface mount package, as compared to the through-hole, is that both sides of the PWB can be used, and therefore allows higher packing density on the board.

Figure 2.1 shows the two categories of packages. Dual-in-line packages (DIP) and pin grid arrays (PGA) are through-hole packages. In DIPs, the I/Os, or the pins, are

distributed along the sides of the package. To achieve higher I/O connections, PGAs are used where the pins are distributed in an area array fashion underneath the package surface. Most of the advances in package design and performance are observed for surface mount packages. The small outline (SOP) package is the most widely used package in modern memory for low I/O applications because of its extremely low cost. The quad flat package (QFP) is an extension of the SOP with larger I/O connections. Both the SOP and QFP have leads that can be attached to the PWB. There are also leadless packages such as leadless chip carrier (LCC) and plastic leader chip carrier (PLCC), but their usage is very limited.

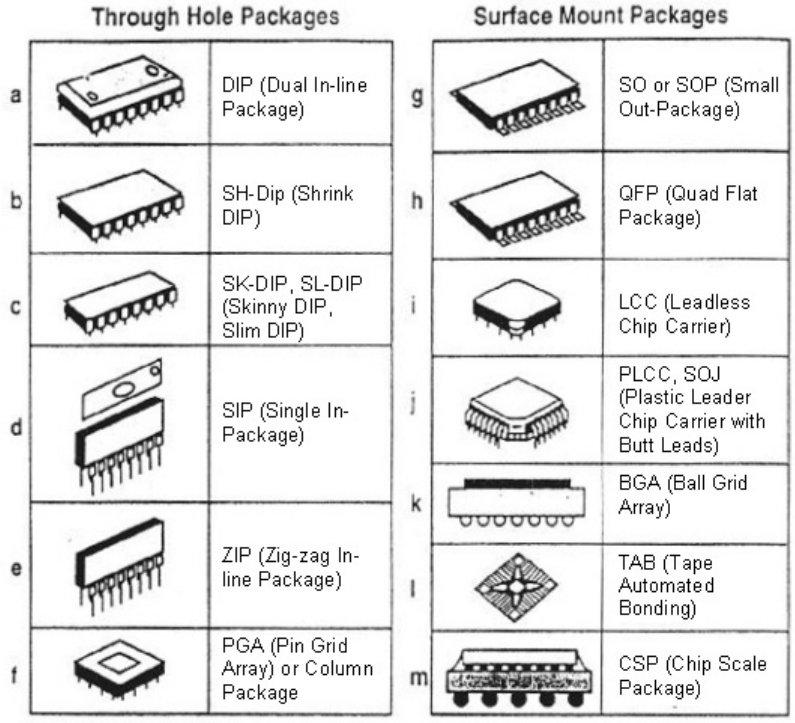

Figure 2.1 Through-hole packages and surface mount packages [Morris and Tummala, 2001].

Packages with solder balls were later developed as an alternative to packages with leads. One example is the ball grid array (BGA) packages. The solder balls can be placed underneath the surface of the package in an area array and significantly increase the I/O

count of surface mount packages. During assembly, surface mount packages are placed on pads patterned on the printed wiring board and pretreated with solder paste. The board is then heated, during which the molten solder paste reflows around the leads, simultaneously forming electrical and mechanical connections.

Smaller, thinner and lighter packages are required in the modern age of portable and hand-held products. Chip scale package (CSP), which is a package whose area is less than 1.2 times the area of the normal IC packages, have been developed to address these demands of modern electronics. To package the various types of ICs and provide high performance and low-cost solutions is a challenging task for package engineers.

2.1.2 Reflow Soldering Process

Reflow soldering, commonly used in assembling surface mount devices, involves remelting (reflowing) solder previously applied to a PWB joint site (pad) in the form of a preform or paste. No solder is added during reflow [Gallo and Munamarty, 1995]. A typical reflow temperature profile involves preheat, dryout, reflow and cooling, as shown in Fig. 2.2. In the preheat zone, the temperature of the assembly is raised to 100^{o}C to 150^{o}C at a rate low enough, usually 2^{o}C/sec, to prevent solvent boiling and the formation of solder balls.

The second stage is the slow heat/dry zone, where the temperature is increased to the solder melting point, activating the flux in the solder paste. The activated flux removes oxides and contaminants from the surfaces of the metals to be joined. The heating is kept short to allow the moisture in the paste to evaporate without splattering the solder.

At the third stage, the temperature of the assembly is raised to about 220°C to 260°C (the melting point of the solder is 183°C). The total time that the solder is above the melting point, or wetting time, is normally 30 to 60 seconds, and is critical to reliable solder joint formation. It is during the wetting time that the solder paste melts and reflows to form the solder joint.

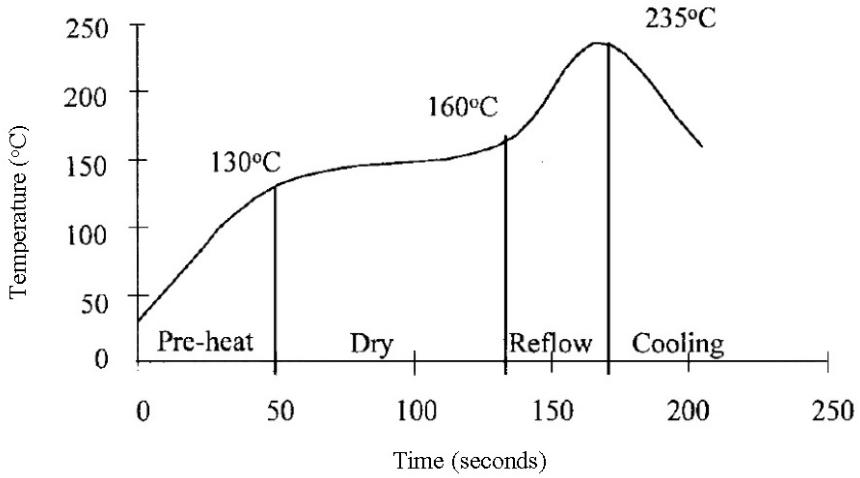

Figure 2.2 A typical reflow soldering time-temperature profile [Pecht, 1999].

2.2 Moisture Induced Failure in IC packages – Popcorn Failure

IC package materials are hygroscopic in nature, i.e. they absorb moisture readily. Popcorn failure is caused by the damaging effects of moisture, which is absorbed due to the storage of plastic IC packages in a noncontrolled humidity environment. The popcorn mechanism for two kinds of IC packages, plastic encapsulated microcircuits (PEM) and plastic ball grid arrays (PBGA), are discussed.

2.2.1 Popcorn failure of plastic encapsulated microcircuits (PEM)

The popcorn failure mechanism of plastic encapsulated microcircuits is showed in Fig. 2.3. When moisture, present in the factory environment, is absorbed through the package exterior, it condenses in micropores and defects in the molding compound and die attach materials, and along interfaces, particularly in the die pad/molding compound, die attach/die pad and die /die attach interfaces.

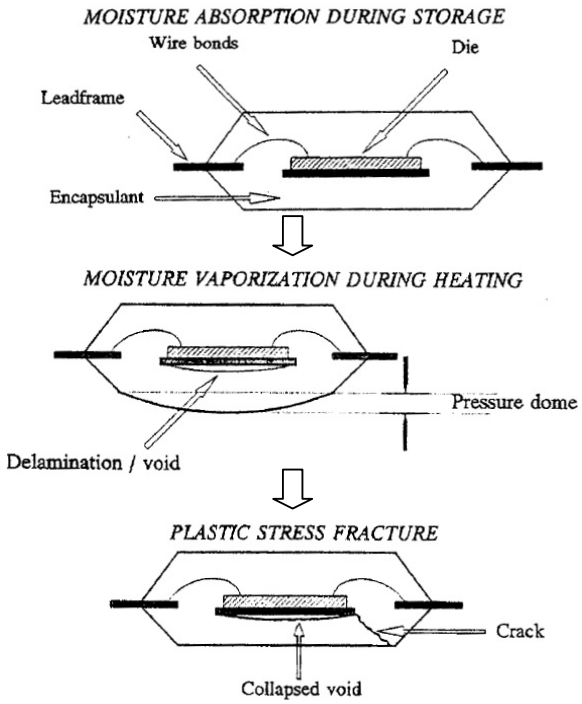

Figure 2.3 Mechanism of popcorn failure of PEMs [Gallo and Munamarty, 1995].

As the PEMs are heated to reflow temperature, thermomechanical and moisture induced stresses are developed. The stresses are caused by:

- rapid vaporizing of absorbed moisture, resulting in steam and build-up of vapor pressure;

- coefficient of thermal expansion mismatch between the various PEM components causing mismatch stress at elevated temperatures;
- decrease in the strength of the PEM polymeric components, such as molding compound and die attach, near the glass transition temperature;
- expansion of molding compounds after absorbing moisture; consequently molding compounds in a moisture saturated package experience approximately 20% more hygrothermal strain when exposed to reflow heating than a dry package [Ngyuyen et al., 1995].

Vaporizing moisture increases the vapor pressure in the delaminated cavity. If the hygrothermal stresses and vapor pressure exceed the adhesion strength and fracture toughness of the molding compound, they become the driving force behind the delamination growth and crack formation. As a result, a crack forms that may propagate laterally outwards. When the crack reaches the package exterior, high pressure water vapor is suddenly released producing an audible popping sound.

Currently, the most reliable solutions in preventing such package cracking have been dry-packing the packages prior to shipping, or baking them before board mounting, but such solutions add costs and time to the manufacturing throughout. To bypass such an approach, extensive work has been done to understand and find alternate solutions, especially on improving the crack resistance of the molding compound. However, with the introduction of more crack-resistant molding compounds, recent studies have indicated the fracture mechanism is tending to shift, from the common delamination at

the die pad/molding compound interface to the interfaces in the die attach, complicating the problem further. [Fukazawa et al., 1985; Chen et al., 1994]

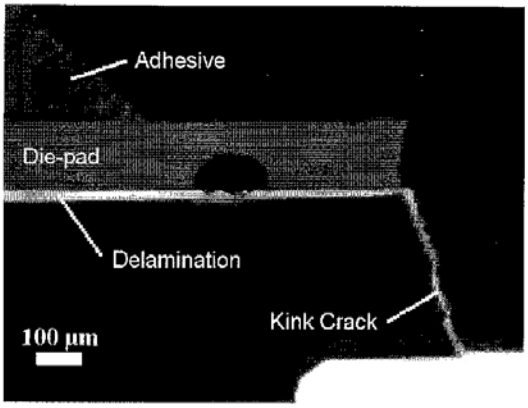

(a)

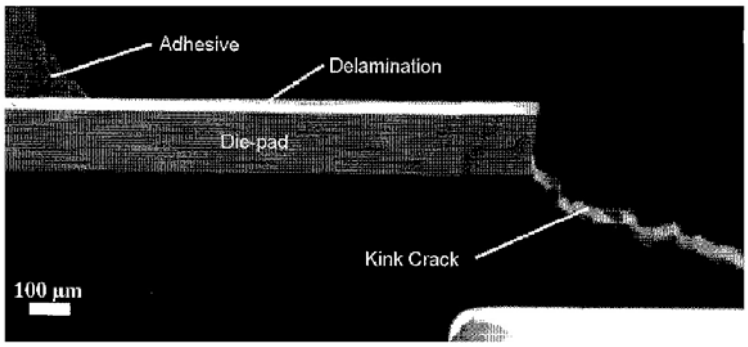

(b)

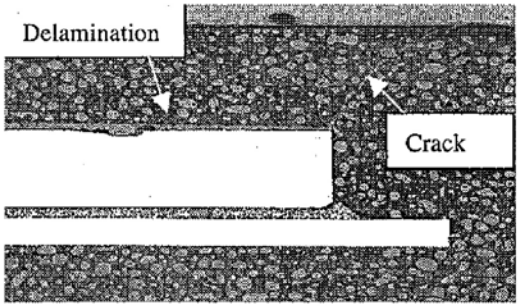

(c)

Figure 2.4 Types of popcorn failure modes:
(a) Type I from the bottom of die pad/molding compound interface [Dudek et al., 1998];
(b) Type II from the die/die attach interface [Dudek et al., 1998];
(c) Type III from the top of molding compound/die interface [Chai et al., 1999].

There are generally three types of popcorn failure modes [Omi et al., 1991] that can be identified in relation to the delaminated interfaces in PEMs. Type I refers to cracking from the bottom of die pad/molding compound interface delamination, type II from the die/die attach interface delamination, and type III from the top of die/molding compound delamination (Figure 2.4).

Another effect of moisture in popcorn cracking, other than the increase in stress due to moisture vaporizing in the delaminated interface, is that it degrades the adhesion between the die pad and the molding compound [Tay and Lin, 1996a; Tanaka and Nishimura, 1995]. It has been found by Tay et al. (1994) that, through measuring the adhesion strength of the die pad/molding compound interface for various levels of moisture preconditioning, the greater the level of moisture, the lower the adhesion strength of the interface. Thus, confirming that moisture degrades the adhesion between the die pad and molding compound.

2.2.2 Popcorn failure of plastic ball grid arrays (PBGA)

In recent years, plastic ball grid arrays have gained in popularity because of their ability to provide increased I/O density, high electrical performance and ease of circuit card assembly [Pecht, 1999]. However, one drawback to PBGA packages is their moisture absorbing characteristics. The most common failure mode in the PBGA packages occurs in the die attach region during solder reflow [Yip et al., 1996]. Similar to PEMs, moisture is absorbed from the surroundings, and condenses in micropores and defects that are present in the substrate, solder mask, die attach materials, and along the interfaces in the die attach. During reflow, condensed moisture vaporizes, creating an

overpressure condition. Under severe conditions, the combined thermal mismatch stress and vapor pressure force the substrate outward away from the die, creating a stress singularity at the edge of the die/overmold, die/die attach or die attach/BT epoxy interface. As a result, a crack forms that may propagate laterally outward. When the crack reaches the package exterior, high pressure water vapor is suddenly increased, producing an audible popping sound.

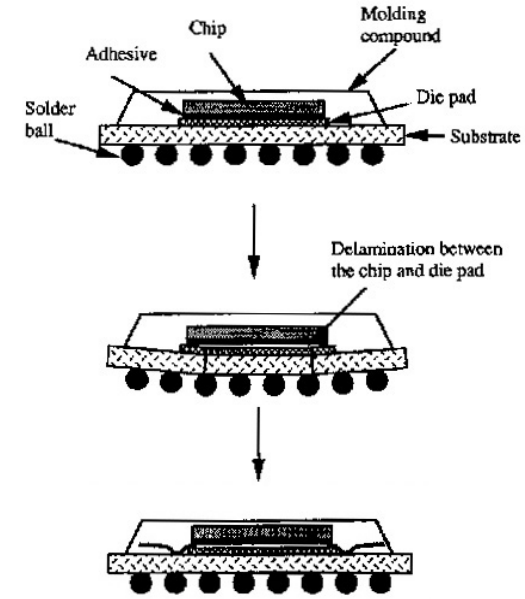

(a)

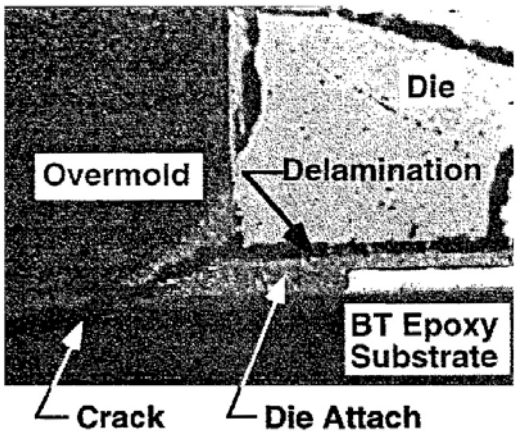

(b)

Figure 2.5 (a) PBGA popcorn failure mechanism [Ahn and Kwon, 1995].
(b) PBGA popcorn failure showing package cracking and delamination [Galloway and Miles, 1997].

For PBGA packages, failure typically initiated by a delamination of the die/die attach interface followed by the propagation of a crack through the overmold or substrate (Fig. 2.5a). Figure 2.5b shows an example of a popcorn failure as evidenced by the cracked package. The die is completely delaminated from the die attach. A crack initiated at the corner of the die and propagated through the die attach fillet into the substrate. Popcorn failure may break wire bonds or degrade long term reliability by the presence of a crack, which provides a path for corrosive material to enter the package. In addition, degradation in the thermal performance results when the die delaminates, in particular for high power devices.

2.3 Moisture diffusion in IC packaging

Moisture-induced failure in IC packaging is not only determined by the absolute moisture level in the package but also by the moisture distribution in the package and moisture concentration at the critical interfaces [Kitano et al., 1988; Tay and Lin, 1996b]. However, experimental data available for moisture is only through measuring the weight gain or loss as a function of time. As such, there is a need for detail modeling of the moisture diffusion process in the IC packaging, especially through a multi-layer package having different diffusion properties in each layer. And through moisture diffusion modeling, the initial porosity in each component can be estimated which will be elaborated further in the next section.

In order to predict the moisture induced stress state, the local moisture concentration in each layer and the critical interfaces must be known. Moisture diffusion models

developed for the external molding compound of plastic encapsulated packages are readily available, but cannot be easily extended to account for materials that are sandwiched between different components, in particular the die attach layers [Galloway and Miles, 1997].

The moisture diffusion process in IC packages can be described using Fick's diffusion equation

$$\frac{\partial^2 C}{\partial x^2} + \frac{\partial^2 C}{\partial y^2} + \frac{\partial^2 C}{\partial z^2} = \frac{1}{\alpha_D}\frac{\partial C}{\partial t} \tag{2.1}$$

where C is the local moisture concentration and α_D the moisture diffusitivity. However, except for simple geometries, it is not analytically viable to solve the partial differential equation. The problem can be solved using the thermal diffusion capabilities of commercial finite element software, due to the similarity between (2.1) and the heat conduction equation [Wong et al., 1998]

$$\frac{\partial^2 T}{\partial x^2} + \frac{\partial^2 T}{\partial y^2} + \frac{\partial^2 T}{\partial z^2} = \frac{1}{\alpha_T}\frac{\partial T}{\partial t} \tag{2.2}$$

where T is the temperature and α_T is the thermal diffusitivity. However, another problem does arise in that unlike temperature, which is continuous in nature, moisture concentration is discontinuous across bi-material interfaces where two materials having different saturated moisture concentrations are joined. Thus, in the early stages, Kitano et al. (1988) and Tay and Lin (1996b) have only applied Fick's diffusion equation with moisture concentration as a field variable to homogenous systems, such as just the molding compound and ignoring the moisture concentrations in the die attach. A new variable that could enforce field continuity is necessary for the modeling of moisture diffusion in a multi-material system such as IC packaging.

The interface discontinuity can be removed by normalizing the moisture concentration C against the moisture solubility S [Fan, 2000]. The solubility S is related to the saturated concentration C_{sat} by

$$S = \frac{C_{sat}}{p_{ext}} \tag{2.3}$$

where p_{ext} is the ambient vapor pressure under given humid conditions. Hence, the continuity across the interface of dissimilar materials is assumed by

$$\frac{C_1}{S_1} = \frac{C_2}{S_2} \tag{2.4}$$

or equivalently, by equation (2.3)

$$\frac{C_1}{S_{1sat}} = \frac{C_2}{S_{2sat}} \tag{2.5}$$

where the subscripts 1 and 2 represent different materials respectively.

The moisture diffusitivity α_D is determined by the Arrhenius equation:

$$\alpha_D = D_0 \exp\left(-\frac{Q}{RT}\right) \tag{2.6}$$

where T is the absolute temperature, Q the activation energy, R universal gas constant.

The moisture saturation concentration, C_{sat}, in equation (2.3) is dependent on temperature, humidity and material type. The concentration becomes a function of temperature and independent of relative humidity when C_{sat} is normalized by the ambient water vapor density, ρ_{ext}. The moisture concentration ratio dependency can be modeled similarly using the form of Arrhenius equation given by

$$\psi = \frac{C_{sat}}{\rho_{ext}} = \psi_0 \, exp\left(\frac{Q_\psi}{R_b T}\right) \tag{2.7}$$

where ψ_0 is the material constant, Q_ψ the activation energy, R_b the Boltzman constant. Assuming that the ambient vapor behaves like an ideal gas, so that

$$p_{ext} V = mRT \text{ or } p_{ext} = \rho_{ext} RT \tag{2.8}$$

where m is the vapor mass and ρ_{ext} is the ambient vapor density. The solubility S can be described in terms of ψ, as follows

$$S = \frac{\psi}{RT} = \frac{\psi_0}{RT} \exp\left(\frac{Q_\psi}{R_b T}\right) \tag{2.9}$$

Using similar approaches to above, moisture diffusion distributions were obtained for various IC package geometries, even across the different material layers [Galloway and Miles, 1997; Wong et al., 1998; Wong et al., 2002a; Liu et al., 2002]. For Thin quad flat packs (TQFP), a typical PEM, the molding compound is usually saturated with moisture and moisture concentrations are predominantly damaging at the molding compound interfaces, such as the die pad/molding compound interface and molding compound/die interface. On the other hand, most of the die attach material in the TQFP is not saturated with moisture. This is a result of the die attach being a very thin layer trapped between the die and the die pad which are both impermeable to moisture. However, at the perimeter of the die attach, it is saturated with moisture.

PBGA package is more susceptible to popcorn failures because other than the molding compound and die attach, the substrate also absorbs moisture [Tan et al., 1996]. In addition, during moisture pre-conditioning, the presence of thermal vias beneath the die

provides an effective path for rapid moisture diffusion into the die attach region. On the other hand, during solder reflow, the thermal vias do not provide any relieve for moisture, and therefore vapor pressure [Wong et al., 2002a]. Hence, it would be reasonable to assume that the whole die attach is saturated with moisture and subjected to the effects of vapor pressure.

The diffusion of heat in the IC packaging was found to be very much faster than that of moisture by various researchers [Tay and Lin, 1996b; Wong et al., 1998]. Gibson (1994) has suggested that thermal diffusion could be a million times faster than moisture diffusion. Thermal equilibrium in the package can be reached within seconds. Hence for the simulations in this work, it is assumed that the change in temperature is uniform within the package while the moisture distribution is assumed to be constant during reflow.

2.4 Estimated initial void size of typical IC package materials

Due to factors such as manufacturing faults or contamination, very small voids or defects exist at interfaces in IC packages. These small interfacial defects cause very high stress concentrations in the material around the defects leading to the debonding of the interface. An approach to estimate the initial void size of typical IC package materials by Fan (2000) is described in this section. This approach is a continuation from the previous section.

The voids are assumed to be distributed randomly but uniformly from the statistical point of view, so that the materials have isotropic behaviors. The initial void volume fraction f_0, can be defined as a scalar quantity to represent its isotropy. When temperature increases, the void volume increases due to the vapor pressure. The moisture density ρ_m in the voids is defined as

$$\rho_m = \frac{C}{f_0} \tag{2.10}$$

At saturation, the local concentration C above is replaced by C_{sat}. Thus, the initial void volume fraction can be expressed as following through equations (2.7) to (2.9).

$$f_0 = \frac{1}{\rho_m}\rho_{ext}\psi = \frac{1}{\rho_m}\rho_{ext}\psi_0 \exp\left(\frac{Q_\psi}{RT}\right) \tag{2.11}$$

Suppose that under 100 ^{o}C/100 %RH condition, the voids in the body are full of water, i.e., ρ_m = 1.0 g/cm^3, then

$$f_0 = C_{sat}\big|_{100/100} = \rho_g\psi_0 \exp\left(\frac{Q_\psi}{RT}\right)\Bigg|_{100/100} \tag{2.12}$$

where ρ_g is the saturated ambient water vapor density.

The above equation provides a simple way to predict the approximate magnitude of the voids existing in materials. It is a low bound estimation since in the voids of the body, it is actually a mixture of water and vapor. Liu et al. (2002) observed that moisture concentrations within the IC package usually exceed the ambient moisture density by many times. As a result, most, but not all, of the moisture exists in the package in liquid state. Thus, confirming that the voids in the body are a mixture of water and vapor during moisture pre-conditioning. Using the equation, Table 2.1 lists the results of the initial void volume fraction for some commonly used plastic materials in IC packages,

according to the material property data measured by Galloway and Munamarty (1995). It showed that the fractions are usually between 1 % and 5 %.

Table 2.1 Initial void volume fraction for some materials in IC packages [Fan, 2000].

Material	BT-epoxy	Die-attach	Molding	Solder mask
f_0 (%)	3.46	3.29	1.46	5.05

2.5 Modeling popcorn failure in IC packages

Various forms of popcorn effect models have been proposed based on the three popcorn failure types described previously in section 2.2.1. Currently, the more dominant field of approach is the cracking of the molding compound itself, where the die pad/molding compound interface (Type I) is assumed to be fully delaminated already. It was assumed that the interface delaminated without much resistance. The focus of such modeling was on the delaminated gap between the die pad/molding compound interface. The interaction between IC package with thermal loading and the vapor pressure by the vaporized moisture that had diffused into the gap was studied [Kitano et al., 1988; Tay and Lin, 1996a; Park and Yu, 1997; Liu and Shi, 2002; Wong et al., 2002b]. The other field of interest is the interface delamination between the layers. The commonly accepted mechanism is that the steam-generated vapor pressure from the evaporated moisture at the interface in the solder reflow process breaks the interface bonding and cracks the molding compound [Guo and Cheng, 2001; Liu et al., 2002; Liu et al., 2003].

Great emphasis has hitherto been placed on modeling and simulating interface failures in plastic IC packages using the assumption of either fully bonded interfaces or pre-cracked interfaces. For fully bonded interfaces, a typical analysis is performed using standard stress analysis; for interfaces containing pre-existing cracks, an analysis may be carried out using conventional fracture mechanics. In the study of moisture effects in electronic packages by Park and Yu (1997), using the methods of interface fracture mechanics, the popcorn failure phenomenon in surface mounted packages is studied by assuming an inherent edge crack at the die pad/molding compound interface which can ultimately lead to the entire interface delamination. A pre-existing macroscopic crack was assumed by Liu and Mei (1995) prior to reflow soldering where vapor pressure was treated as an external traction on the delaminated crack. In recent years, Alpern et al. (2002a, 2002b) has developed a simple model to predict the failure of plastic encapsulated IC packages from various popcorn failure modes, using package stability parameters derived from a totally delaminated package.

Experimental results [Tanaka and Nishimura, 1995], however, show that IC packages without apparent pre-existing cracks at the interfaces can still fail by delamination during solder reflow. A cohesive surface, described by traction-separation law [Tvergaard and Hutchinson, 1992; Tvergaard and Hutchinson, 1994], was introduced as a potential plane for crack growth along interfaces by Liu et al. (2003). This approach offers several advantages. There is no need to assume the interfaces are fully bonded or pre-cracked. Moreover, it has the capability to predict the initiation of delamination and subsequent growth to a macroscopic crack in IC packages. In a similar approach, Huang et al. (1996) identified thermal-stress induced voiding in electronics packages as

a dominant failure mechanism and proposed a micromechanics model to investigate this mechanism. Cheng and Guo (2001), instigated by such an approach, incorporated vapor pressure as an internal variable into the cell element model [Xia and Shih, 1995]. They found that popcorn cracking could be treated as unstable growth of a voided cell when the combined thermal loading and vapor pressure reach the critical traction or intrinsic cavitation stress.

As mentioned previously, popcorn failure actually originates from the delamination and rapid propagation of delamination along the critical interfaces in IC packages, due to the combination of thermal mismatch stress, high vapor pressure and the degradation of adhesive strength by the moisture at reflow temperature. Therefore, it is important to model the initiation of delamination in order to have a more complete mechanical understanding of the entire process of popcorn cracking and is the focus of the present work.

2.6 Moisture Sensitivity Tests

As a solution to popcorn failure, the moisture susceptible IC packages are dry packed with desiccant, in moisture barrier bags that are virtually impermeable to water [Gallo and Munamarty, 1995]. The packing procedure allows the surface mount packages to remain dry when placed in inventory or shipping, and offers the printed circuit board manufacturer the flexibility to mount these packages within a specific time period. The industry has defined several moisture sensitivity levels (MSL) which relate to the maximum allowable time that the parts can be exposed to ambient conditions after

removal from the dry pack prior to solder reflow. The MSL and the corresponding maximum allowable exposure time (floor life) are printed on the moisture barrier bag label. Table 2.2 shows the moisture sensitivity levels. MSL level 1 does not require dry pack, whereas levels 2 to 6 require dry pack.

Table 2.2 Moisture Sensitivity levels [IPC/JEDEC J-STD-020A, 1999].

LEVEL	FLOOR LIFE (TIME OUT OF BAG)		STANDARD MOISTURE SOAK (MOISTURE PRECONDITIONING) REQUIREMENTS	
	TIME	CONDITIONS	TIME (hours)	CONDITIONS
1	Unlimited	≤30°C/85%RH	168	85°C/85%RH
2	1 year	≤30°C/60%RH	168	85°C/60%RH
2a	4 weeks	≤30°C/60%RH	696 [2]	30°C/60%RH
3	168 hours	≤30°C/60%RH	192 [2]	30°C/60%RH
4	72 hours	≤30°C/60%RH	96 [2]	30°C/60%RH
5	48 hours	≤30°C/60%RH	72 [2]	30°C/60%RH
5a	24 hours	≤30°C/60%RH	48 [2]	30°C/60%RH
6	Time on Label (TOL)	≤30°C/60%RH	TOL	30°C/60%RH

The appropriate MSL is determined by following a defined procedure such as given in the specification Joint IPC/JEDEC Standard J-STD-020A (1999), developed by the Joint Electron Device Engineering Council (JEDEC). A sample procedure used for the moisture evaluation is shown in Fig. 2.6. All as-received devices were initially inspected for existing delamination under microscope and using scanning acoustic microscopy (SAM) prior to moisture preconditioning. The devices were then baked at 125°C for 24 hours to remove any residual moisture. After baking, the dry weights were recorded and the devices were placed in humidity chambers for moisture soak under the conditions set forth by the desired level of moisture characterization (Table 2.2). Throughout the temperature/humidity pre-conditioning, the devices were weighed to monitor the rate of moisture absorption. After moisture exposure, the devices were subjected to the same reflow profile three times. The samples were re-examined using

SAM and microscope for evidence of delamination and cracking. In certain cases, devices were cross-sectioned to verify the extent of the damage. If the device samples showed no signs of degradation at, for example, level 4, the process will be repeated for level 3 and subsequent levels until level 1. If the samples exhibit any degradation at any level, they are classified as having failed at that moisture sensitivity level.

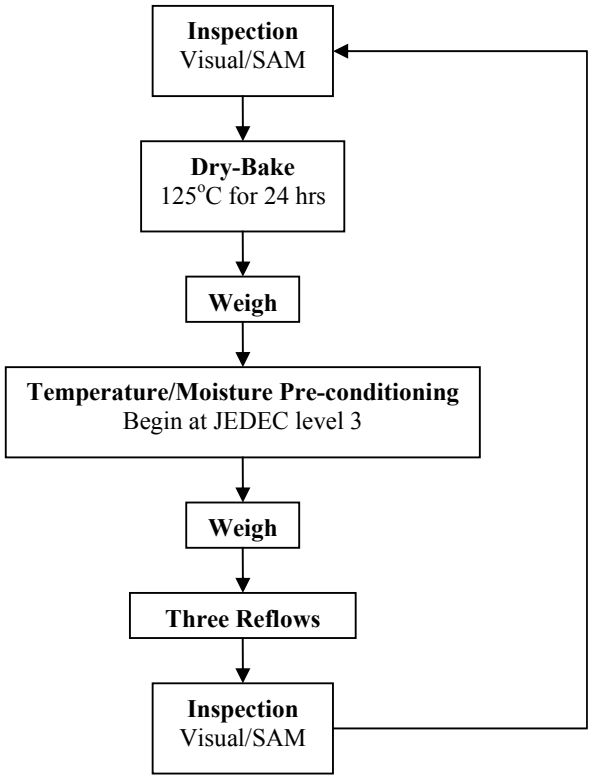

Figure 2.6 Flow chart for moisture sensitivity characterization.

As can be seen, such classifications are time-consuming and add costs to manufacturing. To bypass such methods, extensive work is necessary to understand and find other solutions. As an alternative, reliable and effective simulation models can used to predict, evaluate and qualify the mechanical reliability of IC packages against moisture-induced failures. The three cycles of solder reflow described above, constitutes the approach of simulation loading for the present work.

Chapter 3

Computational Cells and Numerical Implementation

Considerable resources must be committed to experimentally validate new packaging processes, designs or materials using the Joint IPC/JEDEC Standard J-STD-020A (1999). Many moisture studies that focus on the standard's qualification test show a relation between package weight and package cracking or delamination. However, experimental results measured for one specific package design with certain material properties, geometry and process conditions are not easily generalized to predict popcorn failure for new designs or conditions. To predict popcorn failure, the conditions at the location where the failure initiated must be known. As such, a methodology is necessary in providing an in-depth mechanical analysis of popcorn cracking.

3.1 Characteristics of polymeric IC package materials

Polymers are used in the IC packages for applications such as the die attach, interlayer dielectrics, molding compounds, substrates and underfills. Their mechanical behaviors are strongly influenced by their morphology of macromolecules and filled particles. The glass transition temperature T_g is a temperature, or narrow range of temperatures, below which a polymer is in a glassy state, and above which it is rubbery. It is typically measured as a change in the coefficient of thermal expansion or the Young's modulus.

During reflow soldering, the package temperature is raised rapidly to about 220 ^{o}C or more in order to melt the solder. Such temperatures fall near the glass transition temperature T_g of the polymeric materials. For molding compound polymer (epoxy resins) used in IC packages, the Young's modulus E and the ultimate tensile strength σ_{UTS} at temperatures above T_g are about one-tenth of the room-temperature values [Gibson and Ashby, 1997]. As temperature increases well above T_g, the material becomes extremely soft and easier to fail.

In fact, most IC package materials exhibit viscoelastic behavior even at room temperature, even though these polymers are filled as much as 90% by weight with silica filler particles [Groothuis et al., 1995]. Such conditions, couple with the presence of voids and moisture-induced vapor pressure, suggest that elastic-plastic constitutive relations can be used in simulating the behavior of polymeric IC package materials.

3.2 Mechanism-based Fracture Mechanics – Cell Element Model

Mechanism-based fracture mechanics attempts to link the macroscopically measured fracture resistance to the microstructural variables and the continuum properties of the material. Ductile materials which fail by void growth and coalescence display a macroscopically planar fracture process zone of one or two void spacing in thickness. This zone is characterized by intensely strained ligaments between voids which have undergone large amounts of growth; voids away from this zone show little or no growth. Shih and Xia (1995) modeled the process of ductile fracture noted above by confining

void growth and coalescence to a narrow material layer of initial thickness D. The material outside this strip, referred to as the background material, is undamaged by void growth – its response is described by J_2 flow theory of plasticity.

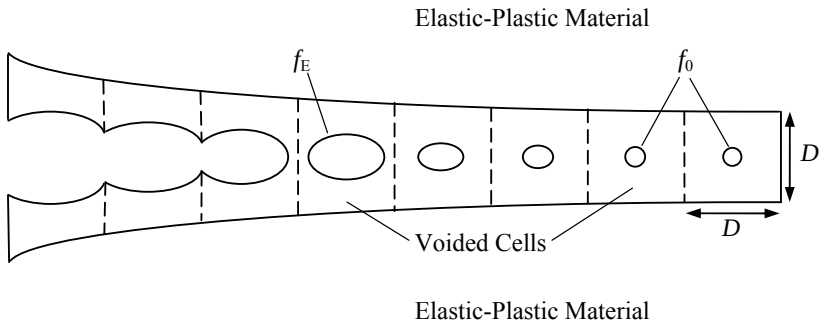

Figure 3.1 Cell model for void growth and coalescence.

Figure 3.1 displays a finite element model of a row of uniformly voided sized cells; each cell contains a void whose initial volume fraction (porosity) of the cell is f_0, which can be regarded as representative of voids nucleated from large inclusions with mean spacing D. Studies by Tvergaard and Hutchinson (1992) have shown that small and large inclusions nucleate voids at stresses that are less than those developed ahead of the crack.

The progressive damage in the cells resulting in material softening and, ultimately, loss of stress carrying capacity is described using the Gurson's stress-strain relation for an elastic-plastic solid containing voids [Gurson, 1977], and will be illustrated in the next section. The model has a sound micromechanical basis and key features of the model have been validated by experiments on voided materials (see review article by Tvergaard, 1990).

3.3 Modified Gurson flow potential

Progressive void growth and subsequent macroscopic material softening in each cell are governed by the Gurson flow potential Φ [Gurson, 1977; Tvergaard, 1990] extended to take account of vapor pressure p present within the voids [Guo and Cheng, 2002 and 2003]. It has the form:

$$\Phi = \left(\frac{\sigma_e}{\sigma_M} \right)^2 + 2q_1 f \cosh\left(\frac{3q_2(\sigma_m + p)}{2\sigma_M} \right) - \left[1 + (q_1 f)^2 \right] = 0 \tag{3.1}$$

where σ_e is the macroscopic effective Mises stress, σ_m the macroscopic mean stress and σ_M the current flow stress of the matrix, and f the current void volume fraction. Factors q_1 and q_2 were introduced by Tvergaard (1990) to improve the model predictions for periodic arrays of cylindrical and spherical voids, and is taken to be 1.25 and 1.0 respectively in the present analysis. In addition to the inherent internal variables of σ_M and f in the Gurson flow potential, extended form of the equation introduces an additional variable p, the internal void vapor pressure [Guo and Cheng, 2002 and 2003].

The vapor pressure, void volume and temperature relationship for a fully vaporized moisture state is recapitulated subsequently [Guo and Cheng, 2001]. Consider a small representative material sample containing a microvoid with void volume V_f and cell volume V. The vapor pressure p at a fully vaporized state obeys the ideal gas law

$$pV_f = mRT \tag{3.2}$$

where R is the universal gas constant, m the moisture weight inside of the microvoid, and T the temperature. Dividing both sides of Eq. (3.2) by V leads to

$$pf = CRT \tag{3.3}$$

where $C = m/V$ is the averaged moisture concentration and $f = V_f / V$ is the void volume fraction. Eq. (3.3), supplemented by moisture diffusion analysis [Tay and Lin, 1996; Galloway and Miles, 1997], permits the evaluation of the initial void volume fraction f_0.

Two states (p, f, T, C) and (p_0, f_0, T_0, C_0) are related by

$$\frac{p}{p_0} = \frac{T}{T_0}\frac{f_0}{f}\frac{C}{C_0} \tag{3.4}$$

where f_0 is the initial void volume fraction, or porosity, of the cell element and p_0 is the initial internal void vapor pressure. T_0, in the present analysis, is assumed to be the curing temperature. During the process of deformation $(V_0 \to V)$ associated with the temperature change $\Delta T (= T - T_0)$, it was assumed that the moisture weight m is conserved. Hence,

$$\frac{p}{p_0} = \frac{T}{T_0}\frac{f_0}{f}\frac{V_0}{V} \tag{3.5}$$

For spherically symmetric void growth in an incompressible solid, the relative volume change V/V_0 of the microvoid cell during mechanical deformation and thermal expansion is given by

$$\frac{V}{V_0} = \frac{1 - f_0}{1 - f} e^{3\alpha\Delta T} \tag{3.6}$$

where α is the thermal expansion coefficient of the matrix material. Being a function of temperature T and void volume fraction f, the relationship for fully vaporized moisture is given by

$$\frac{p}{p_0} = \frac{T}{T_0}\frac{f_0}{f}\frac{1-f}{1-f_0}e^{-3\alpha\Delta T} \tag{3.7}$$

Thus, the continuum description of internal pressure for fully vaporized moisture state is completed.

For the present model, each cell element is rendered extinct when the average void volume fraction over a cell reaches the critical void volume fraction, f_E. That is, the cell stiffness is made zero and nodal forces arising from the remaining stress in the cell are gradually reduced to zero over an elongation equal to $0.5D$ with the aid of a linear-force elongation relationship [Gullerud et al., 2000]. In the works of Cheng and Guo (2003), a typical value of f_E is set as 0.15. This model is used in the early stages of the research and validation studies of the extended Gurson model (3.1) as well as its finite element implementation have been carried out by Guo and Cheng (2002) wherein several initial vapor pressure levels were applied to a range of material parametric combinations.

3.4 Modified Gurson flow potential incorporating coalescence effect, *f* *

To incorporate the coalescence effect, with reference to the works of Tvergaard and Needleman (1984), the extended Gurson flow potential Φ was subsequently modified and has the form:

$$\Phi = \left(\frac{\sigma_e}{\sigma_M}\right)^2 + 2q_1 f^* \cosh\left(\frac{3q_2(\sigma_m + p)}{2\sigma_M}\right) - \left[1 + (q_1 f^*)^2\right] = 0 \tag{3.8}$$

where $f^* = f$ the current void volume fraction. Similarly, q_1 and q_2 is taken to be 1.25 and 1.0 respectively in the present analysis.

The key difference between (3.1) and (3.8) lies in f^*. The function f^* in (3.8) was introduced to model the complete loss of material stress carrying capacity at a realistic void volume fraction, in an effort to incorporate the effects of coalescence into the Gurson model [Tvergaard, 1990]. The continuous damage function has the form

$$f^*(f) = \begin{cases} f, & f \le f_C \\ f_C + \dfrac{f_U^* - f_C}{f_F - f_C}(f - f_C), & f_C < f \le f_F \\ f_U^*, & f > f_F \end{cases} \tag{3.9}$$

where the void volume at final fracture is noted by f_F, so that $f^*(f_F) = f_U^* = 1 / q_1$. According to (3.9), when the void volume fraction reaches a certain critical value f_C, the modification of the yield condition starts due to the effect of coalescence. After f_F, the cell losses all material stress carrying capacity; void coalescence and final failure of the cell occurs. Based on experimental results and numerical analyses [Tvergaard, 1990], the values of f_C and f_F are taken to be 0.15 and 0.25, respectively.

In addition to the inherent internal variables of σ_M and f^* in the Gurson flow potential (3.8), the relationship for vapor pressure p in (3.7) appears as a new internal variable. To be consistent with (3.9), the vapor pressure in (3.7) should be replaced by

$$\frac{p}{p_0} = \begin{cases} \dfrac{T}{T_0}\dfrac{f_0}{f}\dfrac{1-f}{1-f_0}e^{-3\alpha\Delta T}, & f \le f_C \\ \dfrac{T}{T_0}\dfrac{f_0}{f_C}\dfrac{1-f}{1-f_0}e^{-3\alpha\Delta T}\dfrac{f_F - f}{f_F - f_C}, & f_C < f \le f_F \\ 0, & f > f_F \end{cases} \tag{3.10}$$

so that the yield surface (3.8) can shrink to a point when $f \ge f_F$.

3.5 Numerical Implementation

The multiaxial elastic-plastic relation with thermal strains is described hereafter. The elastic response is given by

$$\overset{\nabla}{\boldsymbol{\sigma}} = \mathbf{L}:(\mathbf{d} - \mathbf{d}^{\text{th}} - \mathbf{d}^{\text{p}}) \tag{3.11}$$

where $\overset{\nabla}{\boldsymbol{\sigma}}$ is the Jaumann rate of the Cauchy stress, $\mathbf{L}$ is the fourth-order elasticity tensor, $\mathbf{d}$ is the deformation rate and $\mathbf{d}^{\text{th}}$ is the thermal strain rate:

$$\mathbf{d}^{\text{th}} = \alpha\Delta\dot{T}\mathbf{1} \tag{3.12}$$

where $\mathbf{1}$ is the identity tensor in the current configuration. The plastic response, $\mathbf{d}^{\text{p}}$, follows the normal flow rule:

$$\mathbf{d}^{\text{p}} = \lambda\frac{\partial\Phi}{\partial\boldsymbol{\sigma}} \tag{3.13}$$

where Φ is the Gurson flow potential in Eq. (3.1) and Eq. (3.8), $\boldsymbol{\sigma}$ the Cauchy stress tensor, λ is the flow parameter determined by the consistency condition of the yield function along with plastic work-rate equivalence between the matrix and the macroscopic continuum

$$(1-f)\sigma_M\dot{\bar{\varepsilon}}_M^p = \boldsymbol{\sigma}:\mathbf{d}^{\text{p}} \tag{3.14}$$

The rate of void growth $\dot{f}$ is dependent on the plastic volumetric strain rate as follow:

$$\dot{f} = (1-f)\,\text{tr}\mathbf{d}^{\text{P}}. \tag{3.15}$$

The process of void growth is thus fully described.

The weak formulation of momentum balance equations (the principle of virtual work) is expressed in the current configuration by [Guo and Cheng, 2003]

$$\int_V \delta\boldsymbol{\varepsilon}:\boldsymbol{\sigma}\,\mathrm{d}\upsilon = \int_S \delta\mathbf{u}\cdot\mathbf{T}\,\mathrm{d}s \tag{3.16}$$

in the absence of body forces. Here $\delta\boldsymbol{\varepsilon} = \mathrm{sym}\left(\nabla\delta\mathbf{u}\right)$ is the virtual rate of deformation tensor work-conjugate to the Cauchy stress $\boldsymbol{\sigma}$ with $\delta\mathbf{u}$ denoting an admissible virtual displacement field. $\mathbf{T}$ is the surface traction per unit area in the current configuration and V denotes the current volume with bounding surface S. In the above, the reference configuration is assumed to be stress-free.

Eq. (3.16) is discretized at each time instant t_{n+1}; implicit iterations are employed to enforce global equilibrium. Accompanying the evaluation of the consistent tangent moduli at time t_{n+1}, the plastic constitutive equations are numerically integrated using a backward Euler method in stepping the time increment from t_n to t_{n+1}. Details of numerical implementation within the framework of J_2 flow theory of plasticity are given in the WARP3D manual [Gullerud et al., 2000].

Chapter 4

Vapor pressure assisted interface delamination and failure of thin quad flat pack (TQFP)

4.1 Introduction

Surface mount plastic IC packages are vulnerable to a moisture-induced fracture mechanism known as popcorn failure, in which cracking occurs during the vapor phase or infrared solder reflow processes [Kitano et al., 1988]. In such processes, the package is heated up to 220-260 ^{o}C for up to 2 minutes. The moisture within the package turns to steam at these elevated temperatures, and the vapor pressure exerted is greater than the plastic can withstand. As such, the plastic fails and releases the pressure, resulting in an external crack [Gallo and Munamarty, 1995].

Three distinct types of temperature- and moisture-induced popcorn cracking have been reported for surface mount plastic encapsulated microcircuits (PEMs) [Omi et al., 1991]. Type I refers to package crack originating from the die pad/molding compound interface delamination, Type II refers to package crack originating from the die/die attach interface delamination and Type III refers to package crack originating from the die surface/molding compound interface delamination. Of the three, type II package cracking has been studied by Guo and Cheng (2003), Cheng and Guo (2003) and Chew et al. (2004a). They showed that high vapor pressure within cavities accelerates void growth and coalescence, causing die-attach failure and brittle-like interface

delamination. In some cases, high vapor pressure combined with high porosity brings about severe reduction in the joint toughness.

In the present work, the combined effect of thermal mismatch stress and internal vapor pressure on a thin quad flat pack (TQFP) while undergoing the moisture sensitivity test (MST) is investigated. The vapor pressure incorporated cell element model (from Chapter 3, section 3.3), is adapted to model damage and predict the onset of delamination at the die pad/molding compound interface and the die/die attach interface. This contributes towards an approach for predicting interface delamination in plastic encapsulated microcircuits.

4.2 Problem Formulation

4.2.1 Material model

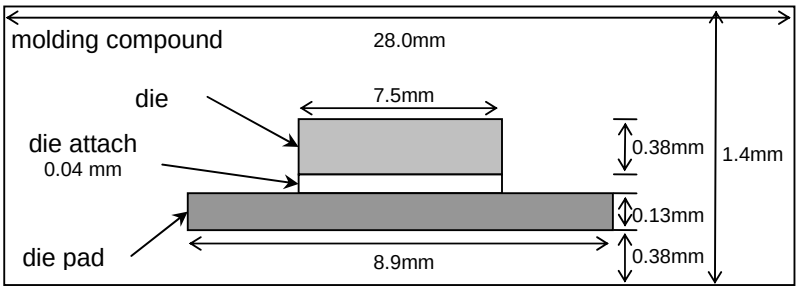

Figure 4.1 A simplified TQFP package.

A simplified Thin Quad Flat Pack (TQFP) package used for the simulations modeling is shown in Fig. 4.1. The die and die pad are assumed to be linear elastic isotropic materials. The die is made up of silicon and the die pad's material is copper, unless otherwise stated. The die attach and molding compound are taken to be polymers in

which their behavior is governed by a power-law hardening behavior of initial tensile yield stress σ_0, and a true stress-logarithmic strain curve in uniaxial tension specified by:

$$\varepsilon = \begin{cases} \dfrac{\sigma}{E}, & \sigma \le \sigma_0 \\ \dfrac{\sigma_0}{E}\left(\dfrac{\sigma}{\sigma_0}\right)^{1/N}, & \sigma \ge \sigma_0 \end{cases} \tag{4.1}$$

where N is the strain hardening exponent. The tensile behavior is generalized to multiaxial stress states assuming isotropic hardening and characterized by the J_2 flow theory.

Table 4.1 Material properties of TQFP components.

Components	***Material***	***E* (GPa)**	**σ_0 (MPa)**	**ν**	**α ($\times 10^{-6}$/°C)**
Die	Silicon	190.0	-	0.278	3.1
Die Attach	Ag filled epoxy	0.2	2	0.30	184.0
Die Pad	Copper	119.3	-	0.348	16.9
	Alloy42	147.0	-	0.30	3.4
Molding Compound	Biphenyl epoxy resin	2.6	25.5	0.25	71.4

The material properties are assumed to be constant with the changes in temperature, and can be found in the Table 4.1. Except for molding compound and die attach, whose properties are varied using the material properties from Chen et al. (1994) and Proctor and Solc (1999), the properties of the other components are extracted from Amagai (1999).

4.2.2 Cell model application at die pad/molding compound interface

Figure 4.2a shows a plane view of the finite element mesh used for the simulations. Due to symmetry, only one half of the whole specimen needs to be modeled with the appropriate boundary condition of traction-free in the respective symmetry planes.

Plane strain conditions are achieved by imposing zero out-of-plane displacements on all the nodes. The mesh composed of a total of 5354 three dimensional, 8-noded linear elements and 11068 nodes.

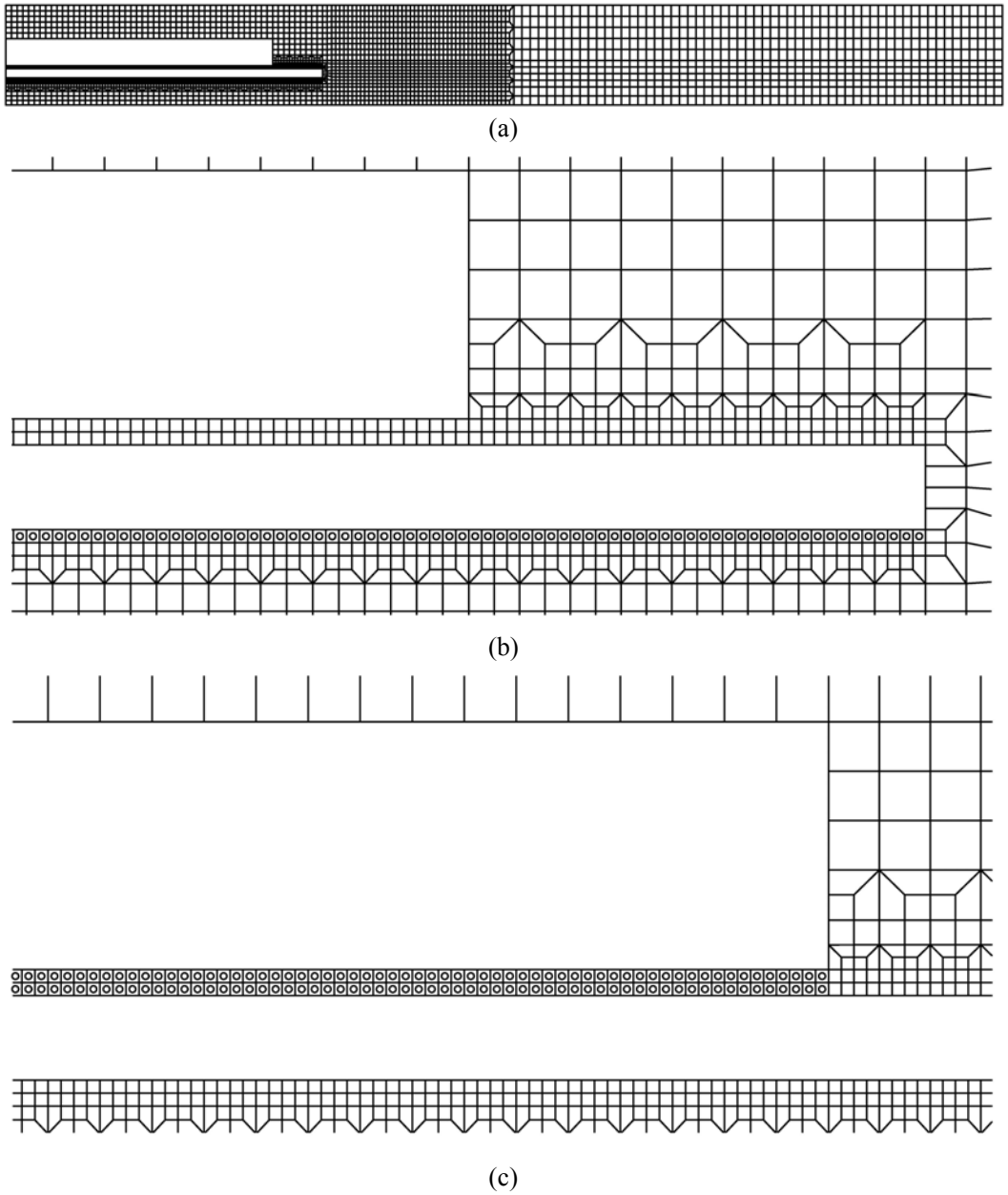

Figure 4.2 Finite element mesh of Thin Quad Flat Pack (TQFP):
(a) Plane view of half package;
(b) Close-up view of cell elements at die pad/molding compound interface;
(c) Close-up view of cell elements in die attach (FPA model).

The most common form of popcorn failure to date is mode I, where delamination initiates from the die pad/molding compound interface. Delamination usually starts at the corners of the die pad and progresses towards the center [Lewis et al., 1994]. Thus, failure analysis is to be carried out at the die pad/molding compound interface.

The vapor pressure incorporated cell element model [Xia and Shih, 1995; Cheng and Guo, 2003] is applied to study delamination at the die pad/molding compound interface during thermal loading. A single layer of 224 of uniformly sized cell elements is used to model the interface (Fig. 4b). Each cell element, of size $D \times D$ (D = 0.02mm), contains porosity of initial void volume fraction f_0. Progressive void growth and subsequent macroscopic material softening in each cell are described by the modified Gurson flow potential discussed in Chapter 3, Section 3.3.

4.2.3 Cell model application at die attach

Interface delamination at the die attach layer (Type II popcorn failure) is one of the primary failure mechanisms in plastic IC packages and often lowers the threshold for other mechanical and electrical failure mechanisms [Tay and Goh, 2003]. Hence, the overall reliability of plastic packages strongly depends on the integrity of the die attach layer, since its delamination may precipitate other failure mechanisms.

While the mechanism of cracks originating from the die pad/molding compound interface (mode I) have been extensively studied, little information is found for cracks that emanate from the interfaces involving the die attach [Chan et al., 1998; Chai et al.,

1999]. As such, the effect of thermal mismatch stress and vapor pressure at the die/die attach interface, using the same material properties from Table 4.1, is analyzed.

Using the methodology stated in the works of Chew et al. (2004b), a similar approach to section 4.2.2 is adapted. The die attach is modeled by two rows of 188 uniformly sized cell elements (Fig. 4.2c). Each cell element, of the size $D \times D$ (D = 0.02 mm), contains porosity of initial void volume fraction f_0. Progressive void growth and subsequent macroscopic material softening in each cell are described by the modified Gurson flow potential discussed in Chapter 3, Section 3.3. The remaining parameters and boundary conditions follow the same as the analysis for the die pad/molding compound interface. This computational model is referred as the fully porous adhesive (FPA) model by Chew et al. (2004b). It is different from the previous applications of the cell model which confined the cell elements to a single layer.

4.2.4 Moisture distribution modeling at die attach

Currently, all the interfaces under analysis are assumed to be of uniform moisture concentration, and therefore, uniform initial vapor pressure. However, as stated in Chapter 2.3, the die attach of the TQFP may not be of uniform moisture concentration. In fact, from the works of Liu et al. (2002), it was found that most of the die attach is not saturated with moisture. This is a result of the die attach being a very thin layer trapped between the die and the die pad which are both impermeable to moisture, causing only the perimeter of the die attach to be saturated with moisture. As such, there is a cause to alter the scenario presented thus far for further analysis.

Three cases of moisture penetration are presented here. Firstly, the die attach is assumed to be of uniform moisture concentration and vapor pressure up to a certain length $X_{piecewise}$ from the die attach/molding compound interface (Fig. 4.3), i.e. moisture is piecewise constant until $X_{piecewise}$.

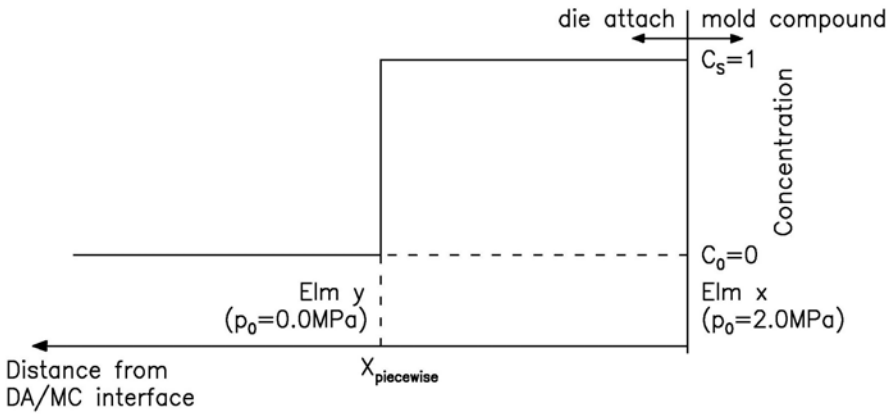

Figure 4.3 Piecewise Moisture Concentration Distribution.

The other case is where the moisture distribution is assumed to be linearly distributed. With the concentration at the die attach/molding compound interface assumed to be unity, while X_{linear} is the furthest distance from the die attach/molding compound interface that moisture has diffused and is assumed to be zero as shown in Fig. 4.4.

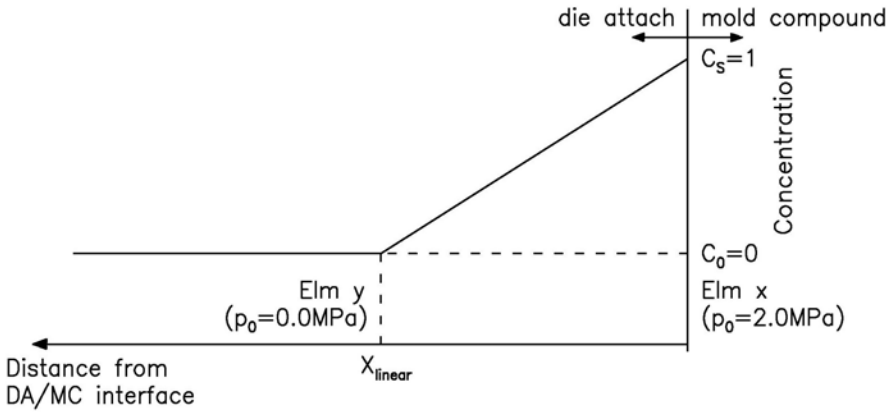

Figure 4.4 Linear Moisture Concentration Distribution.

Finally, a case of transient diffusion is considered, where the Fick's Second Law is applied. Transient diffusion describes the non-steady state change in moisture concentration before equilibrium is achieved. The general diffusion equation for the time-dependent diffusion is described by:

$$\frac{\partial C}{\partial t} = D\frac{\partial^2 C}{\partial x^2} \quad \Rightarrow \quad \frac{\partial c_x}{\partial t} = D\frac{\partial^2 c_x}{\partial x^2} \tag{4.2}$$

where x is the distance from the saturated die attach/molding compound interface, c_x the variable concentration at distance x, D diffusion coefficient and t time. This equation specifies the time-dependent change of the diffusion in one direction, or, the time-dependent change of local concentration gradient at that position for materials of different diffusion coefficient.

The diffusion coefficient can be obtained using $D = D_0 \exp\left(-\frac{Q}{RT}\right)$, where T is the absolute temperature, Q the activation energy, R universal gas constant. From Kitano et al. (1988), Q = 4.84 × 10^4 J/mol and D_0 = 47.2 mm^2/s. Moisture preconditioning is usually carried out at 85°C, and D works out to be 4.093 × 10^{-12} m^2/s.

Solving the differential equation,

$$\frac{c_s - c_x}{c_s - c_0} = erf\left(\frac{x}{2\sqrt{Dt}}\right) \tag{4.3}$$

where c_s is the constant concentration at surface (x=0), c_0 initial concentration (assume c_0=0) and *erf* the error function (Table 4.2). A typical Fick's moisture concentration distribution at time t is shown in Fig. 4.5. X_{fick} is the furthest distance from the die attach/molding compound interface that moisture has diffused and is assumed to be zero.

Table 4.2 Table of the Error Function [Flinn and Trojan, 1981].

z	erf z	z	erf z	z	erf z	z	erf z
0	0	0.40	0.4284	0.85	0.7707	1.6	0.9763
0.025	0.0282	0.45	0.4755	0.90	0.7970	1.7	0.9838
0.05	0.0564	0.50	0.5205	0.95	0.8209	1.8	0.9891
0.10	0.1125	0.55	0.5633	1.0	0.8427	1.9	0.9928
0.15	0.1680	0.60	0.6039	1.1	0.8802	2.0	0.9953
0.20	0.2227	0.65	0.6420	1.2	0.9103	2.2	0.9981
0.25	0.2763	0.70	0.6778	1.3	0.9340	2.4	0.9993
0.30	0.3286	0.75	0.7112	1.4	0.9523	2.6	0.9998
0.35	0.3794	0.80	0.7421	1.5	0.9661	2.8	0.9999

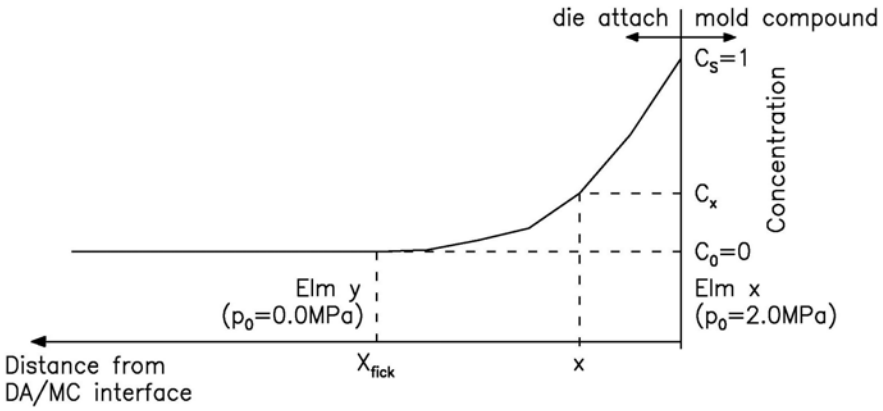

Figure 4.5 Fick's Moisture Concentration Distribution.

For the present work, a direct relationship between vapor pressure and moisture concentration is assumed. From Fig. 4.3 to Fig. 4.5, concentration at surface (molding compound, c_s = 1, and initial concentration of die attach, c_0 = 0; c_s = 1 is assumed to be equivalent to p_0/σ_0=1.0 while c_0 = 0 is assumed to be equivalent to p_0/σ_0=0.0. The following (Fig. 4.6 and Table 4.3 to Table 4.5) show the modeling of cell element initial vapor pressures for moisture penetration at X = 0.1 mm, 0.2 mm and 0.3 mm with the three different cases.

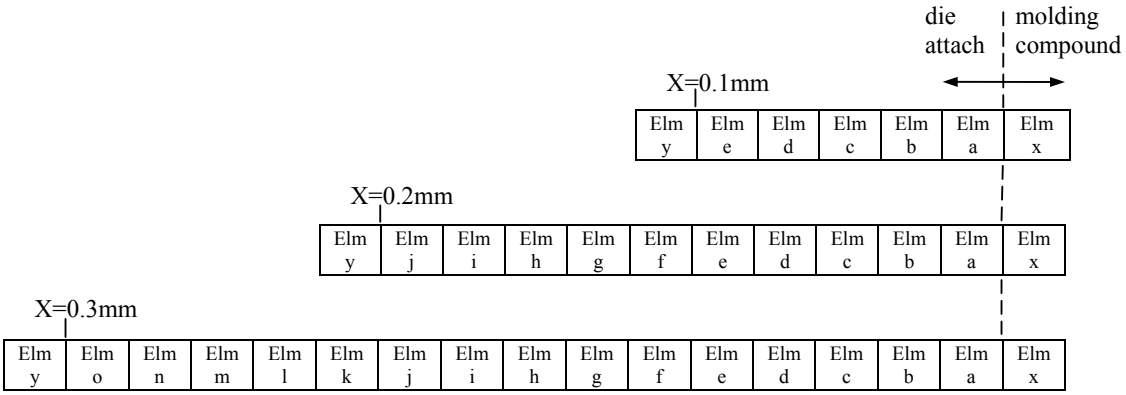

Figure 4.6 Cell moisture concentration and vapor pressure configuration for moisture penetration at X = 0.1 mm, 0.2 mm and 0.3 mm.

Table 4.3 Cell element initial vapor pressure for moisture penetration at X=0.1 mm

Moisture Distribution	Piecewise		Linear		Fick's 2nd Law	
	c_x	p_0 (MPa)	c_x	p_0 (MPa)	c_x	p_0 (MPa)
Elm x	1.00	2.00	1.00	2.00	1.00	2.00
Elm a	1.00	2.00	0.8333	1.6667	0.6060	1.2121
Elm b	1.00	2.00	0.6667	1.3333	0.3023	0.6047
Elm c	1.00	2.00	0.5000	1.0000	0.1218	0.2437
Elm d	1.00	2.00	0.3333	0.6667	0.0395	0.0790
Elm e	1.00	2.00	0.1667	0.3333	0.0100	0.0200
Elm y	0.0	0.0	0.0	0.0	0.0	0.0

Table 4.4 Cell element initial vapor pressure for moisture penetration at X=0.2 mm

Moisture Distribution	Piecewise		Linear		Fick's 2nd Law	
	c_x	p_0 (MPa)	c_x	p_0 (MPa)	c_x	p_0 (MPa)
Elm x	1.00	2.00	1.00	2.00	1.00	2.00
Elm a	1.00	2.00	0.9091	1.8182	0.7965	1.5930
Elm b	1.00	2.00	0.8182	1.6364	0.6060	1.2121
Elm c	1.00	2.00	0.7273	1.4545	0.4390	0.8780
Elm d	1.00	2.00	0.6364	1.2727	0.3023	0.6047
Elm e	1.00	2.00	0.5455	1.0909	0.1972	0.3944
Elm f	1.00	2.00	0.4545	0.9091	0.1218	0.2437
Elm g	1.00	2.00	0.3636	0.7273	0.0714	0.1429
Elm h	1.00	2.00	0.2727	0.5455	0.0395	0.0790
Elm i	1.00	2.00	0.1818	0.3636	0.0206	0.0411
Elm j	1.00	2.00	0.0909	0.1818	0.0100	0.0200
Elm y	0.0	0.0	0.0	0.0	0.0	0.0

Table 4.5 Cell element initial vapor pressure for moisture penetration at X=0.3 mm

Moisture Distribution	Piecewise		Linear		Fick's 2nd Law	
	c_x	p_0 (MPa)	c_x	p_0 (MPa)	c_x	p_0 (MPa)
Elm x	1.00	2.00	1.00	2.00	1.00	2.00
Elm a	1.00	2.00	0.9375	1.8750	0.8635	1.7270
Elm b	1.00	2.00	0.8750	1.7500	0.7309	1.4619
Elm c	1.00	2.00	0.8125	1.6250	0.6060	1.2121
Elm d	1.00	2.00	0.7500	1.5000	0.4917	0.9833
Elm e	1.00	2.00	0.6875	1.3750	0.3899	0.7798
Elm f	1.00	2.00	0.6250	1.2500	0.3023	0.6047
Elm g	1.00	2.00	0.5625	1.1250	0.2286	0.4572
Elm h	1.00	2.00	0.5000	1.0000	0.1691	0.3382
Elm i	1.00	2.00	0.4375	0.8750	0.1218	0.2437
Elm j	1.00	2.00	0.3750	0.7500	0.0859	0.1717
Elm k	1.00	2.00	0.3125	0.6250	0.0591	0.1182
Elm l	1.00	2.00	0.2500	0.5000	0.0395	0.0790
Elm m	1.00	2.00	0.1875	0.3750	0.0256	0.0513
Elm n	1.00	2.00	0.1250	0.2500	0.0161	0.0321
Elm o	1.00	2.00	0.0625	0.1250	0.0100	0.0200
Elm y	0.0	0.0	0.0	0.0	0.0	0.0

4.2.5 MST Loading and Numerical Procedure

The finite element model is subjected to a loading profile analogous to Moisture Sensitivity Test (MST), where the loading profile is shown in Fig. 4.7. In the physical test itself, the package is cured at 175 ^{o}C (point A), where it is assumed to be at a stress free state. After the package is cooled down to room temperature (point B) from the curing temperature, according to Joint IPC/JEDEC Standard J-STD-020A (1999), it undergoes 3 cycles (C1, C2, C3) of heating up to the reflow temperature at 235 ^{o}C and cooling down to room temperature of 25 ^{o}C.

As temperature changes, thermal stresses are induced in the package due to thermal mismatch. With rapid thermal diffusion, it is assumed uniform change in temperature within the package. Since the volume fraction of micro-defects at the interfaces is much higher than that within the molding compound and die attach, the moisture content at

the interfaces will also be higher. Thus, only vapor pressure at the interfaces is modeled for the present analysis.

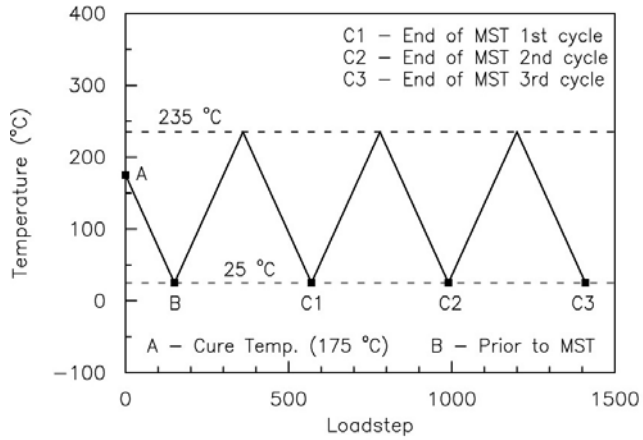

Figure 4.7 MST thermal loading profile

4.3 Results and Discussions – Die Pad/Molding Compound Interface Analysis

4.3.1 Effects of Strain Hardening Exponent, *N*

In this section, the effects of changing the material's hardening are demonstrated and a representative hardening value of the materials will be chosen for the subsequent sections. The values $N = 0, 0.05, 0.10$ represent an ideally plastic solid, a low hardening material and a moderate hardening material respectively.

The current porosity and mean stress distribution for different material hardening across the interface from the center ($X_1/D=0$) to the corner ($X_1/D=224$) is shown in Fig. 4.8. Lowering the hardening exponent induces higher void growth and reduces the mean stress, but it does not affect the damage (void growth) trend significantly. An

elastic-ideally plastic solid (N = 0) will be chosen to represent the materials for the following sections on the die pad/molding compound interface analysis.

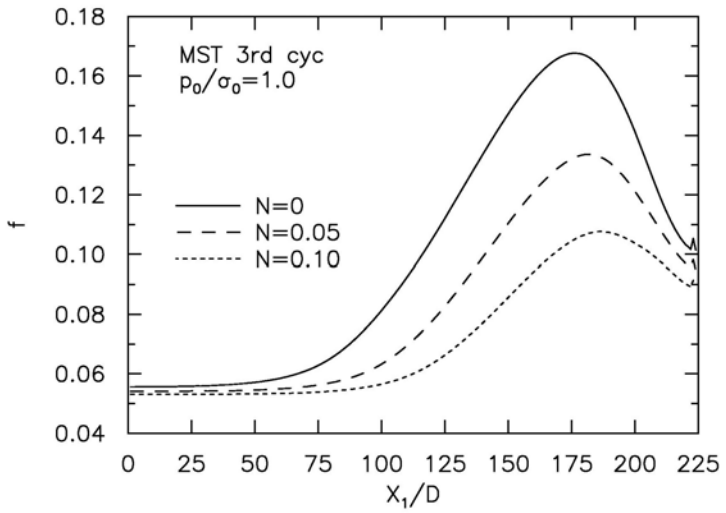

(a)

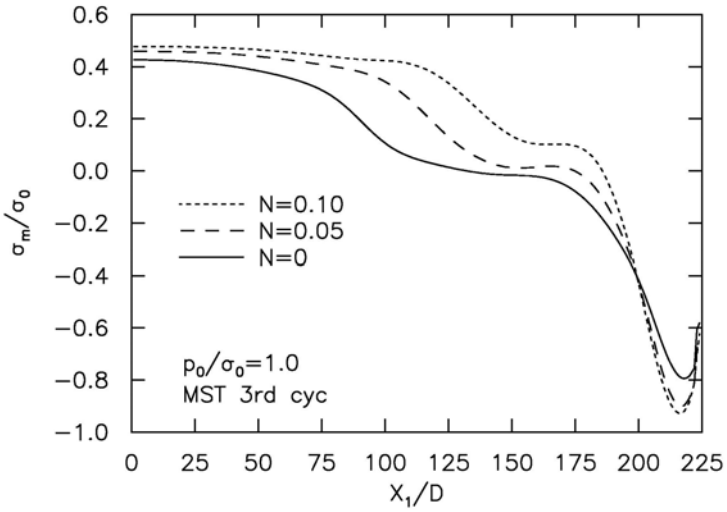

(b)

Figure 4.8 (a) Current void volume fraction f, and (b) mean stress σ_m/σ_0, along the die pad/molding compound interface at the end of MST for N = 0, 0.05 and 0.10.

The stress distribution is observed to decrease from the center to the corner, with the negative stresses at the corner reflecting the compressive state at the end of the MST 3rd cycle. Nevertheless, void growth is observed to occur at the corner despite such

compressive stresses due to the effects of vapor pressure and the contribution of mismatch stress to the accumulated damage during other stages of the MST loading.

4.3.2 Effects of Initial Void Volume Fraction, f_0

The estimated void volume fractions of typical IC package materials ranged from 1 % to 5 %. The effects of high initial porosity (f_0 = 0.05) and low initial porosity (f_0 = 0.01) in the die attach are described next in Fig. 4.9. A decrease in f_0 increases the mean stress carry capacity across the interface and results in much lesser void growth. With higher initial void volume fraction, the progressive void growth at the end of each MST cycle is significantly larger and void activity spreads over a larger area across the interface. Similar to the observations in the works of Chong et al. (2004), high initial porosity significantly weakens the interface toughness. For the subsequent sections on die pad/molding compound interface analysis, the initial void volume fraction is assumed to be 0.05 throughout.

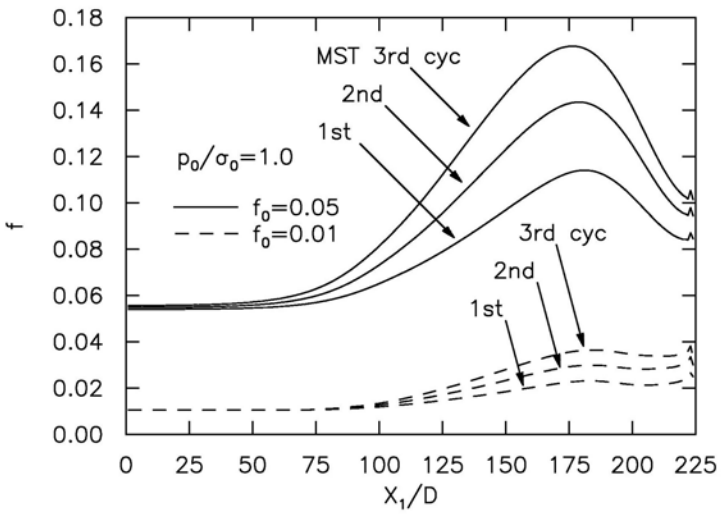

(a)

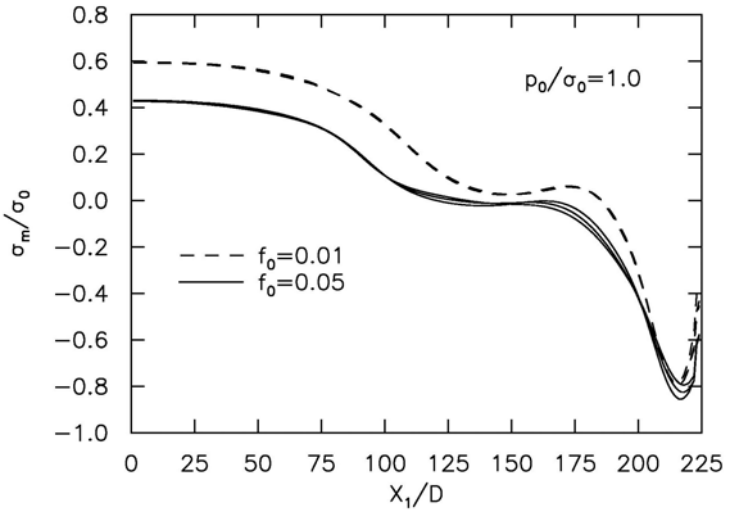

(b)

Figure 4.9 (a) Current void volume fraction f, and (b) mean stress σ_m/σ_0, along the die pad/molding compound interface at the end of MST for f_0 = 0.01 and 0.05.

4.3.3 Effects of vapor pressure

Figure 4.10a displays the porosity distribution along the die pad/molding compound interface for p_0/σ_0 = 0, 0.5, 1.0, 1.5 at the end of the MST test (after MST 3rd cycle). It can be seen that vapor pressure accelerates void growth. Under similar thermal conditions, porosity levels at p_0/σ_0 = 1.5 is higher than those for p_0/σ_0 = 0, growing to a peak of 0.23 from the initial void size of 0.05. With the increase in vapor pressure, voids near the die pad corner (at X_1/D=224) grow at a significantly faster pace. This shows that with higher initial vapor pressure, there tends to be increased void growth and it tends to be localized close to the die pad corner, forming the possible delamination initiation site at the interface.

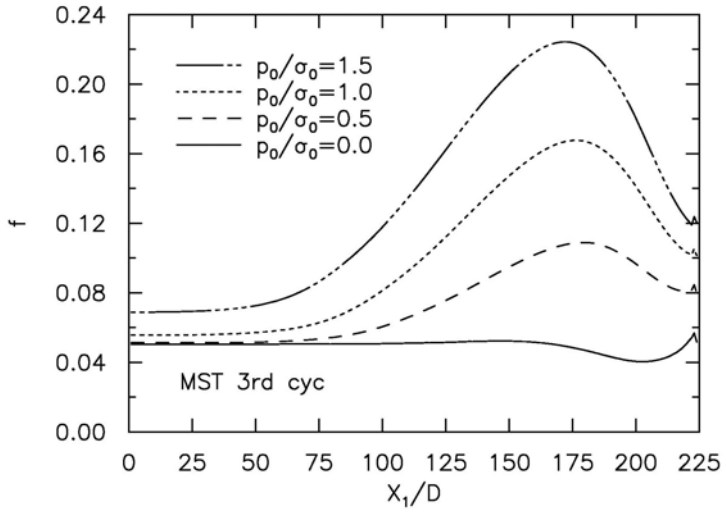

(a)

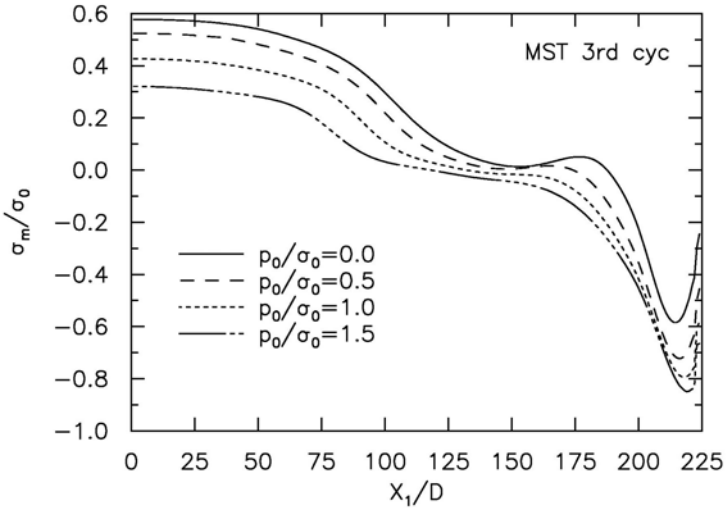

(b)

Figure 4.10 (a) Current void volume fraction f, and (b) mean stress σ_m/σ_0, along the die pad/molding compound interface at the end of MST for p_0/σ_0 = 0.0, 0.5, 1.0 and 1.5.

Figure 4.10b compares the normalized mean stress distribution associated with different vapor pressure, p_0/σ_0 = 0, 0.5, 1.0, 1.5 at the end of the MST tests. With the rise in vapor pressure, the stress levels reached across the whole interface is lowered. The stress distribution across the interface is observed to decrease from the center (X_1/D=0) to the corner (X_1/D=224), reflecting the greater loss of stress carrying

capacity near the die pad corner. This shows that higher void growth is coupled with the further loss of stress carrying capacity.

4.3.4 MST cycle effect

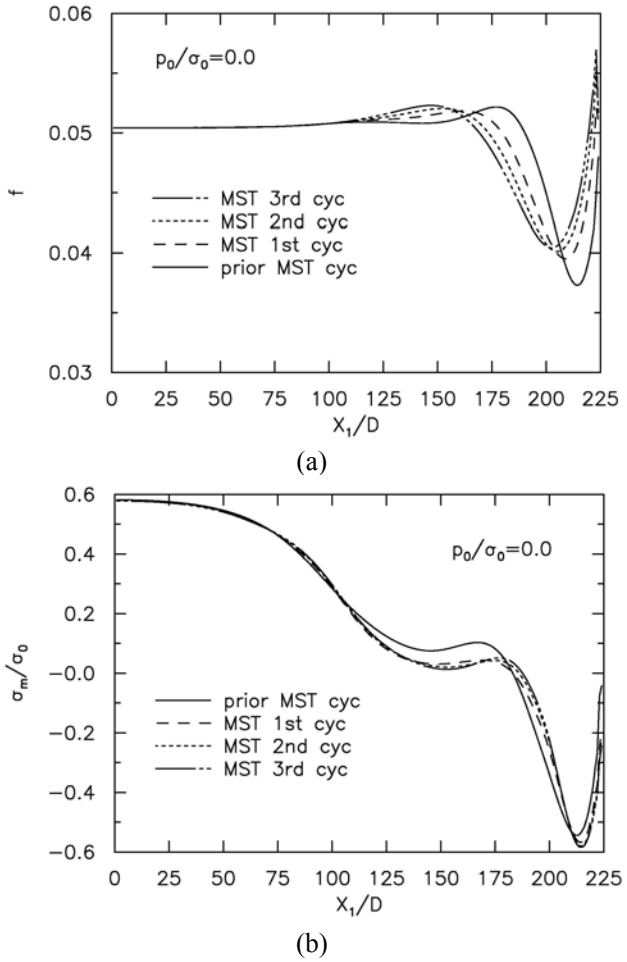

Figure 4.11 (a) Current void volume fraction f, and (b) mean stress σ_m/σ_0, along the die pad/molding compound interface at each MST cycle for $p_0/\sigma_0 = 0.0$.

The study of the whole interface behavior at the progress of each MST cycle is shown subsequently. The current void porosities for $p_0/\sigma_0 = 0.0$ at the end of each MST cycle is noticed to fluctuate near to the die pad corner (Fig. 4.11a). At the progress of each MST cycle, though very limited void growth take place, the peak being reached by void

growth at the interface corner increases steadily. The stress carrying capacity showed similar trends at the end of each MST cycle as the void activity is down to a minimal (Fig. 4.11b).

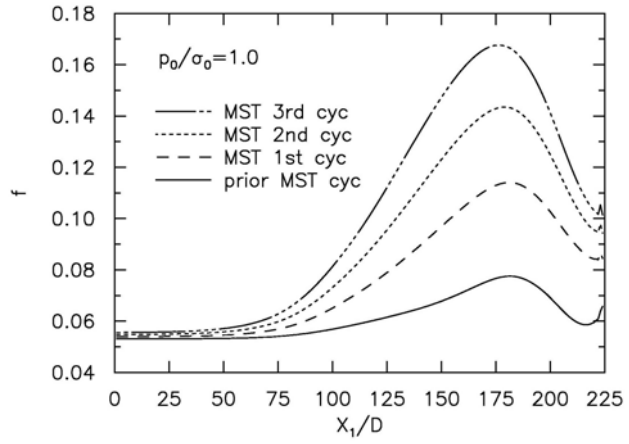

(a)

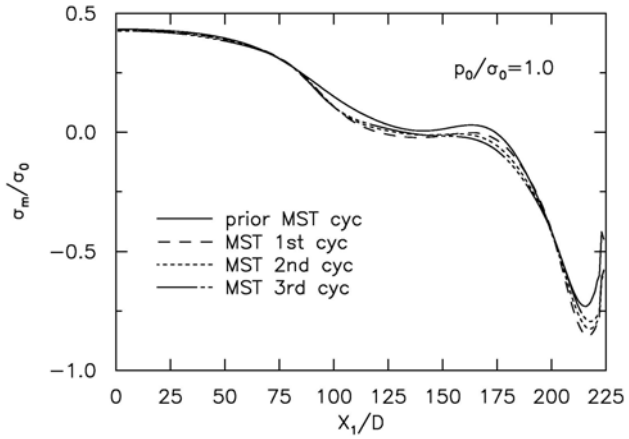

(b)

Figure 4.12 (a) Current void volume fraction f, and (b) mean stress σ_m/σ_0, along the die pad/molding compound interface at each MST cycle for $p_0/\sigma_0 = 1.0$.

Figure 4.12 shows that the current void porosities for $p_0/\sigma_0 = 1.0$ at the progress of each MST cycle grows steadily while the mean stress distribution decreases. At the end of each MST cycle, the peak being reached by void growth near the interface corner is noticed to be more intense than general void growth (from about 0.08 before the MST

cycles to close to 0.17), highlighting the increased possibility of forming sites of interface delamination.

4.3.5 Behavior of Individual Elements along the die pad/molding compound interface

In this section, the behavior of individual cell elements at certain positions along the die pad/molding compound interface is presented for the duration of the MST loading. First of all, the element closest to the package center is considered at $X_1/D = 221$. From Fig. 4.10, the analysis showed that the element at $X_1/D = 175$ is one of the elements which reached the highest porosity levels at the various vapor pressure levels, and is possible of being the crack initiation site. As such, the loading history of the cell element at $X_1/D = 175$ is presented next to find out the void and mean stress behavior. Finally, the behavior of a cell element close to the die pad corner is investigated ($X_1/D = 223$). Two cases of initial vapor pressure are presented here, $p_0/\sigma_0 = 0.0$ and $p_0/\sigma_0 = 1.0$.

With the progress of the MST loading, the combined effects of thermal mismatch stress and vapor pressure at the package center along the die pad/molding compound interface are not pronounced (Fig. 4.13). At $p_0/\sigma_0 = 0.0$, with the progress of each load step, the void growth remains constant at close to 0.05, indicating that there is no further interface damage; at $p_0/\sigma_0 = 1.0$, though there is a gradual rise in void growth with each load step, the void growth levels are actually very small — about 0.5% change in void volume fractions (Fig. 4.13b). The mean stress trends for $p_0/\sigma_0 = 0.0$ and $p_0/\sigma_0 = 1.0$ are very similar but the mean stress peaks at the progress of each cycle is found to be

getting lower and lower for p_0/σ_0 = 1.0, reflecting a little gradual loss of stress carrying capacity for the cell element.

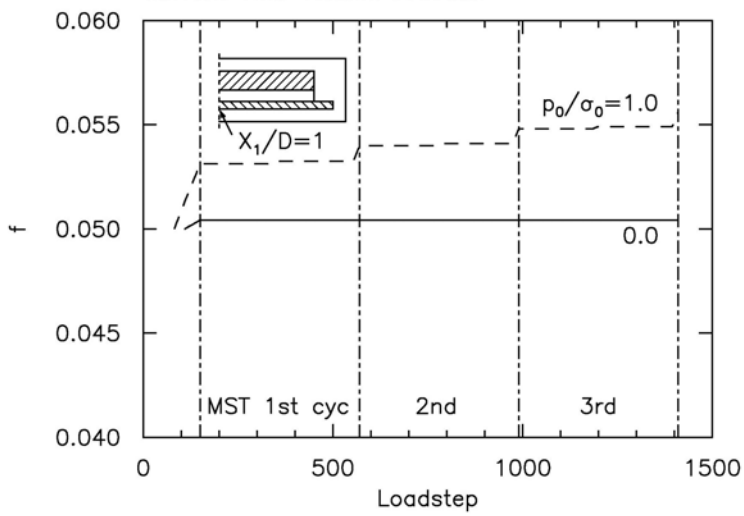

(a)

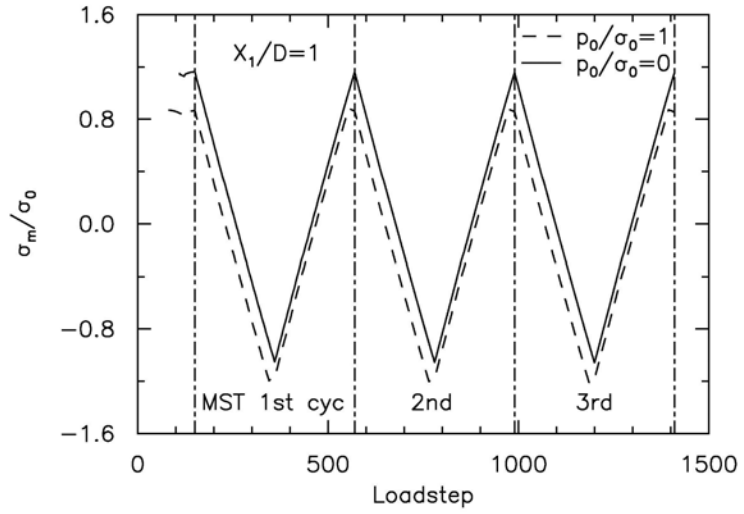

(b)

Figure 4.13 (a) Current void volume fraction f, and (b) mean stress σ_m/σ_0, at X_1/D=1, along the die pad/molding compound interface for p_0/σ_0 = 0.0, 1.0.

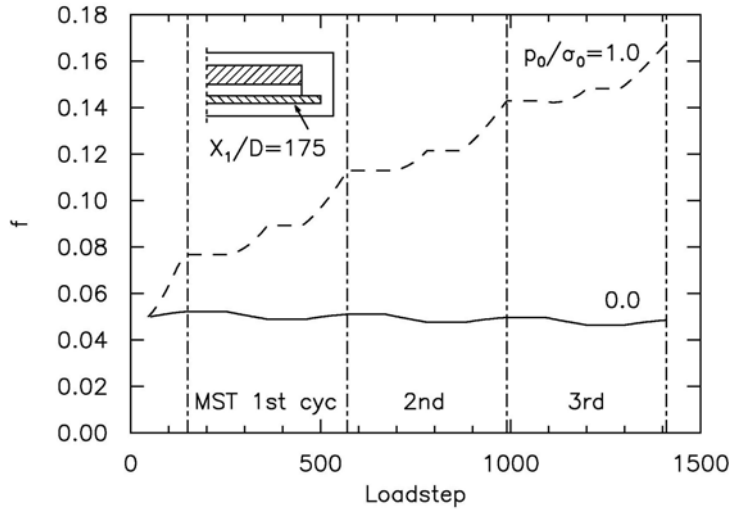

(a)

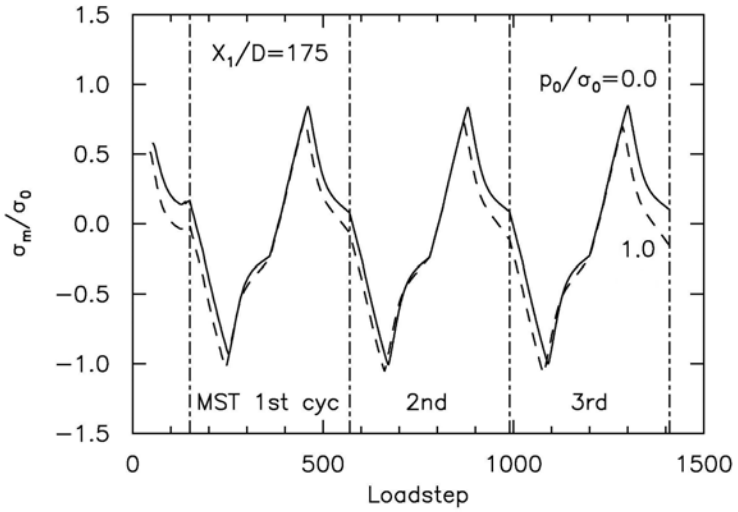

(b)

Figure 4.14 (a) Current void volume fraction f, and (b) mean stress σ_m/σ_0, at X_1/D=175, along the die pad/molding compound interface for p_0/σ_0 = 0.0, 1.0.

At X_1/D = 175, there is significant and steady increase in void growth with each load step of the MST test (Fig. 4.14). For each cycle, the greatest increase in void growth actually occurs during the fall in temperature. This could be because during the fall in temperature at each MST cycle, the molding compound which has a higher coefficient of thermal expansion, contracts at a much faster rate than the die pad. As such, the cell elements bonded to the die pad experience a tensile force from the die pad, resulting in

void growth. Also, with the increase in MST cycles, the increase in amount of void growth actually gets progressively lower. The mean stress trends for both vapor pressure levels are very similar but the mean stress peaks at the progress of each cycle is found to be getting lower and lower for p_0/σ_0 = 1.0, reflecting the gradual loss of stress capacity for the cell element.

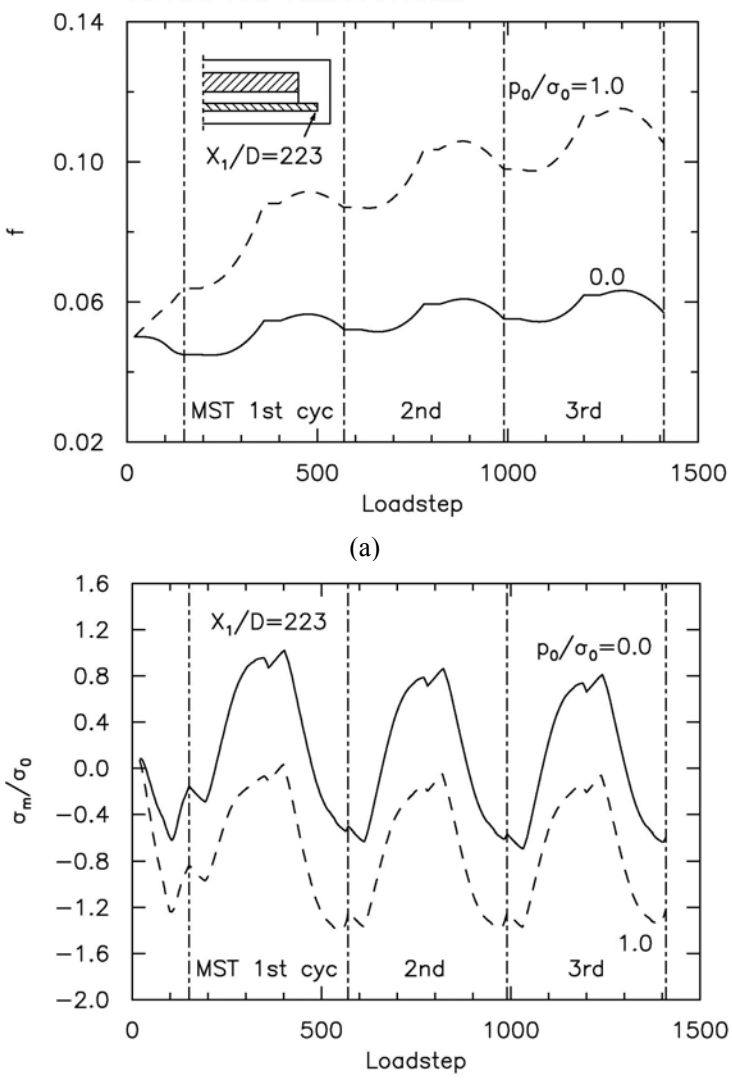

Figure 4.15 (a) Current void volume fraction f, and (b) mean stress σ_m/σ_0, at X_1/D=223, along the die pad/molding compound interface for p_0/σ_0 = 0.0, 1.0.

For the cell element at X_1/D=223, without vapor pressure, the void growth is the highest as compared to other cell elements (Fig. 4.15). At p_0/σ_0 = 1.0, there are periods where the element undergoes void contraction, despite the progressive rise in void activity. The loss in stress capacity is more apparent with the mean stress starting off much lower for p_0/σ_0 = 1.0 and widening the gap with p_0/σ_0 = 0.0 as the MST progresses. Among the three cell elements considered, without initial vapor pressure, the interface corner (X_1/D=223) is the one that undergoes the most void growth, but with the introduction of vapor pressure a higher damage zone is formed away from the die pad corner.

4.3.6 Crack initiation and propagation along the die pad/molding compound interface

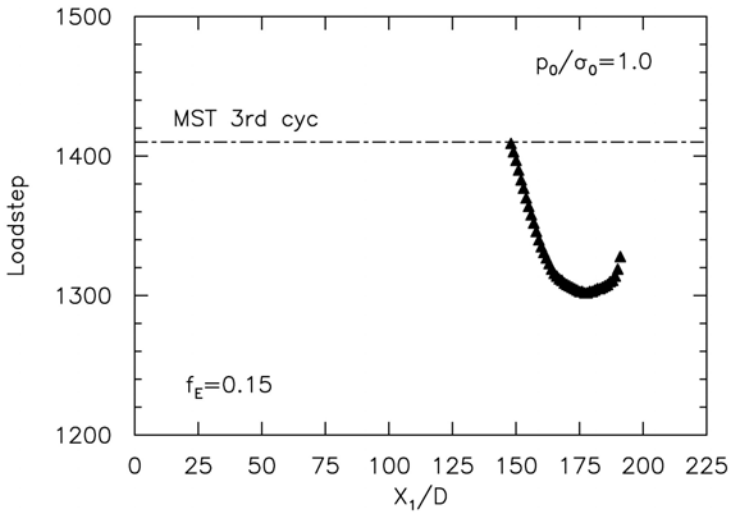

Figure 4.16 History of crack initiation and propagation along the die pad/molding compounding interface with f_0 =0.05, p_0/σ_0 = 1.0 and f_E =0.15.

It was concluded previously that the most probable crack initiation location is near to the die pad corner. To provide further insights into vapor pressure assisted interface

delamination, the history of crack initiation and propagation, and the deformed configuration of the TQFP package with the delaminated zone along the die pad/molding compound interface are presented in this section. Each cell element is rendered to have failed when the average void volume fraction over a cell reaches the critical void volume fraction f_E. The history of crack initiation and propagation for p_0/σ_0 = 1.0 and f_E =0.15 is summarized in Fig. 4.16. Crack initiates close to the die pad/molding compound interface corner at X_1/D = 178 near the end of the 3rd MST cycle (at step 1302), and propagates in both directions towards the interface corner and center, resulting in a delaminated zone of 44 cell elements.

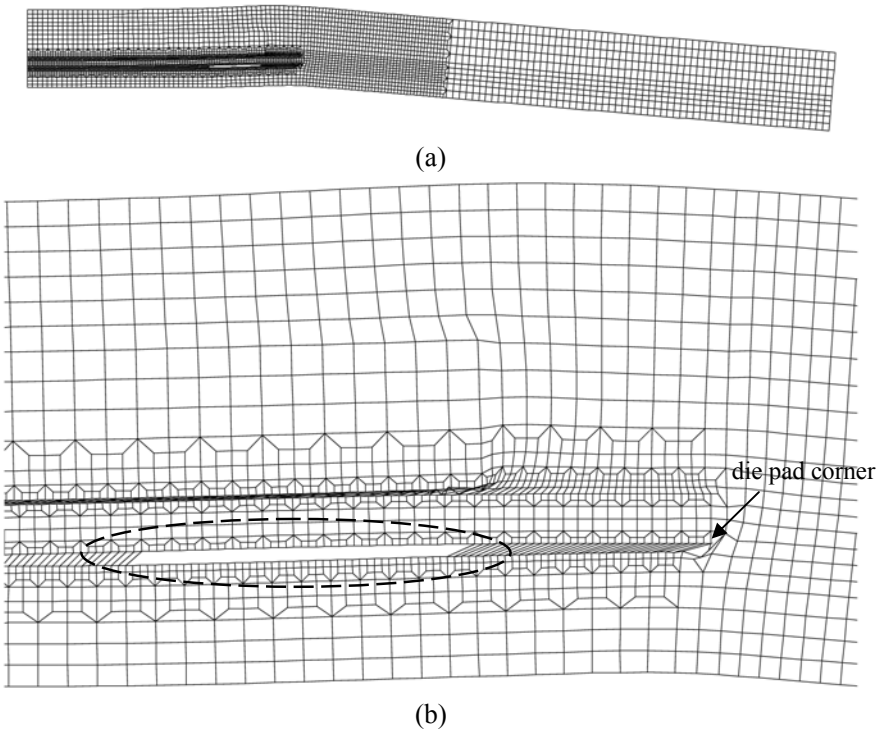

Figure 4.17 Deformed configuration of the TQFP package: (a) half the package, and (b) close up of the delamination site along the die pad/molding compounding interface.

Figure 4.17 shows the deformed configuration of the die pad/molding compound interface in the TQFP package with p_0/σ_0 = 1.0 and f_E =0.15 at the end of the MST

loading. The 44 cell elements (equivalent to 0.88 mm) that had delaminated along the interface at the end of the MST 3rd cycle are highlighted.

4.3.7 Effects of die pad materials

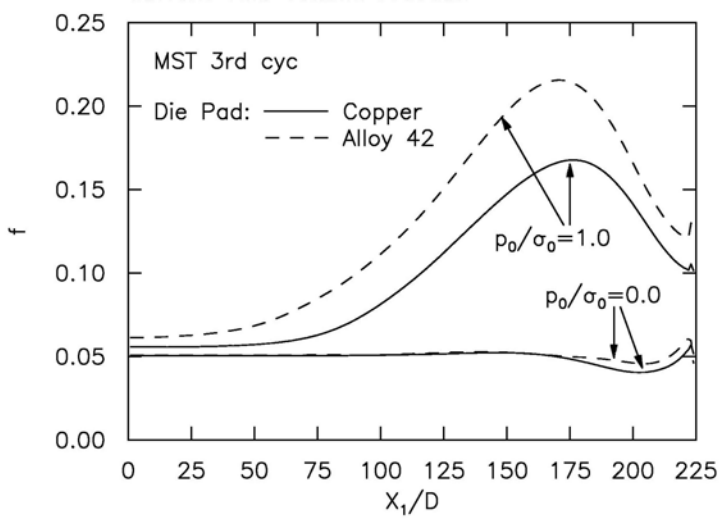

(a)

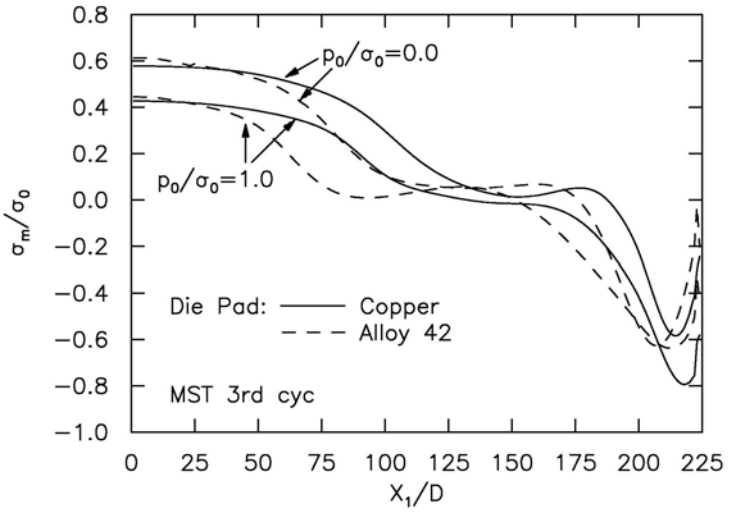

(b)

Figure 4.18 (a) Current void volume fraction f, and (b) mean stress σ_m/σ_0, along the die pad/molding compound interface for copper and alloy42 die pad, with p_0/σ_0 = 0.0, 1.0.

Up to this point, all the analysis has been done for copper as the die pad material. Generally, the die pad material would be copper or alloy42. Though copper is of lower cost, excellent thermal conductivity and higher malleability, but it has a lower stiffness and higher coefficient of thermal expansion (Table 4.1). As such, a further analysis is done by using the material properties of alloy42 as the die pad material. Similar to that of copper, the material is assumed to be linear elastic.

The current void porosities and normalized mean stress distribution for $p_0/\sigma_0 = 0.0$ and 1.0 at the end the MST test are shown in Fig. 4.18. Though the trends are quite similar, it can be seen that at the end of each cycle, the void growth is larger for the alloy42 die pad while the mean stress distribution decreases. As compared to a copper die pad, the zone of localized void activity at the alloy42 die pad/molding compound interface is much larger and higher peak values of void growth are being reached. Such behavior is largely attributed to the greater difference between the coefficients of thermal expansion of the molding compound and the alloy42 die pad.

4.4 Results and Discussions – Die/ Die Attach Interface Analysis

For this section, the analysis will focus on the die/die attach interface as described by the approach highlighted in section 4.2.3. Note that from this point onwards, $X_1/D=1$ is the die/die attach interface center while $X_1/D=188$ is the interface corner.

4.4.1 Effects of Strain Hardening Exponent, *N*

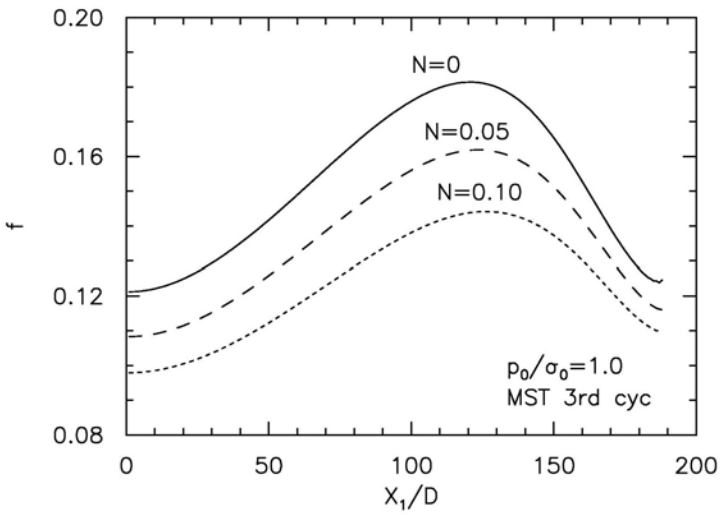

(a)

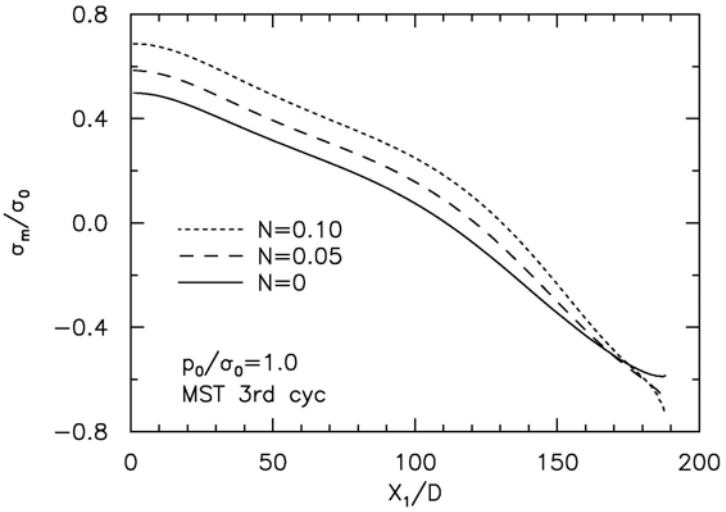

(b)

Figure 4.19 (a) Current void volume fraction *f*, and (b) mean stress σ_m/σ_0, along the die/die attach interface at the end of MST for $N = 0$, 0.05 and 0.10.

Figure 4.19 compares current porosity and mean stress distribution for different material hardening, with $N = 0$ representing an ideally plastic solid, $N = 0.05$ a low hardening material, $N = 0.1$ a moderate hardening material. Lowering the hardening exponent induces higher void growth and reduces the mean stress, but it does not affect the damage (void growth) trend significantly. Similar to the section 4.3, an elastic-

ideally plastic solid (N = 0) will be chosen to represent the materials for the sections hereafter.

4.4.2 Effects of Initial Void Volume Fraction, f_0

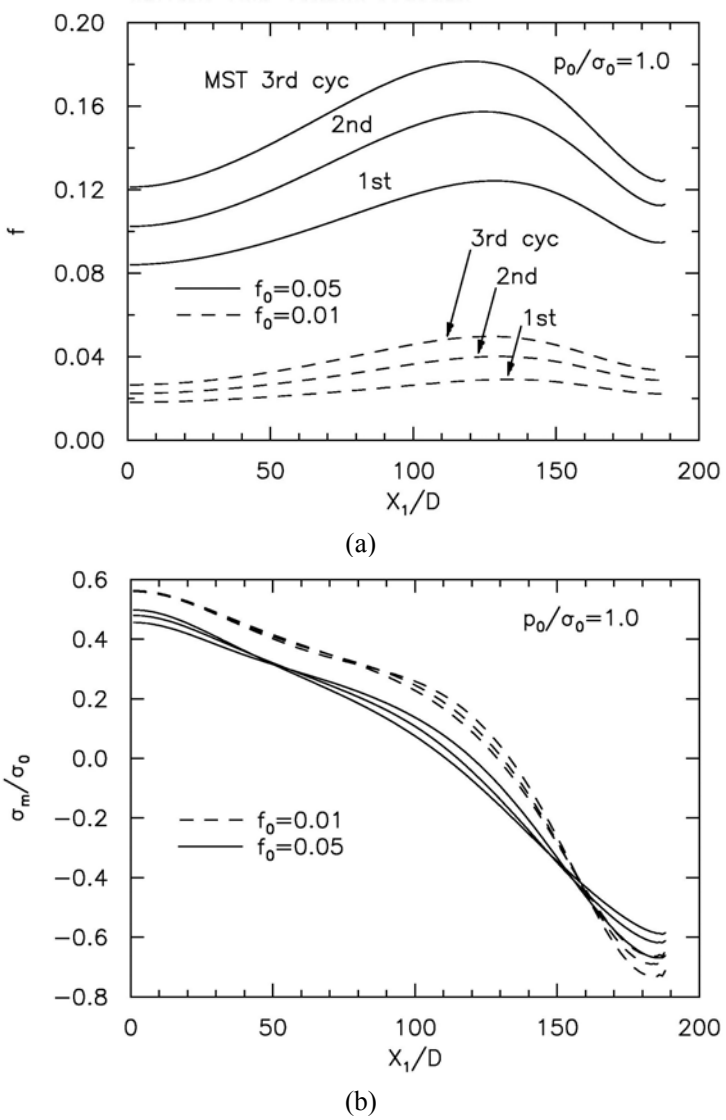

Figure 4.20 (a) Current void volume fraction f, and (b) mean stress σ_m/σ_0, along the die/die attach interface at the end of MST for f_0 = 0.01 and 0.05.

The role of f_0 is amply demonstrated in Fig. 4.20; a decrease in f_0 increases the mean stress carry capacity across the interface and results in much lesser void growth. The

works of Chew et al (2004a) showed that high porosity brings about reduction in joint toughness along the interfaces of a polymeric film joining elastic substrates. With higher initial void volume fraction, the progressive void growth at the end of each MST cycle is significantly larger and void activity spreads over a larger area across the interface. For subsequent sections, the die attach is assumed to have an initial void volume fraction of 0.05.

4.4.3 Effects of Initial Vapor Pressure, p_0/σ_0

Vapor pressure accelerates void growth along the die/die attach interface (Fig. 4.21). At $p_0/\sigma_0 = 0$, voids near the die attach corner undergo contraction, shrinking from $f_0 = 0.05$ to less than 0.025. However, with the increase in vapor pressure, a localized zone of intense void activity and the possible sites of delamination at the interface form away from the die attach corner. At $p_0/\sigma_0 = 1.5$, voids grow to as high as 0.23 (at $X_1/D=115$). The possible delamination site is also noticed to become progressively larger with the rise in p_0/σ_0. With the rise in vapor pressure, the stress levels reached is slightly lowered (Fig. 21b). The stress distribution along the interface appears to be gradually decreasing as it approaches the die attach corner.

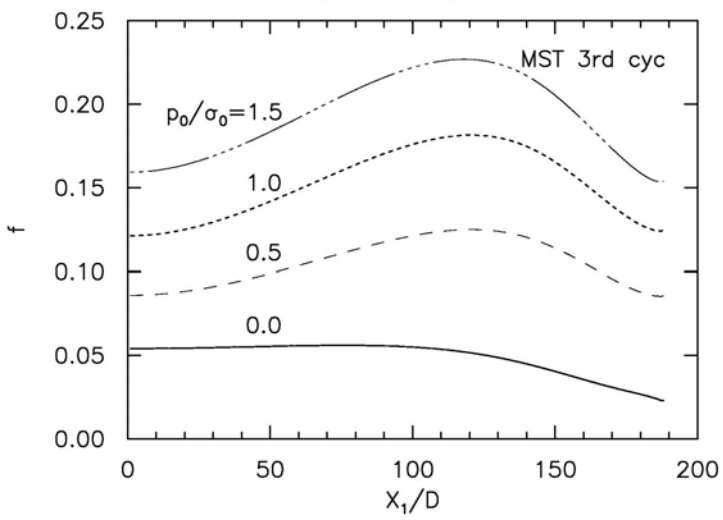

(a)

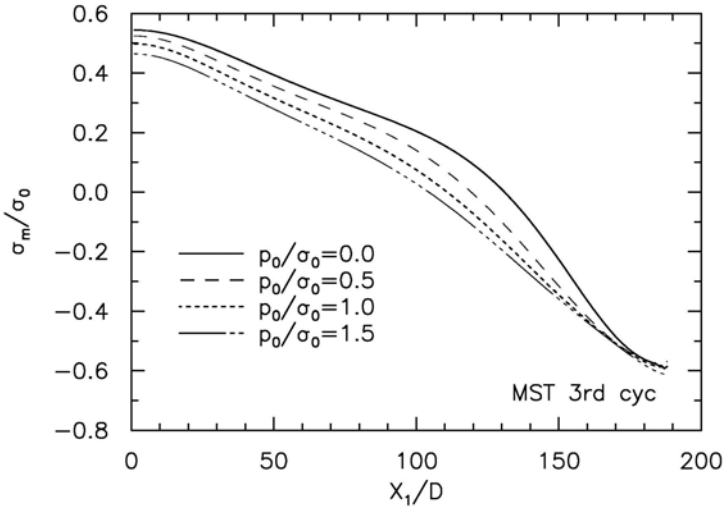

(b)

Figure 4.21 (a) Current void volume fraction f, and (b) mean stress σ_m/σ_0, along the die/die attach interface at the end of MST for p_0/σ_0 = 0.0, 0.5, 1.0 and 1.5.

4.4.4 MST cycle effect

At the end of each MST cycle, the voids near the die attach corner actually experience further contraction in the absence of vapor pressure (Fig. 4.22); the mean stress across the interface follows a similar decreasing trend as each cycle proceeds.

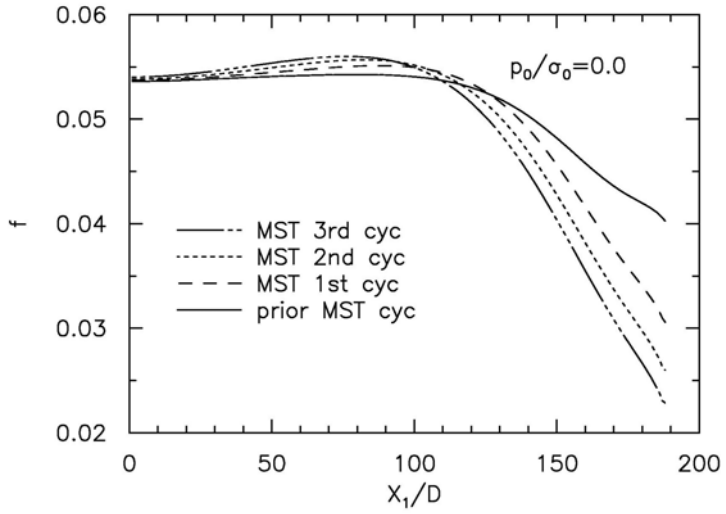

(a)

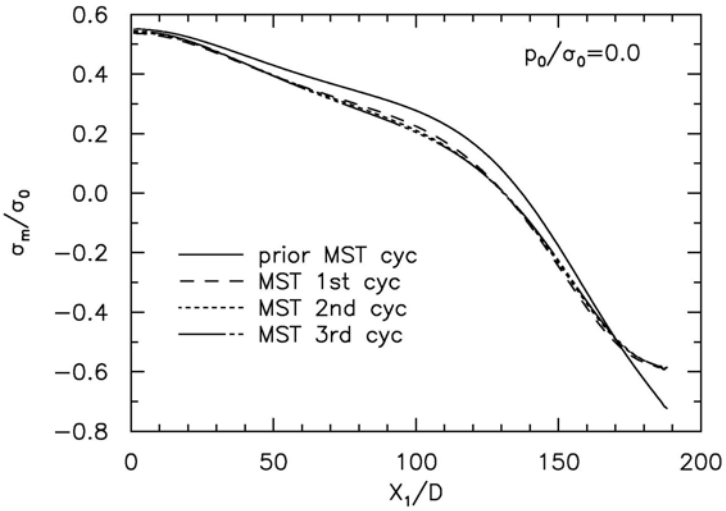

(b)

Figure 4.22 (a) Current void volume fraction f, and (b) mean stress σ_m/σ_0, along the die/die attach interface at each MST cycle for $p_0/\sigma_0 = 0.0$.

With the progress of MST cycles, the voids grow steadily across the die/die attach interface for $p_0/\sigma_0 = 1.0$ while the mean stress distribution decreases (Fig. 4.23). The peak being reached at the localized zone of intense void activity increases as it shifts away from the corner. However, at the end of each MST cycle, the amount of increase in void growth gets progressively lower. The void growth peak increases with a

difference of 0.03, from about 0.125 at the end of the MST 1st cycle to 0.155 at the end of the 2nd cycle, while the difference is about 0.25 from the 2nd cycle to the 3rd cycle.

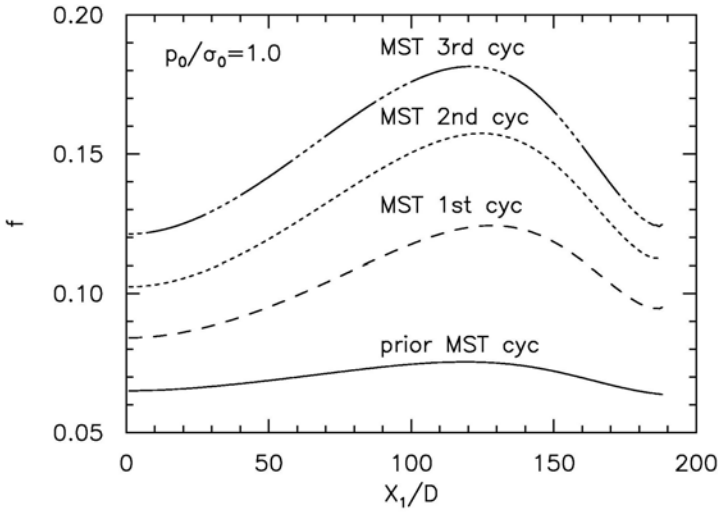

(a)

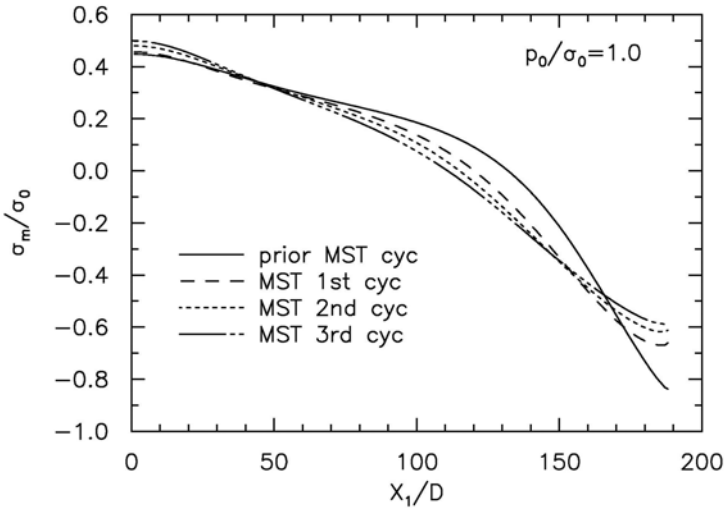

(b)

Figure 4.23 (a) Current void volume fraction f, and (b) mean stress σ_m/σ_0, along the die/die attach interface at each MST cycle for $p_0/\sigma_0 = 1.0$.

High initial void volume fraction and vapor pressure favors formation of a continuous damage zone for a ductile film sandwiched between two elastic substrates [Guo and Cheng, 2003]. The same phenomenon can be observed thus far from Fig. 4.21 and

Fig.4.23. With high initial vapor pressure, the continuous damage zone actually grows larger.

4.4.5 Behavior of Individual Element along the die/die attach interface

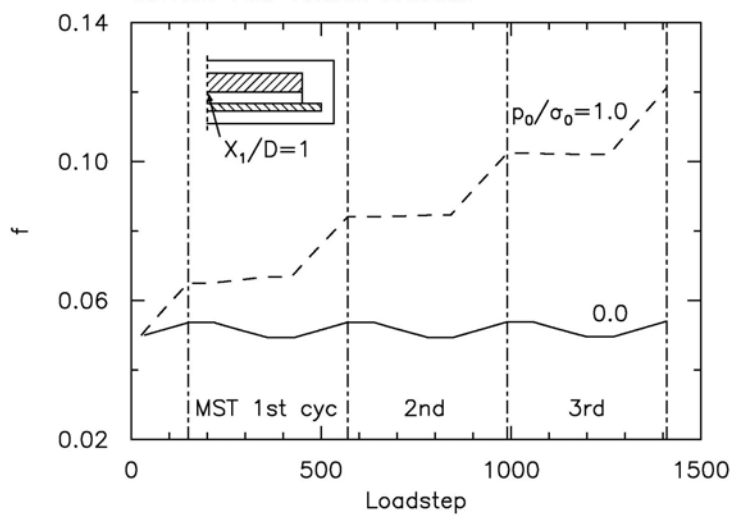

(a)

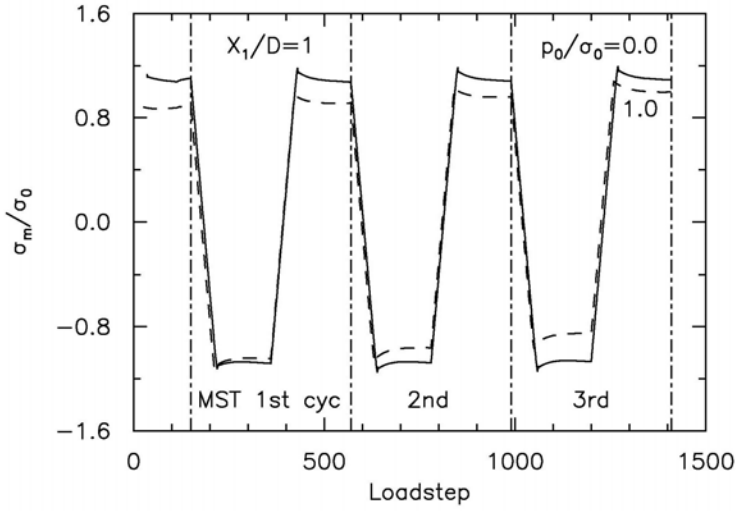

(b)

Figure 4.24 (a) Current void volume fraction f, and (b) mean stress σ_m/σ_0, at $X_1/D=1$, along the die/die attach interface for $p_0/\sigma_0 = 0.0, 1.0$.

Unlike the cell element at the package center along the die pad/molding compound interface, along the die/die attach interface, the cell element at $X_1/D=1$ undergoes

progressive void activity under the combined effects of thermal mismatch and vapor pressure (Fig. 4.24). At $p_0/\sigma_0 = 0.0$, with the progress of each load step, the void growth though remains close to 0.05, there are cycles of void expansion and contraction; at $p_0/\sigma_0 = 1.0$, there is a gradual rise in porosity with each load step. The mean stress trends for $p_0/\sigma_0 = 0.0$ and $p_0/\sigma_0 = 1.0$ are very similar and the mean stress peaks are where void growth occurs (Fig. 4.24b).

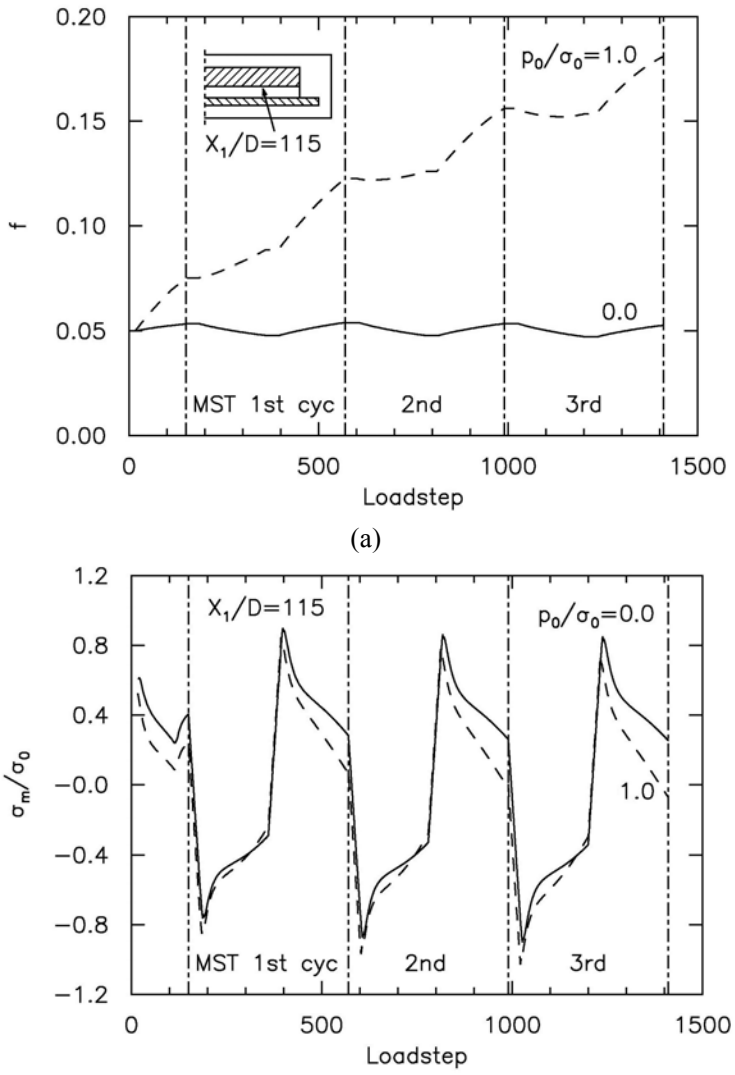

Figure 4.25 (a) Current void volume fraction f, and (b) mean stress σ_m/σ_0, at X_1/D=115, along the die/die attach interface for $p_0/\sigma_0 = 0.0, 1.0$.

The loading history of the cell element at X_1/D = 115, which experienced the highest void growth at various pressure levels is showed in Fig. 4.25. With vapor pressure, the rate of increase in void is significantly higher; there is no significant increase in void growth without vapor pressure. It is noted that for p_0/σ_0 = 0.0, at some stages of the MST cycles there is void contraction.

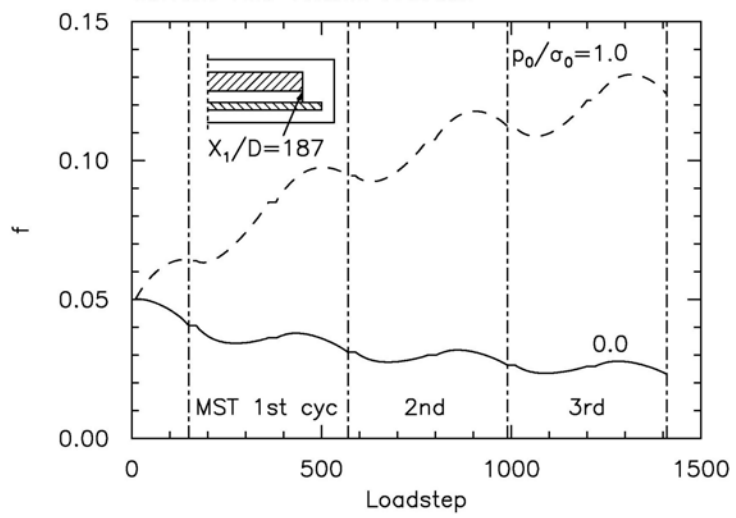

(a)

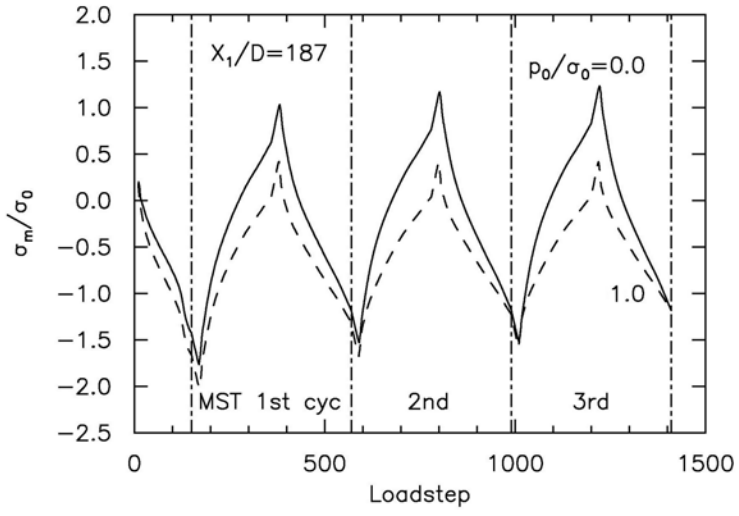

(b)

Figure 4.26 (a) Current void volume fraction f, and (b) mean stress σ_m/σ_0, at X_1/D=187, along the die/die attach interface for p_0/σ_0 = 0.0, 1.0.

For the cell element at X_1/D=187, without vapor pressure, it undergoes progressive void contraction (Fig. 4.26). At p_0/σ_0 = 1.0, there are periods where the element undergoes void contraction, despite the progressive rising trend in void activity. The loss in stress capacity is more apparent with the mean stress starting off much lower for p_0/σ_0 = 1.0 and widening the gap with p_0/σ_0 = 0.0 as the MST progresses. For the cell element at X_1/D=187, it experiences a more complicated thermal stress state than other cell elements away from the die corner. Other than thermal mismatch stress at the die/die attach interface, there is also contribution from the die attach/molding compound interface.

4.4.6 Crack initiation and propagation along the die/die attach interface

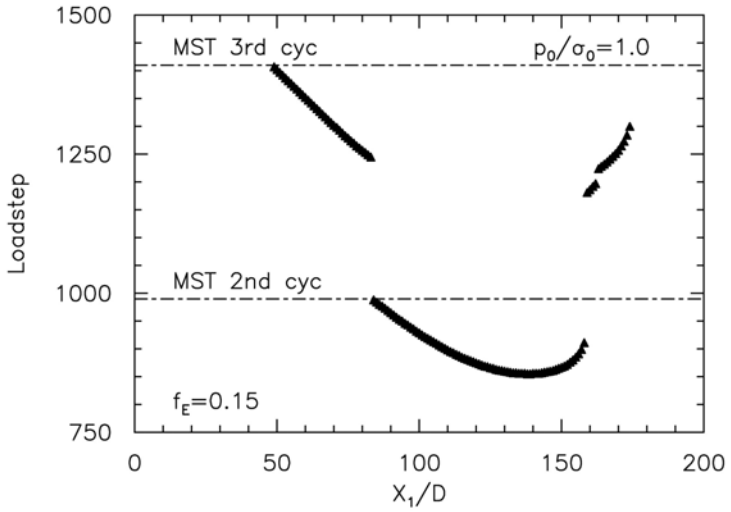

Figure 4.27 History of crack initiation and propagation along the die/die attach interface with f_0 =0.05, p_0/σ_0 = 1.0 and f_E = 0.15.

Figure 4.27 shows the history of crack initiation and propagation for p_0/σ_0 = 1.0 and f_E = 0.15 along the die/die attach interface. Crack initiates close to the interface corner (X_1/D = 156) at X_1/D = 138 near the end of the 2nd MST cycle (at step 855).

Subsequent crack propagation occurs in both directions towards the interface corner and center, resulting in a delaminated zone of 126 cell elements. Most of the cell elements failed to form new crack surface during the ramp-down of temperature at each MST cycle.

The deformed configuration of the die/die attach interface in the TQFP package with p_0/σ_0 = 1.0 and f_E =0.15 at the end of the MST loading is showed in Fig. 4.27. The 126 cell elements (equivalent to 2.52 mm) that had failed to form the delaminated zone along the interface are highlighted.

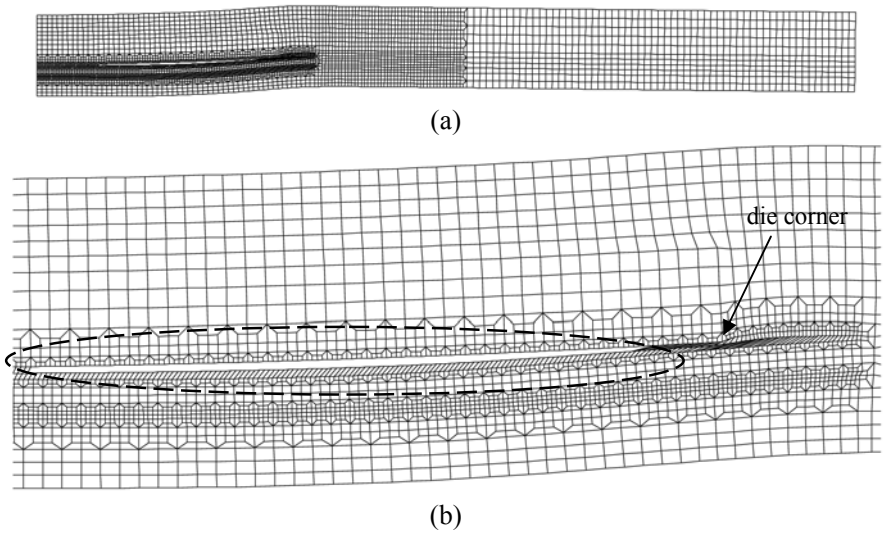

Figure 4.28 Deformed configuration of the TQFP package: (a) half the package, and (b) close up of the delamination site along the die/die attach interface.

4.4.7 Effects of die pad materials

In this section, a comparison is made between having a copper die pad and an alloy42 die pad in Fig. 4.29. The resulting effect on the die/die attach interface is quite different from the die pad/molding compound interface. For p_0/σ_0 = 0.0, the cell elements along

the interface with an alloy42 die pad is found to undergo greater void growth than a copper die pad. However, for $p_0/\sigma_0 = 1.0$, the reverse occurs where the interface with a copper die pad experiences more void growth. Having an alloy42 die pad also results in higher mean stress across the interface in general except at the die center and corner. Such behavior could be due to the alloy42 having a higher Young's modulus and a lower coefficient of thermal expansion. A similar observation was also made by Chew et al. (2004a) in that higher levels of film-substrate coefficient of thermal expansion mismatch result in faster interface cracking. From the works of Tay and Goh (1999), it was reflected that delamination of the die attach is more likely to occur with a copper pad than with an alloy42 pad, due to the greater difference between the coefficients of thermal expansion of copper and silicon. Cheng and Guo (2003) showed that stiffer substrates, i.e. higher Young's modulus for the die pad, offer larger shielding effects on the die attach. This also suggests that the failure of the constrained die attach is affected considerably by the substrates that it is sandwiched between.

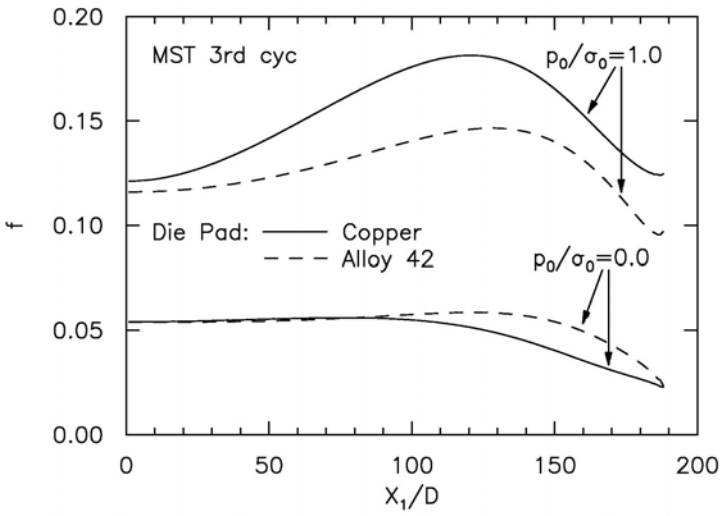

(a)

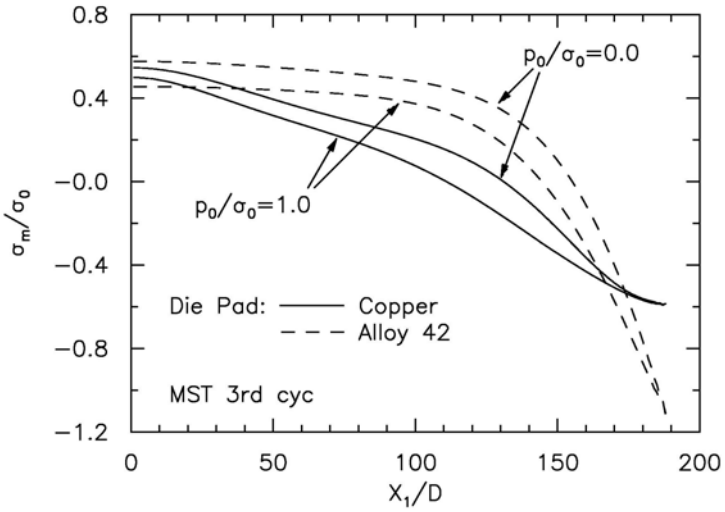

(b)

Figure 4.29 (a) Current void volume fraction *f*, and (b) mean stress σ_m/σ_0, along the die/die attach interface for copper and alloy42 die pad, with p_0/σ_0 = 0.0, 1.0.

4.5 Results and Discussions – Moisture Distribution Effects at Die/Die Attach Interface

4.5.1 Piecewise Constant Distribution

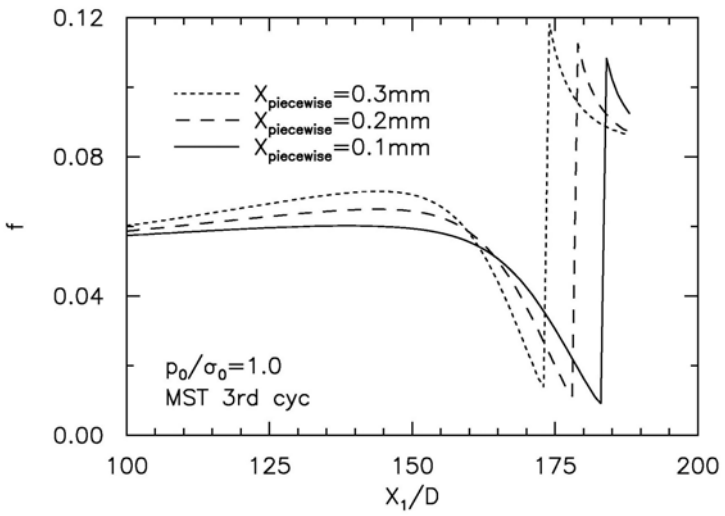

(a)

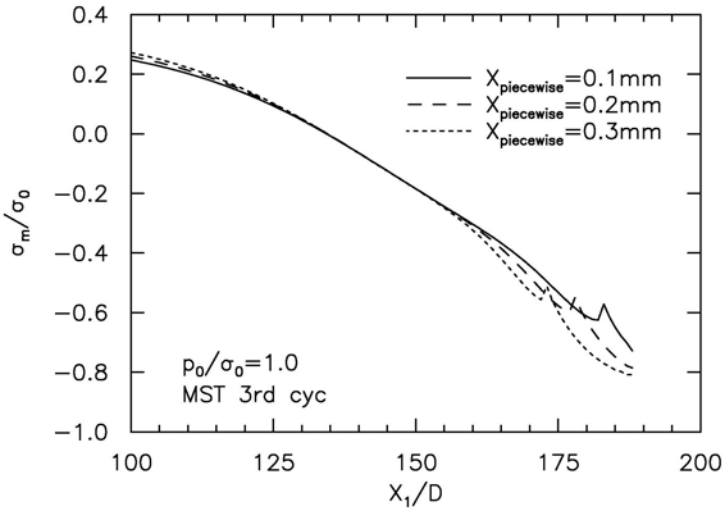

(b)

Figure 4.30 (a) Current void volume fraction *f*, and (b) mean stress σ_m/σ_0, along the die/die attach interface for p_0/σ_0 with $X_{piecewise}$ = 0.1 mm, 0.2 mm and 0.3 mm.

With 0.1 mm of uniform moisture penetration into the die attach at p_0/σ_0 = 1.0, the area of intense void activity is limited to near the interface corner (Fig. 4.30). It was, however, noticed that the peak (of void growth) do not congregate about the die attach corner. In fact, the void growth peak appeared at a distance slightly away. True enough, on subsequent simulations of various uniform moisture penetration ($X_{piecewise}$ = 0.02 and 0.03) the peaks of void growth for each level of moisture penetration occur further away from the interface corner. Also, it was found that each of the peak follows the behavior of the results obtained for full saturation along the die/die attach interface (Fig. 4.21a, p_0/σ_0 = 1.0).

4.5.2 Linear Distribution

For a linear distribution of moisture penetration, void growth occurs mainly at the interface corner (Fig. 4.31). With increase in X_{linear}, the whole interface is observed to

experience increased void growth. The peaks at the corner are observed to spread over a larger region with increased moisture penetration. The fluctuations in mean stress at the corner are observed to be much less than that in Fig. 4.30.

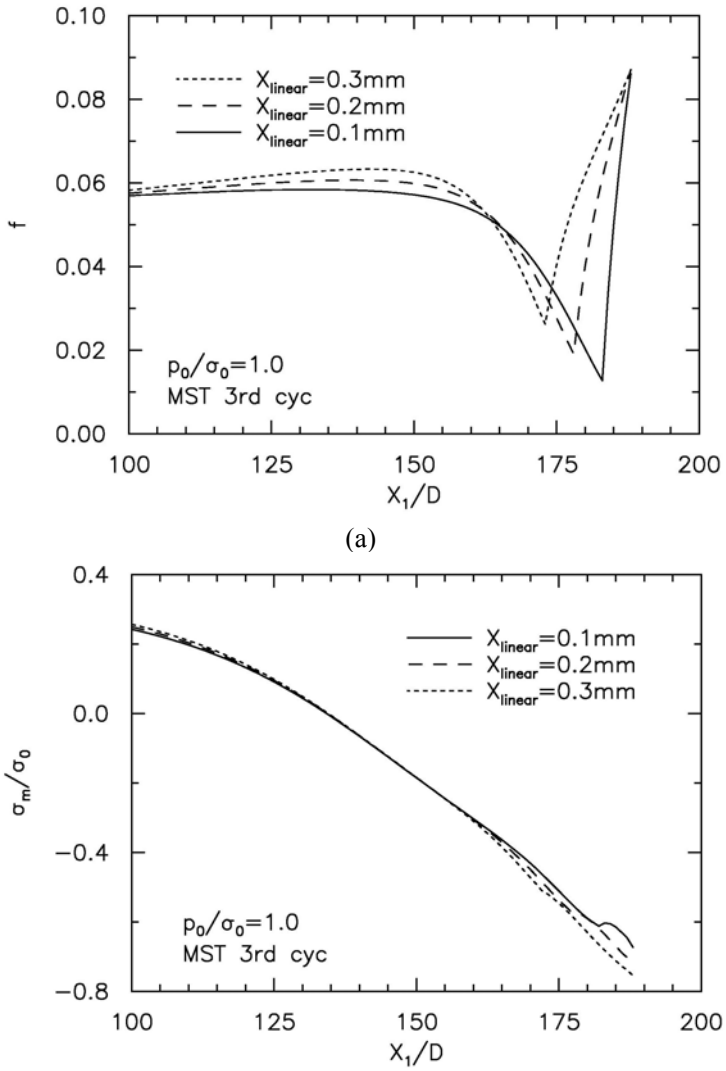

Figure 4.31 (a) Current void volume fraction f, and (b) mean stress σ_m/σ_0, along the die/die attach interface for p_0/σ_0 with X_{linear} = 0.1 mm, 0.2 mm and 0.3 mm.

4.5.3 Fick's Second Law Distribution

With increase in X_{fick}, there is an increase in void growth across the whole interface (Fig. 4.32). Though the void activity at the interface center is similar to Fig. 4.31, the void growth at the die attach corner is observed to increase smoothly and gradually. With the increase in moisture penetration distance, the mean stress carrying capacity at the corner is also observed to fall, due to the effects of vapor pressure.

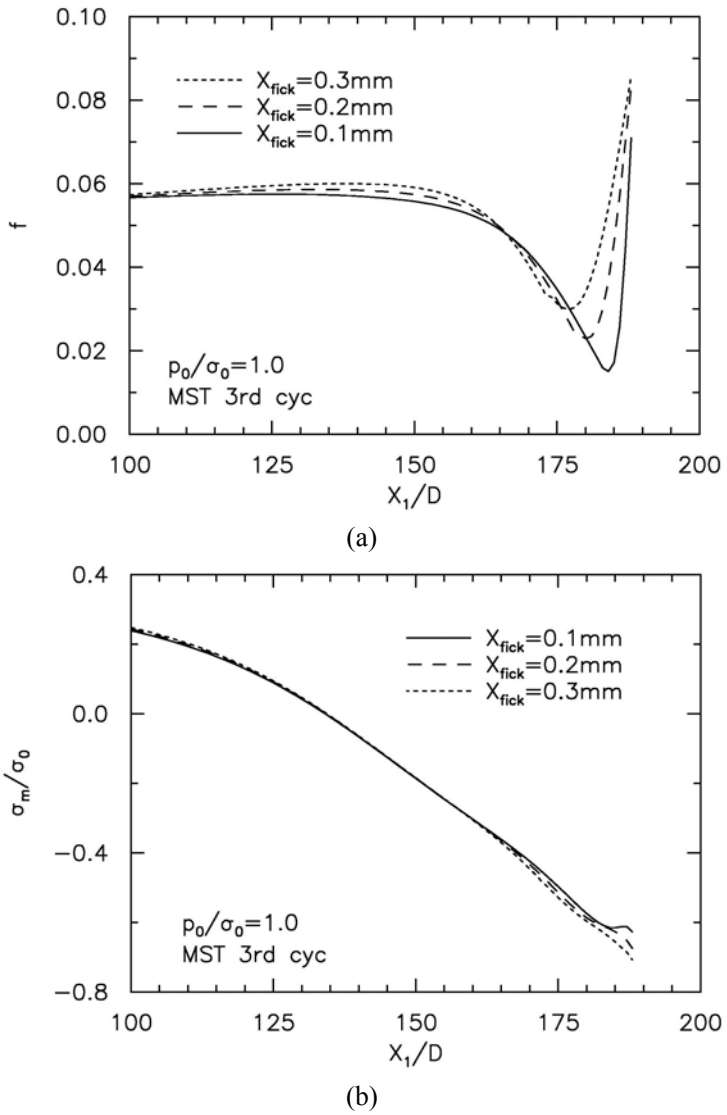

Figure 4.32 (a) Current void volume fraction f, and (b) mean stress σ_m/σ_0, along the die/die attach interface for p_0/σ_0 with X_{fick} = 0.1 mm, 0.2 mm and 0.3 mm.

With the limited moisture penetration into the die attach, it is still possible to cause the interface corner to experience substantial void growth. Therefore, the moisture absorption characteristics of die attach needs to be carefully considered in assessing the mechanical reliability of TQFPs.

4.6 Chapter Conclusion

A micromechanics model is devised to investigate vapor pressure assisted interface delamination in thin quad flat packs. In this study, the interfaces are modeled by rows of voided cell elements governed by the modified Gurson flow potential. The interfaces under analysis were the die pad/molding compound interface and the die/die attach interface. In general, increased vapor pressure levels are detrimental to the interfaces as it brings about an overall increase in void growth and loss in stress carrying capacity across the interfaces.

The analysis at the die pad/molding compound interface shows that the region close to the die pad corner to be highly possible delamination sites, due to intense void growth brought about by increased vapor pressure levels, which is in line with experimental observations. Crack initiation occurs at close to the interface corner and propagates in both directions towards the interface center and corner. By changing the die pad material properties from copper to alloy42, the void growth behavior is affected where the corners experience greater damage with the passing of each MST cycle.

High initial porosity and vapor pressure favor formation of a continuous damage zone along the die/die attach interface. The zone of intense void growth appears to be close to the interface corner, but the region of void growth appears to be more wide spread than the die pad/molding compound interface. Similarly, crack initiates near to the die/die attach interface corner and propagates in both directions towards the interface center and corner. With an alloy42 die pad, a different observation is made where the die/die attach interface experiences less void growth, suggesting that the failure of the constrained die attach is affected considerably by the substrates that it is sandwiched between. Using copper as the die pad material will increase the possibility to Type II popcorn failure (from the die/die attach interface), while alloy42 promotes Type I popcorn failure (from the bottom of die pad/molding compound interface). Hence, in terms of mechanical performance, there is a trade off between the two die pad materials.

The work hitherto assumes that the interfaces of interest in TQFPs are of uniform moisture concentration and so uniform vapor pressure. Although the assumption holds true for die pad/molding compound interface since the molding compound is saturated with moisture, for interfaces involving die attach, the same assumption may not hold. In the works of Liu et al. (2002), it was found that most of the die attach is not saturated with moisture, leaving only the die attach corner filled with moisture. This is likely since the die attach is a very thin layer trapped between the die and die pad which are both moisture impermeable, leaving the only path of moisture diffusion at the die attach corner. As such, a study is made involving modeling the die/die attach interface with non uniform vapor pressure levels. It was found that with the limited moisture

penetration into the die attach, it is still possible to cause the interface corner to experience substantial void growth.

Chapter 5

Thermo-mechanical analysis of Plastic Ball Grid Arrays with vapor pressure effects

5.1 Introduction

Over the years, numerous researchers have done in depth study of interface delamination and popcorn failure in IC packages. Kitano et al. (1988), Gallo and Munamarty (1995), Liu and Mei (1995) have provided a clear illustration of the moisture induced delamination of the interface between the die pad and epoxy molding compound interface for plastic encapsulated IC packages under reflow conditions. In recent years, Alpern et al. (2002a, 2002b) has developed a simple model to predict the failure of plastic encapsulated IC packages from various popcorn failure modes, using package stability parameters derived from a totally delaminated package. Lau and Lee (2000), using fracture mechanics, performed a temperature dependent popcorn failure analysis of plastic ball grid array package (PBGA). All these works postulate a pre-existing delamination prior to reflow soldering where vapor pressure was treated as an external traction on the crack surface. Such approaches do provide solutions in preventing the propagation of delamination and package cracking during reflow, but do not indicate clearly the position of delamination onset and provide a less detailed fracture process.

Liu et al. (2003), on the other hand, introduced a cohesive surface, described by traction-separation law [Tvergaard and Hutchinson, 1992; Tvergaard and Hutchinson,

1994], as a potential plane for crack growth along interfaces to predict the initiation of delamination and subsequent growth to a macroscopic crack in IC packages; effects of moisture were investigated through the introduction of micro-defects at the interface. Huang et al. (1996) identified thermal-stress induced voiding in electronics packages as a dominant failure mechanism and proposed a micromechanics model to investigate this mechanism. Cheng and Guo (2003), instigated by such an approach, incorporated vapor pressure as an internal variable into the interface cracking of a polymeric film bonded between two silicon substrates. A model problem of a ductile film bonded between two elastic substrates, with a centerline crack is also studied [Guo and Cheng, 2003]. Their studies show that polymeric films can fail by one of several mechanisms: near-tip void growth and coalescence with the crack; void growth within a single extending damage zone joined to the crack; and void growth at highly stressed sites at large distances ahead of the main crack, resulting in the formation of multiple damaged zones.

The above studies affirm vapor pressure assisted void growth and coalescence as a key mechanism of popcorn failure. A mechanism-based approach - the cell element model by Xia and Shih (1995) constitutes the methodology adapted in this work to provide an in-depth mechanical analysis of the effects of vapor pressure and thermal mismatch stress on popcorn failure in a PBGA package. The model, without assuming any pre-existing crack, is adapted to model void damage and crack initiation, a precursor to interface delamination and popcorn failure, at the die/die attach interface. The model is also extended to consider the effects of Pb-free reflow soldering. Interface damage analysis of the die/die attach interface using temperature dependent material properties

is subsequently discussed. Finally, a full field analysis is performed by implementing the Gurson constitutive law throughout the polymeric overmold, to predict the likely popcorn failure mode from identifying the severely damaged regions within the package.

5.2 Problem Formulation

5.2.1 Material Model

Figure 5.1 presents a 68 I/O Plastic Ball Grid Array (PBGA) package used as the finite element model [Galloway and Miles, 1997]. With the demand of smaller components and high-density mounting for electronic products, there is a rise in the applications of Ball Grid Arrays (BGA). The PBGA package, however, consists of organic substrate materials, such as polyimide, glass epoxy, or bismaleimide-triazine (BT) resin, resulting in relatively higher moisture absorption rates and susceptibility to popcorn cracking.

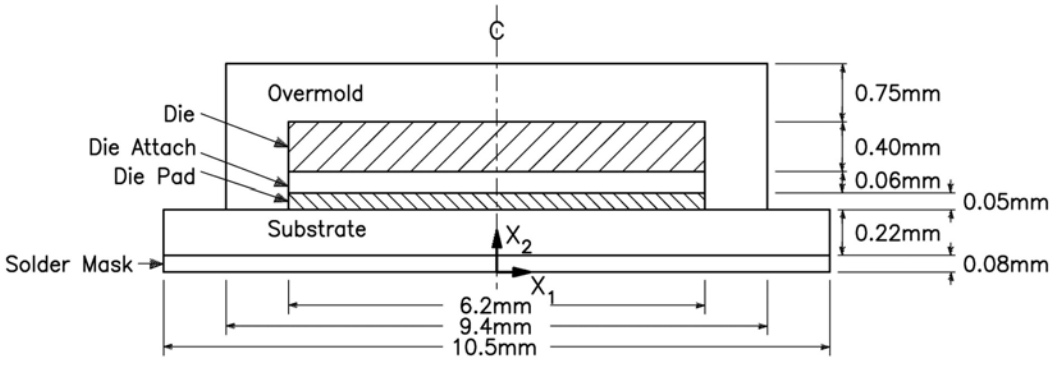

Figure 5.1 68 I/O PBGA package [Galloway and Miles, 1997].

The die and die pad are assumed to be temperature independent elastic isotropic materials. On the other hand, during reflow conditions, the overmold, substrate, solder mask and die attach exhibit extensive ductility and their yield strengths decrease considerably. As such, they are taken as elastic-plastic materials with power-law hardening. The tensile behavior are generalized to multiaxial stress states assuming isotropic hardening and characterized by the J_2 flow theory. The true stress-logarithmic strain relation in uniaxial tension is specified by:

$$\varepsilon = \begin{cases} \dfrac{\sigma}{E}, & \sigma < \sigma_0 \\ \dfrac{\sigma_0}{E}\left(\dfrac{\sigma}{\sigma_0}\right)^{1/N}, & \sigma \geq \sigma_0 \end{cases} \tag{5.1}$$

where σ_0 signifies the initial tensile yield stress, N the strain hardening exponent and E the elastic modulus, which is assumed to be temperature dependent in certain cases of analysis.

The overmold, die attach and BT substrate are the main components that contribute to moisture absorption in the PBGA [Yip, 1996]. In particular, moisture concentrates predominantly and is most damaging in the overmold and the die attach [Lam, 2000]. In the moisture analysis of PBGA packages, Galloway and Miles (1997) indicated that at equilibrium for the 23°C/70% relative humidity conditions, the saturated concentrations of moisture in BT epoxy and die-attach are 0.0066 g/cm^3 and 0.017g/cm^3 respectively. These condensed moisture levels signify that the overmold and the die attach are highly porous. By available moisture analyses [Fan, 2000], the estimated initial void volume fractions of typical polymeric materials used in IC packages range from 1% to 5%. Studies have shown that after moisture exposure and

reflow, severe delamination initiates and occurs in the die attach area [Lau and Lee, 2000; Galloway and Miles, 1997; Lau et al., 1998].

In this section, the yield stress σ_0, elastic modulus E and coefficient of thermal expansion α, of the die attach and the overmold are assumed to be temperature independent, and assumes the values at reflow conditions (T = 235°C), as obtainable from Table 1 (indicated by *). Currently, the exact yield stress at each thermal state is not available to the author's knowledge. For typical polymeric materials, the values of σ_0/E range from 0.01 to 0.04 [Cheng and Guo, 2003]. As such, an estimate is made at σ_0/E=0.01 throughout, assuming loss of proportionality, and is showed in Table 5.1. The material properties of other components are stated in Table 5.1 as well. By applying the vapor pressure incorporated cell element model [Xia and Shih, 1995; Cheng and Guo, 2003], the damaging effects of thermal mismatch and vapor pressure in the die attach, during MST loading, are presented hereafter, and followed by a consideration of the effects of Pb-free reflow soldering and a full field analysis of the overmold.

Table 5.1 Material properties of PBGA components.

Material Property	E (MPa)	σ_0(MPa)	ν	α ($\times 10^{-6}$/°C)
BT Substrate	26000	260.0	0.39	15.0
Silicon Die	131000	-	0.30	2.8
Overmold	9500	95.0	0.25	16.3 (53°C)
	4000	40.0		38.0 (25°C)
	1000	10.0		60.0 (175°C)
	200 *	2.0 *		69.3 * (235°C)
Die Attach	2200	22.0	0.30	59.0 (25°C)
	800	8.0		59.0 (53°C)
	250	2.5		195.0 (175°C)
	200 *	2.0 *		195.0 * (235°C)
Solder Mask	6870	68.7	0.35	19.0
Copper Die Flag	76000	-	0.34	17.0

*material properties used for temperature independent analysis

5.2.2 Cell Model application with coalescence effect at Die Attach

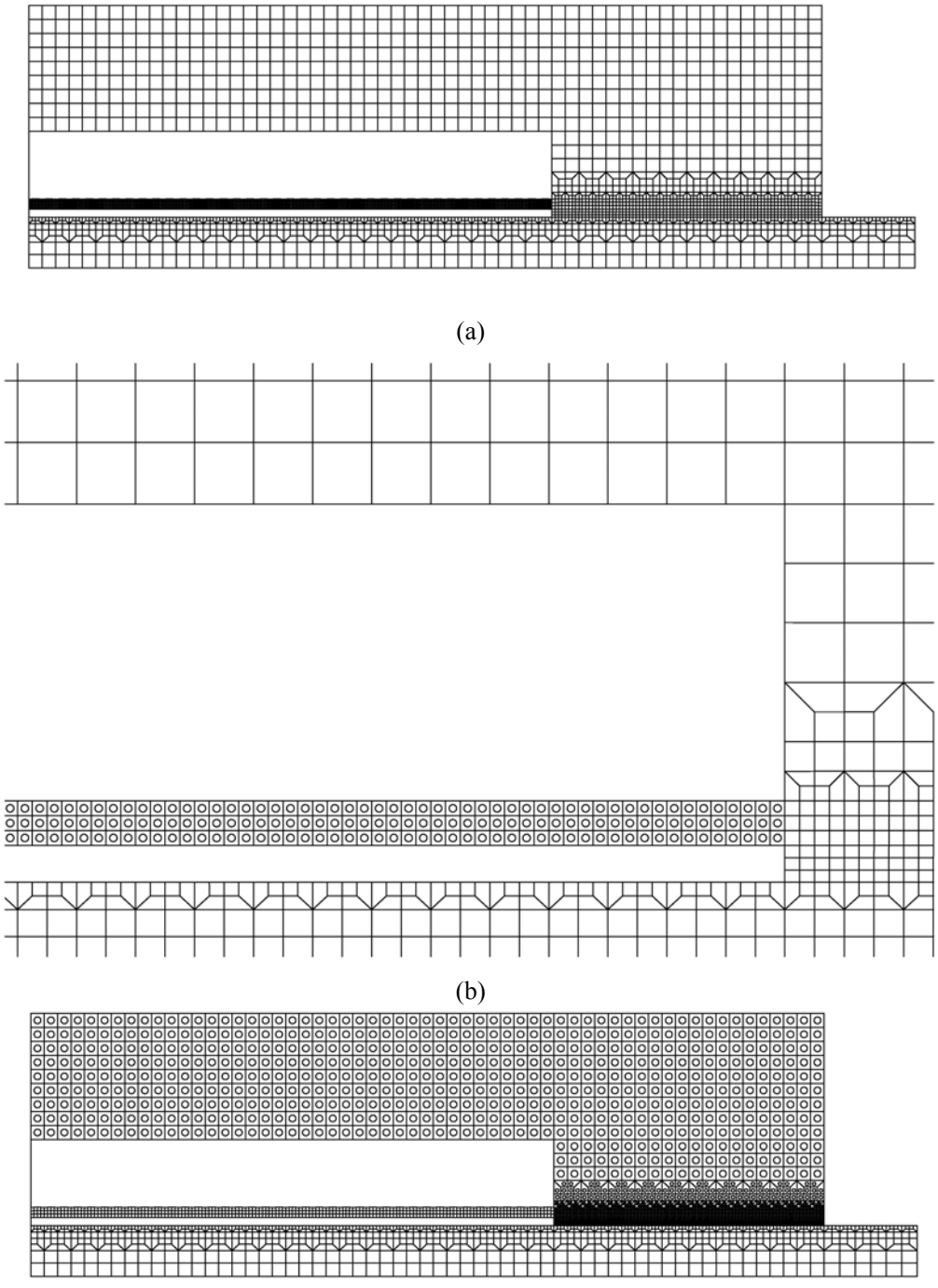

(a)

(b)

(c)

Figure 5.2 Finite element mesh [Cheong et al., 2004]:
(a) Half of PBGA package is modeled ($X_1 \geq 0$);
(b) Close-up of voided cell elements in the die attach;
(c) Full field analysis on overmold.

Figure 5.2 shows the finite element mesh of the PBGA used, consisting of a total of 3618 three dimensional, 8-noded linear elements and 7440 nodes. By symmetry, only half of the model is analyzed. Plane strain conditions are achieved by imposing zero out-of-plane displacements on all the nodes. The computations are implemented via a three-dimensional finite element method (FEM) program, WARP3D [Gullerud et al., 2000].

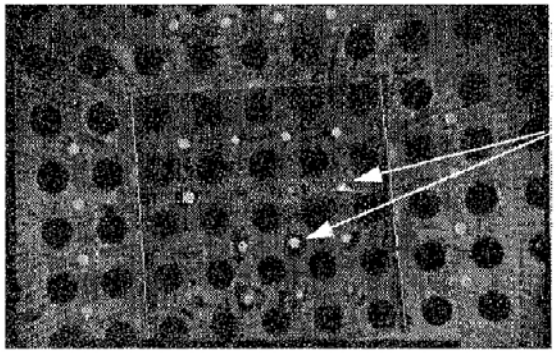

Figure 5.3 X-ray micrograph of die attach voids in PBGA package [Tan et al., 1996].

The vapor pressure incorporated cell element model [Xia and Shih, 1995; Cheng and Guo, 2003] is applied to study delamination at the interfaces under the combined loading of thermal mismatch and vapor pressure. The die attach contains voids that absorb moisture and cause high stress concentrations in the material around the voids (Fig. 5.3). Hence, the die attach is modeled by three rows of 156 uniformly sized cell elements. Each cell element, of the size $D \times D$ (D = 0.02 mm), contains a void of initial volume fraction f_0 associated with initial vapor pressure p_0 (Fig. 5.2b). Progressive void growth and subsequent macroscopic material softening in each cell are described by the modified Gurson flow potential with coalescence effect discussed in Chapter 3, Section 3.4. This computational model is referred to as the fully porous adhesive (FPA) model [Chew et al., 2004b].

5.2.3 Full Field Analysis of Overmold

A full field analysis [Cheong et al., 2004] involves evaluating the PBGA package when the whole overmold is modeled by void-containing cell elements governed by the Gurson flow potential (Chapter 3, section 3.4), as shown in Fig. 5.2c. The analysis will reveal the critical regions that undergo severe damage in the event of combined thermal mismatch and vapor pressure effects during the MST loading, indicating the likely paths of cracking during popcorn failure. The material properties of the components assume the values of the corresponding analysis of the die attach in section 5.2.2.

5.2.4 Moisture Sensitivity Tests and Numerical Procedure

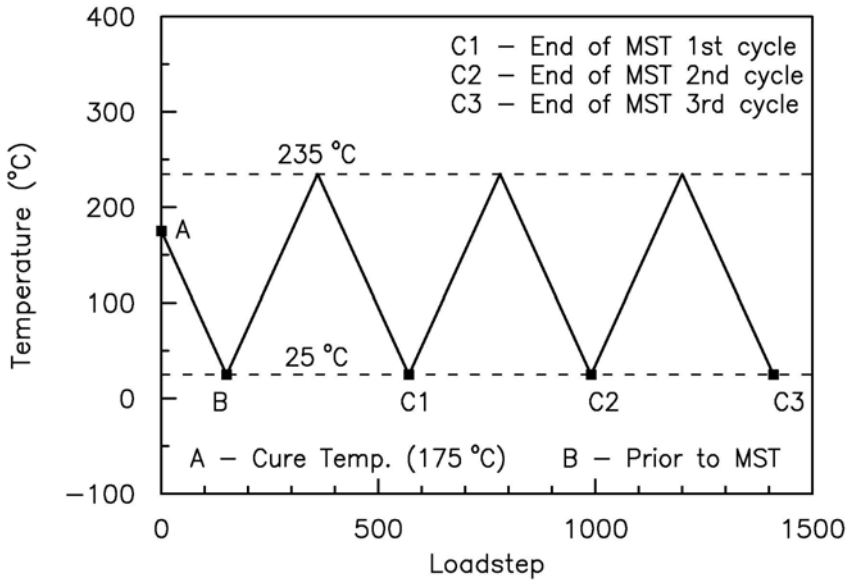

Figure 5.4 Thermal Loading Profile of moisture sensitivity test (MST) with reflow temperature at 235 ^{o}C.

The finite element model is subjected to a loading profile analogous to Moisture Sensitivity Test (MST), shown in Fig. 5.4, according to the Joint IPC/JEDEC Standard J-STD-020A (1999). In the physical test itself, the package is cured at 175 ^{o}C (point A,

Fig. 5.4), T_0, where it is assumed to be at a stress free state [Tay and Lin, 1996a]. After the package is cooled down to room temperature (point B) from the curing temperature, according to the standards, it undergoes 3 cycles (points C1, C2, C3) of heating up, after moisture preconditioning, to the reflow temperature at 235 ^{o}C and back to room temperature of 25 ^{o}C.

Due to the lack of test data for polymeric materials, it is difficult to apply a viscoelastic model to represent the stress relaxation behavior during the sudden change in temperatures. As such, the loading procedure is assumed to be quasistatic at 1 ^{o}C per loadstep. With rapid thermal diffusion, it is assumed the moisture distribution in the package is unchanged and the change in temperature is uniform throughout. With MST loading, the background stress is for the most part of thermal origin and is also, cyclic in nature. The thermal mismatch in thermal expansion coefficients induces a strong mode II loading component on the interfaces of the packages, especially the silicon-polymer interfaces. Void growth and coalescence can occur under high vapor pressures superposed on the background stress.

5.3 Results and Discussion – Die Attach Analysis

The results discussed in this chapter are primarily grouped into two main sections: (i) Die Attach Analysis and (ii) Overmold Full Field Analysis. Studies in the Die Attach Analysis focus on interfacial debonding via void growth in the die attach. The critical interface in the die attach is first being identified, with subsequent analyses in the section being directed on the critical interface.

5.3.1 Identification of critical layer in die attach

Recent moisture reliability assessments of PBGAs by Lau et al. (2000) have indicated that cracks are likely to initiate from the die attach near the die corner. In this section, the layer in the die attach that undergoes the most damage due to thermal mismatch stress and vapor pressure assisted void growth and coalescence during MST loading is identified by modeling the die attach with three rows (top, middle and bottom) of 156 uniformly sized cell elements (Fig. 5.2b).

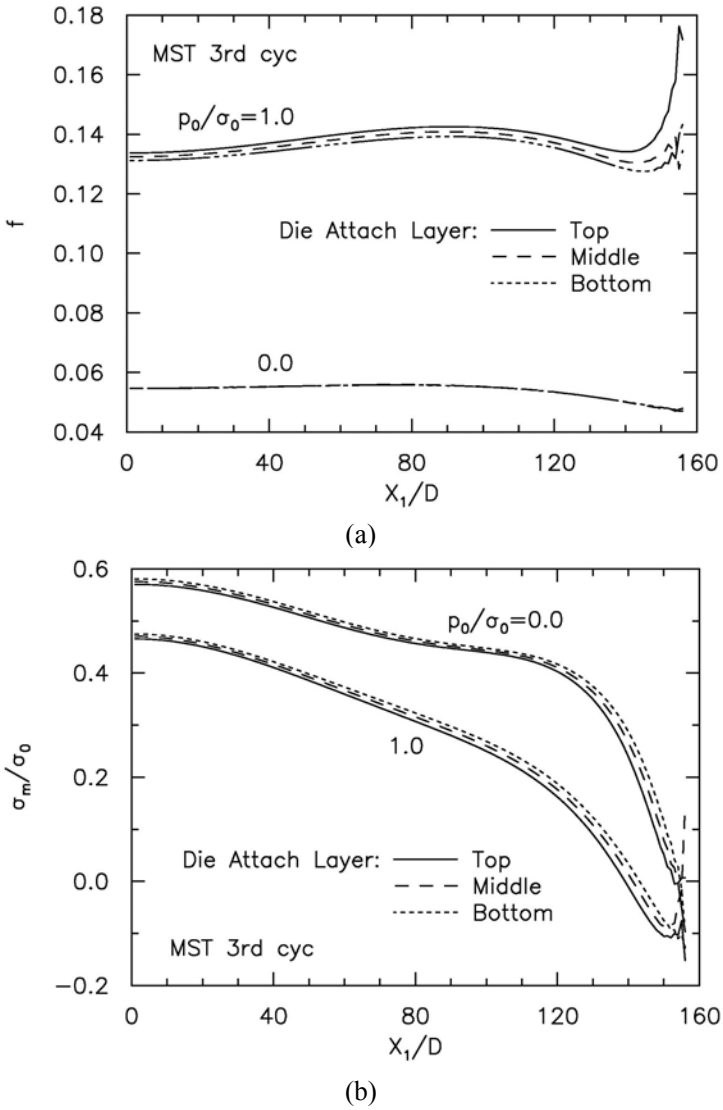

Figure 5.5 (a) Current void volume fraction f, and (b) mean stress σ_m/σ_0, along the top, middle and bottom layer in the die attach at the end of MST.

Void growth and stress distribution along each layer in the die attach are shown in Fig 5.5. With zero initial vapor pressure, the void growth and stress distribution along each layer are similar with minimal differences. However, with $p_0/\sigma_0 = 1.0$, the top die attach layer is observed to have the highest void activity at the corner, making it the most critical layer susceptible to thermal mismatch and moisture induced damage. Another observation is that judging from the void growth in the middle and bottom die attach layers, a possible failure mechanisms is that the initiation of delamination will happen at the corner of the die attach and occur across all three layers. Subsequent delamination will continue into the top layer due to the higher overall porosity. Nevertheless, to simplify the analysis, the presentation will be concentrated on the die/die attach interface hereafter.

5.3.2 Effects of Strain Hardening Exponent, *N*

During the reflow process, temperature of the entire package is raised rapidly to 220^{o}C or higher [Gallo and Munamarty, 1995], falling well within the range of glass-transition temperature, T_g, of typical IC polymeric materials ($150^{o}C < T_g < 300^{o}C$). At such thermal states, the overmold and die attach undergo a tenfold decrease in yield strengths as compared to room-temperature values and exhibit extensive ductility associated with strain hardening.

Figure 5.6 compares current porosity and mean stress distribution for different material hardening, with $N = 0$ representing an ideally plastic solid, $N = 0.05$ a low hardening material and $N = 0.1$ a moderate hardening material. It can be seen that lowering the

hardening exponent induces higher void growth and reduces the mean stress, and so, represents a weaker material. As mentioned earlier, at reflow temperatures, the polymeric materials are to exhibit extensive ductility, and N = 0 to N = 0.05 would be a more suitable representation of the IC package materials. Thus, $N = 0$ will be employed for the analyses that follow.

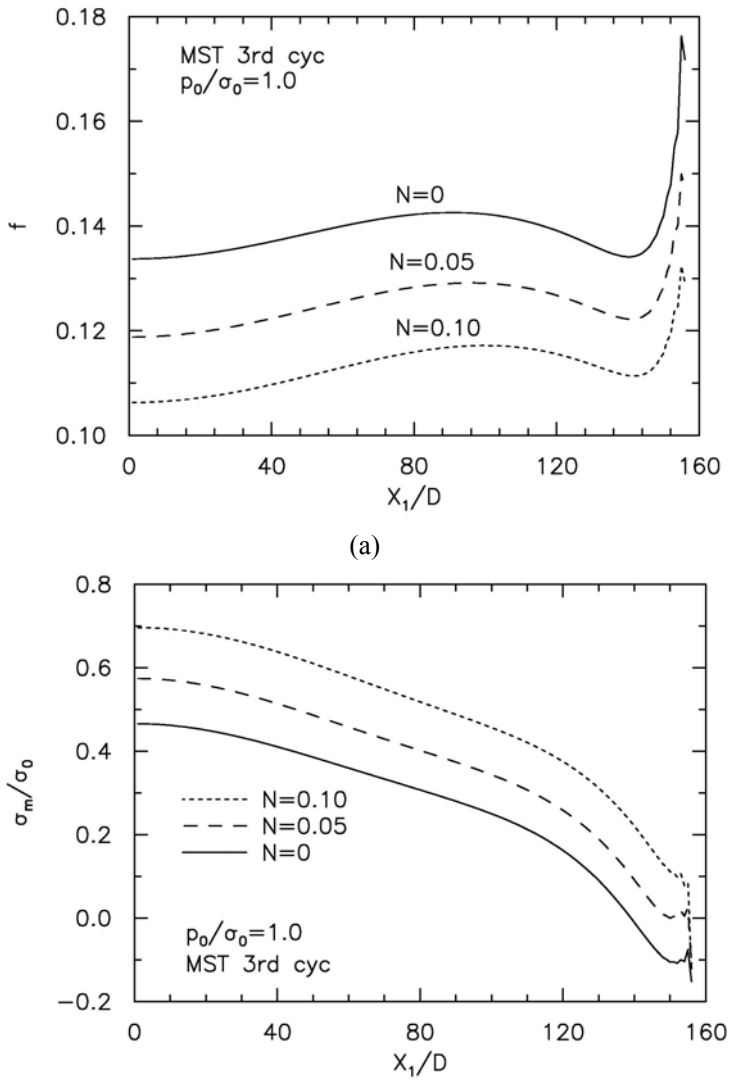

Figure 5.6 (a) Current void volume fraction f, and (b) mean stress σ_m/σ_0, along the die/die attach interface at the end of MST for $N = 0$, 0.05 and 0.10.

5.3.3 Effects of Initial Void Volume Fraction, f_0

As stated previously, typical polymeric materials used in IC packages are highly porous, with the estimated initial void volume fractions ranging from 1% to 5%. Consequently, the present analysis is based on $f_0 = 0.01$ and $f_0 = 0.05$.

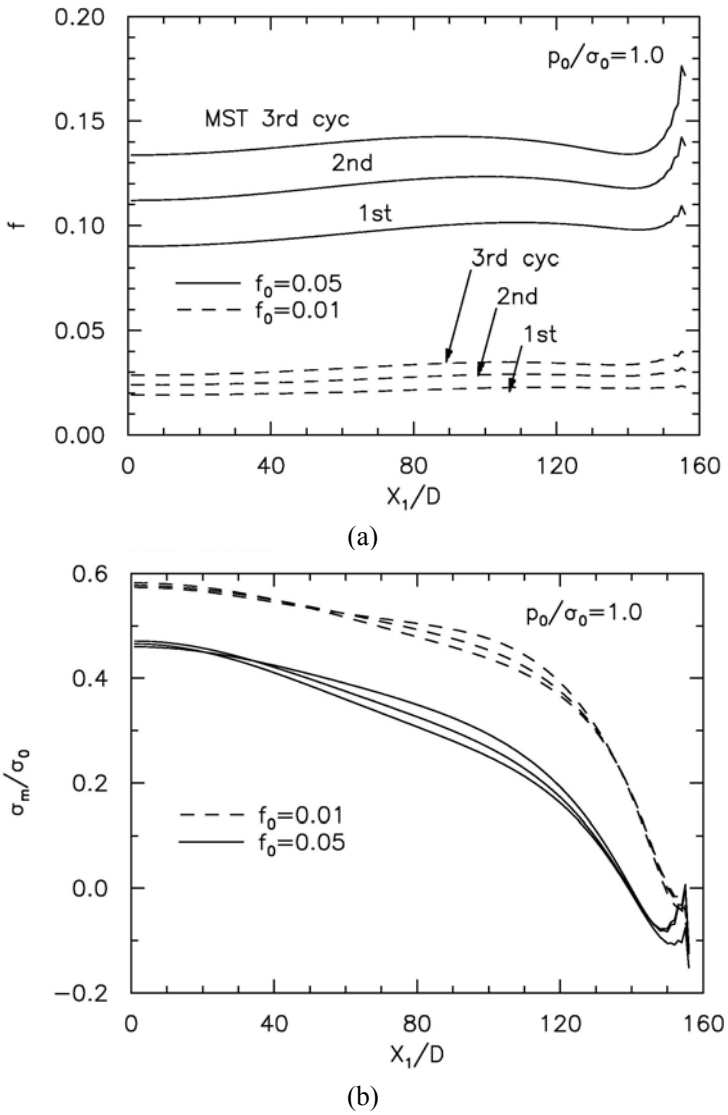

Figure 5.7 (a) Current void volume fraction f, and (b) mean stress σ_m/σ_0, along the die/die attach interface at the end of MST for $f_0 = 0.01$ and 0.05.

For $p_0/\sigma_0 = 1.0$, higher f_0 decreases the mean stress carry capacity across the interface and results in much higher void growth (Fig. 5.7). At $f_0 = 0.05$, the void growth at the

progress of each MST cycle is significantly larger. For the subsequent sections on die/die attach interface analysis, the initial void volume fraction is assumed to be 0.05.

5.3.4 Effects of Initial Vapor Pressure, p_0/σ_0

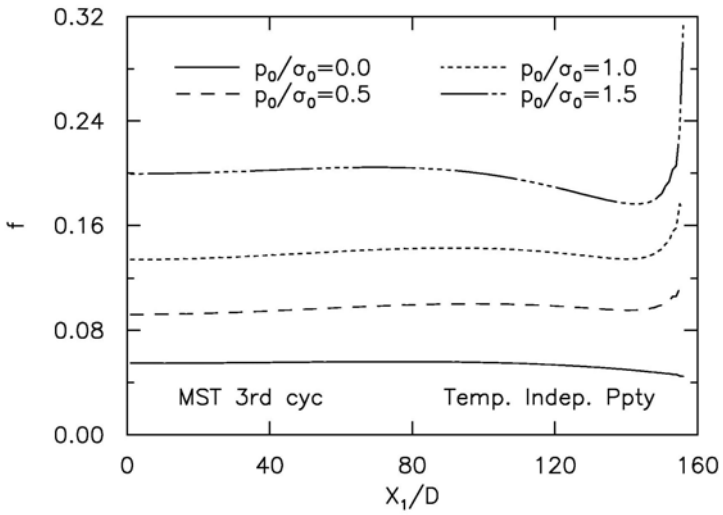

(a)

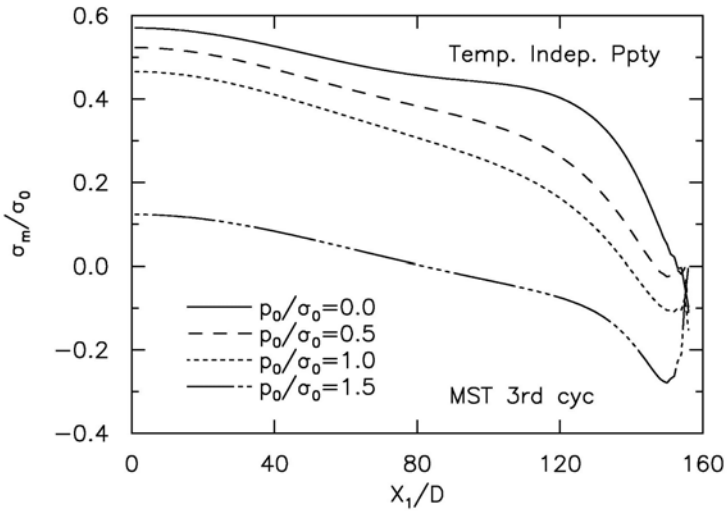

(b)

Figure 5.8 (a) Current void volume fraction f, and (b) mean stress σ_m/σ_0, along the die/die attach interface at the end of MST at various levels of p_0/σ_0.

The vapor pressure exerted by the moisture within the package can reach levels of 3 to 6 MPa [Liu and Mei, 1995]. Combined with the thermal mismatch generated, it is

sufficient to drive the processes of unstable void growth and void rupture and, ultimately, package failure [Guo and Cheng, 2002]. The effects of initial vapor pressure are isolated in this section. Figure 5.8a shows how void growth is affected by the presence of vapor pressure at the interface. High initial vapor pressure, p_0/σ_0 = 1.5, induces voids to grow rapidly with f reaching above 0.16 across the whole interface. In addition, with the intensified initial vapor pressure, voids near the interface corner can grow by as much as 60% more than the rest of the interface. At p_0/σ_0 = 1.5, where void activity levels in general exceeds 0.15, the further loss of material stress carrying capacity sets in as stated in (3.7) when $f > f_C$ and void growth is observed to progress at a much faster rate.

A localized zone of intense void activity forms at the die/die attach interface corner creating the possible delamination sites, in line with the experimental observations stated previously. Another observation by Lau et al. (2000) is that though the above is entirely possible, in reality, the initiation of the crack is difficult to determine. Nevertheless, as vapor pressure levels increased, the intense void activity zone further enlarge while shifting away from the corner and progressing towards the die attach center – highlighting the possible formation of larger and multiple competing interface delamination sites.

Figure 5.8b presents mean stress plots that are normalized versus the yield stress of die attach, σ_0 = 2 MPa. The fall in mean stress carrying capacity reflects the extensive damage across the interface with the rise in initial vapor pressure. The mean stress declines toward the interface corner and more so with increased vapor pressure.

Similarly, at $p_0/\sigma_0 = 1.5$, as void activity levels exceed 0.15, the means stress carrying capacity across the interface drops drastically by more than $0.4\sigma_0$. At the interface corner, when all stress carrying capacity is lost (goes to zero), the material further softens and void level grows beyond 0.25 ($f = f_F$), crack initiation occurs.

5.3.5 MST cycle effect

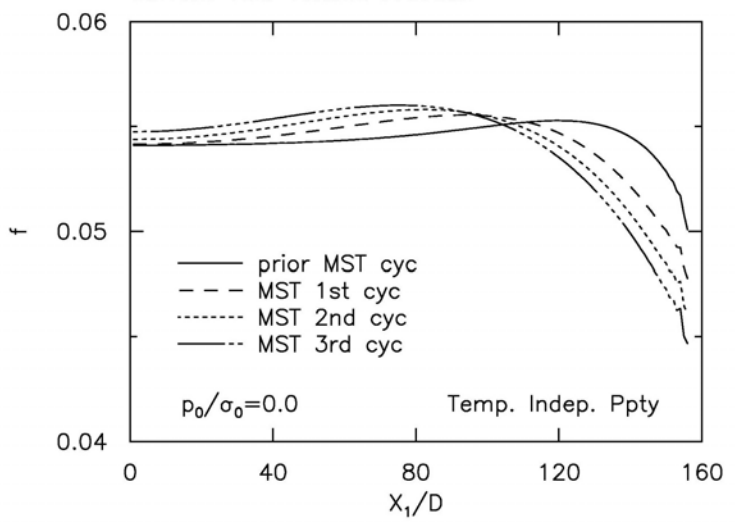

(a)

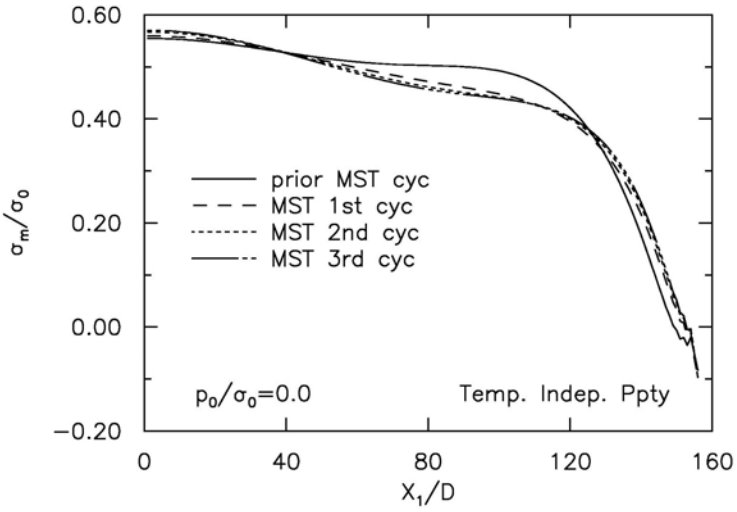

(b)

Figure 5.9 (a) Current void volume fraction f, and (b) mean stress σ_m/σ_0, along the die/die attach interface at the end of each MST cycle with $p_0/\sigma_0 = 0.0$.

At the end of each MST cycle, the behavior of the die/die attach interface is investigated. For p_0/σ_0 = 0.0, at the end of each MST cycle, the voids are noticed to contract near the die pad corner (Fig. 5.9a). Though very limited void activity takes place, the stress carrying capacity pretty much showed the same trend as void activity is minimal (Fig. 5.9b).

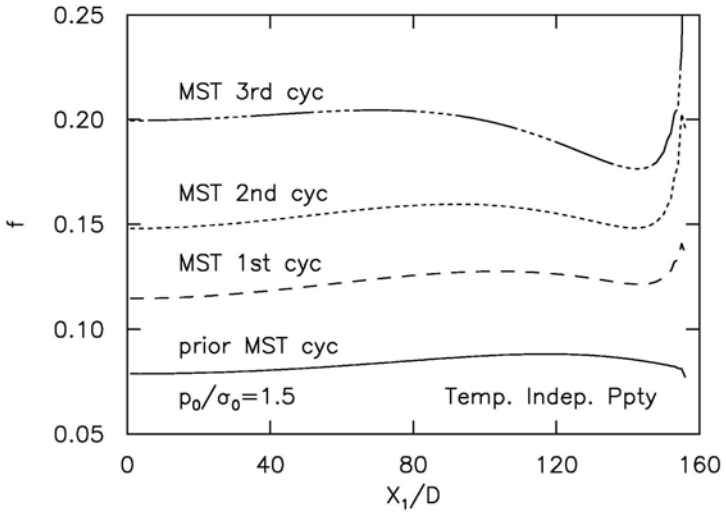

(a)

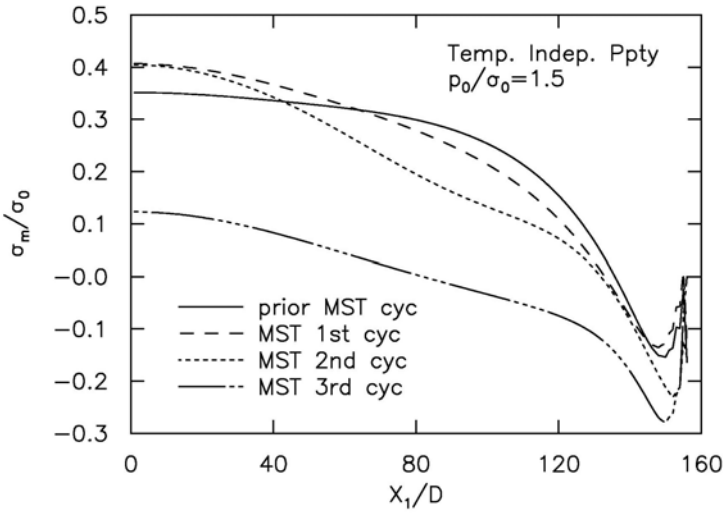

(b)

Figure 5.10 (a) Current void volume fraction f, and (b) mean stress σ_m/σ_0, along the die/die attach interface at the end of each MST cycle with p_0/σ_0 = 1.5.

From Fig. 5.10, at the end of each MST cycle, the peaks being reach by void growth at the corner of the interface are noticed to be more and more intense. The peaks (of void growth) not only congregate about the interface corner, but in fact form smoother secondary peaks at distances slightly away. This enables two possible competing damage zones of crack initiation along the interface and clearly accounts for the fast and complete delamination of the whole die/die attach interface during the short time span of reflow soldering.

5.3.6 Behavior of Individual Element at various positions

The behavior of individual cell elements at various points along the die/die attach interface during MST loading is presented in this section. First of all, the element closest to the center of the package is considered at $X_1/D = 1$. From Fig. 5.8, the analysis showed that the element at $X_1/D = 80$ is one of the elements which reached the highest porosity levels at the various initial vapor pressure levels, other than the die attach corner. As such, the loading history of the cell element at $X_1/D = 80$ is further presented in Fig. 5.12 to find out the void and mean stress behavior. Finally, the behavior of a cell element at the die attach corner is investigated ($X_1/D = 156$). The cases of initial vapor pressure presented here are $p_0/\sigma_0 = 0.0$ and $p_0/\sigma_0 = 1.5$.

The cell element, along the die/die attach interface at $X_1/D=1$, experiences progressive void activity under the combined effects of thermal mismatch and vapor pressure (Fig. 5.11). At $p_0/\sigma_0 = 0.0$, with the progress of each load step, the void growth though remains close to 0.05, there are cycles of void expansion and contraction; at $p_0/\sigma_0 = 1.5$, there is a gradual rise in void growth with each load step. The mean stress trends for

p_0/σ_0 = 0.0 and p_0/σ_0 = 1.5 are very similar and at the peaks of mean stress is where void growth occurs. However, for p_0/σ_0 = 1.5, as f reaches 0.15 near load step 1250, it can be see that there is a significant fall in mean stress due to the coalescence effect when $f > f_C$.

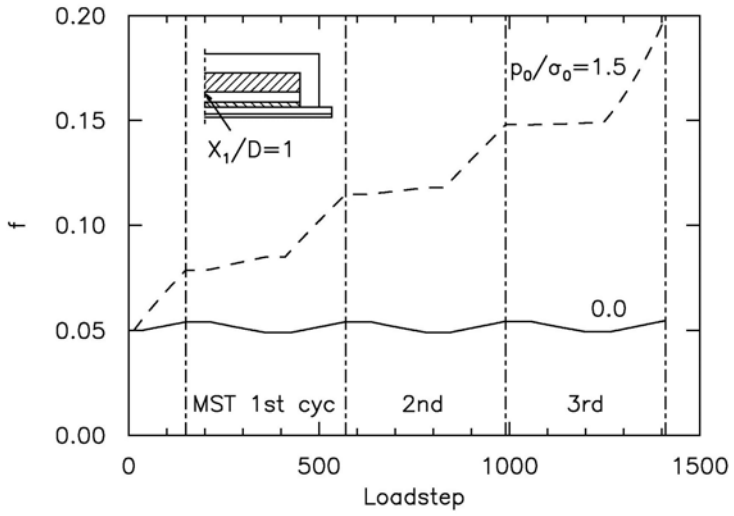

(a)

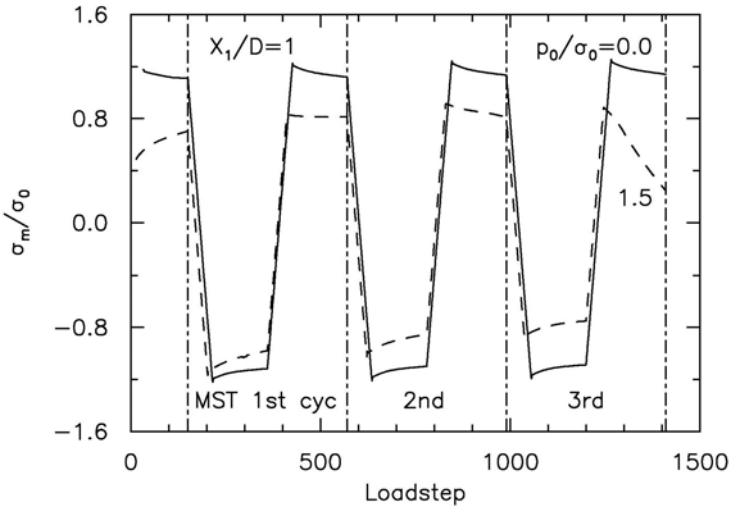

(b)

Figure 5.11 (a) Current void volume fraction f, and (b) mean stress σ_m/σ_0, at X_1/D=1, along the die/die attach interface for p_0/σ_0 = 0.0, 1.5.

The void volume fraction and mean stress distribution at X_1/D = 80 are very similar to that at X_1/D = 1, with void growth being slightly higher at X_1/D = 80. Similarly, at f >

f_C (=0.15), it can be see that there is a gradual fall in mean stress, indicating a loss in stress carrying capacity by the cell element (Fig. 5.12).

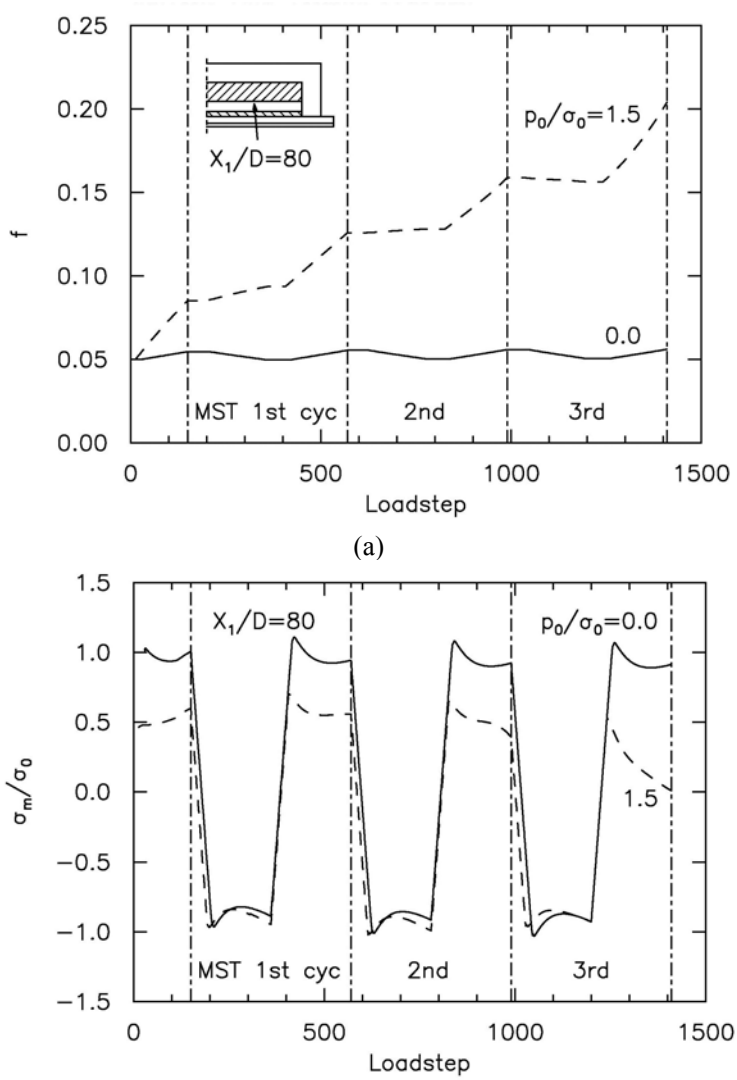

Figure 5.12 (a) Current void volume fraction f, and (b) mean stress σ_m/σ_0, at X_1/D=80, along the die/die attach interface for p_0/σ_0 = 0.0, 1.5.

The cell element at X_1/D=156, the die attach corner, experiences the largest increase in void growth during the MST loading (Fig 5.13). In the middle of the second MST cycle, f has already reach 0.15 and the mean stress is found to decrease drastically thereafter, due to the coalescence effect. Near the end of the MST loading, when $f = f_F$, the

element has lost all it stress carrying capacity (mean stress goes to zero) and the void in the element is free to coalescence to cause crack initiation. The effects of void growth, coalescence and final fracture are fully demonstrated.

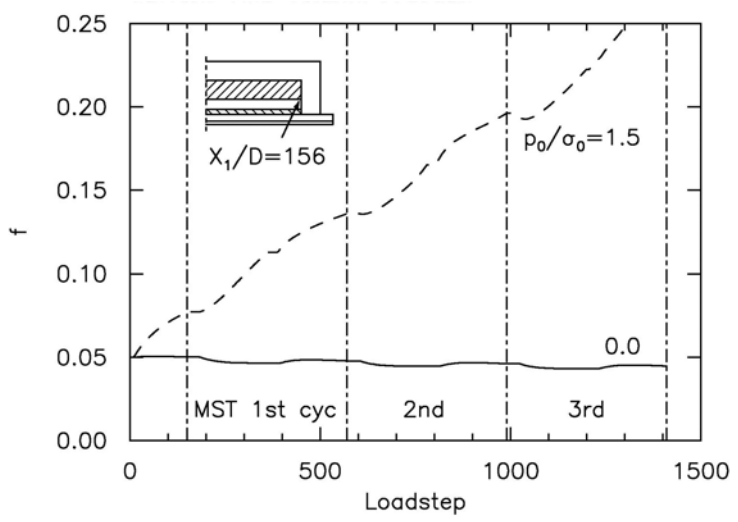

(a)

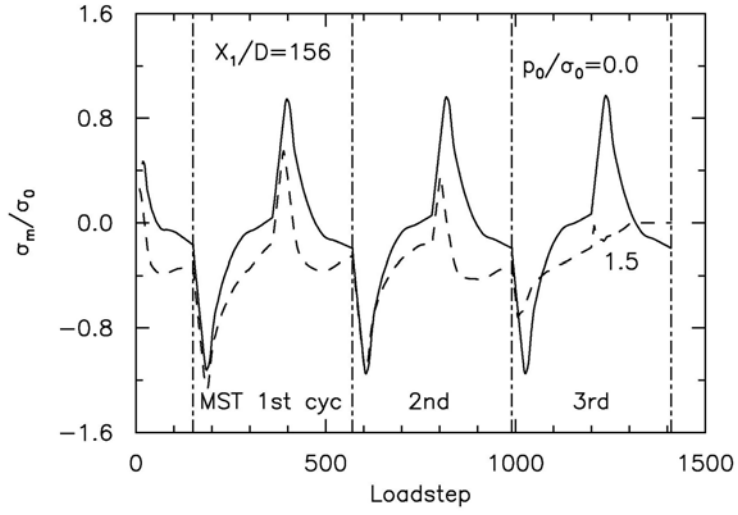

(b)

Figure 5.13 (a) Current void volume fraction f, and (b) mean stress σ_m/σ_0, at X_1/D=156, along the die/die attach interface for p_0/σ_0 = 0.0, 1.5.

5.3.7 Effects of Pb-free Reflow Soldering

With a global trend of using more environmental-friendly materials, the application of lead (Pb) in electronic components and assemblies is being impeded. As such, a raise in

maximum soldering temperature to 260 ^{o}C (or higher) is expected in preparation for lead-free soldering materials. An immensely drastic and adverse impact on the moisture sensitivity of surface mounted integrated circuit packages is expected with such changes. Using a loading profile similar to Fig. 5.4, the effects of raising the reflow soldering temperature to Pb-free soldering temperature (260 ^{o}C) are characterized.

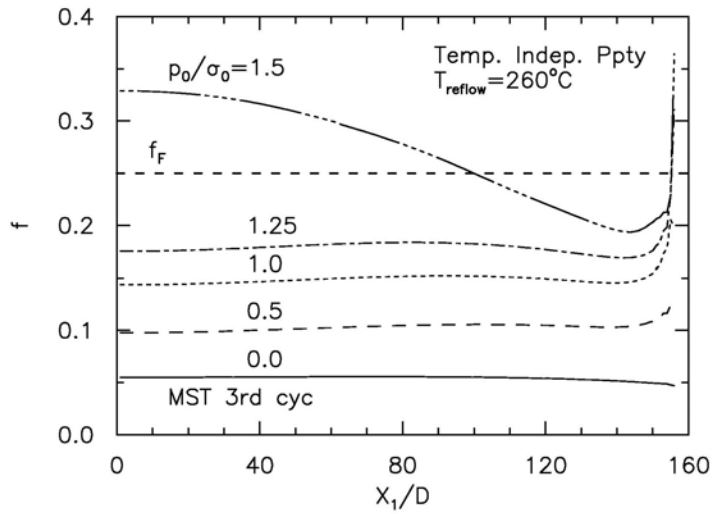

(a)

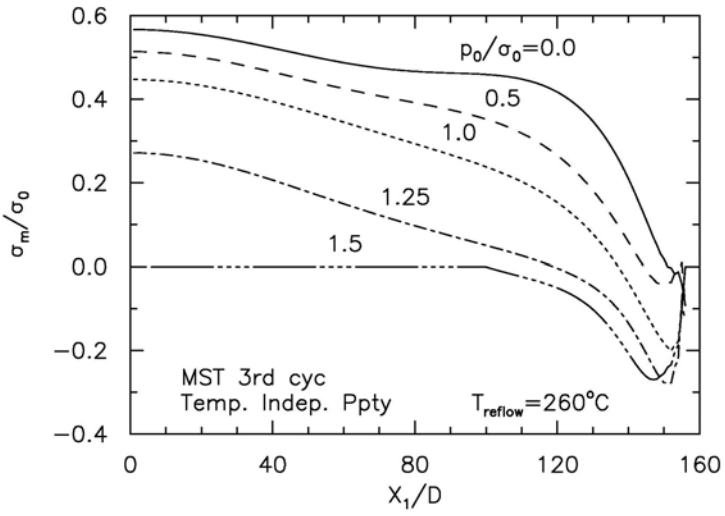

(b)

Figure 5.14 (a) Current void volume fraction f, and (c) mean stress σ_m/σ_0, along the die/die attach interface at the end of MST at various levels of p_0/σ_0, with Pb-free reflow temperature at 260^{o}C.

As temperatures are raised for Pb-free soldering, an interface damage trend similar to the original MST loading (Fig. 5.8a) is observed in Fig. 5.14a. With the increase in initial vapor pressure, voids near the interface corner grow at a significantly faster pace. However, the overall void growth across the whole interface is observed to be larger than when the reflow temperature was at 235 ^{o}C; reaching void levels of 0.20 (Fig. 5.14) as compared to 0.17 (Fig. 5.8) at p_0/σ_0=1.0. Such high void activity hints at the possibility of the fast delamination of the whole interface well before the end of the moisture sensitivity tests. As can be seen at p_0/σ_0 = 1.5, with the further loss of material stress carrying capacity beyond f = 0.15, void growth is observed to progress at an accelerated rate. At void growth above 0.25, each cell element loses all its stress carrying capacity, and a new crack surface is formed with the voids free to grow at will, reaching levels of 0.30 at both the interface center and corner. This confirms the postulation of two competing crack initiation zones along the interface. Figure 5.14b further shows that at p_0/σ_0=1.5, the stress carrying capacity at the interface center and corner goes to zero, and crack initiation and propagation along the interface have occurred.

5.3.8 Effects of Initial Vapor Pressure, p_0/σ_0, without f^*

The key difference in this section lies in the absence of the coalescence effect after f reach f_C; instead of using the Gurson flow potential in Section 3.3, a similar methodology to Chapter 4 is used, by adapting the Gurson flow potential in Section 3.4. Under similar MST thermal conditions, increased vapor pressure accelerates void growth; porosity levels at p_0/σ_0 = 1.5 exceed those for p_0/σ_0 = 0 (Fig 5.15). In addition,

with the intensified initial vapor pressure, voids near the interface corner grow considerably faster. A localized zone of intense void activity forms at the die/die attach interface corner creating the possible delamination sites, and such damage at the interface corner is also reflected by the fall in mean stress capacity.

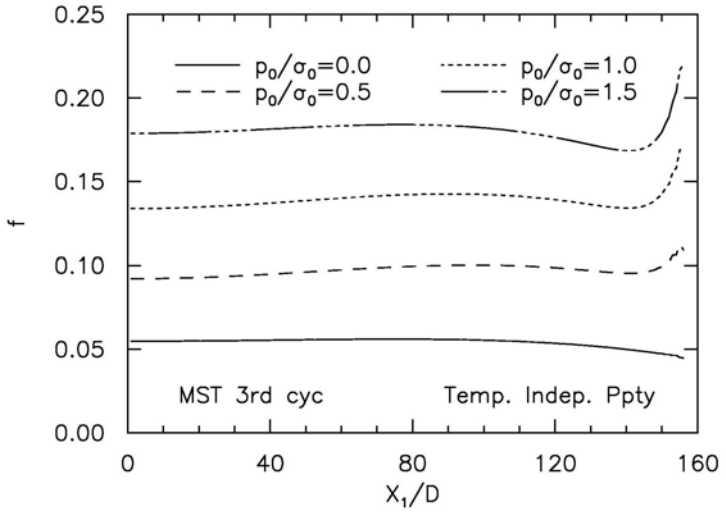

(a)

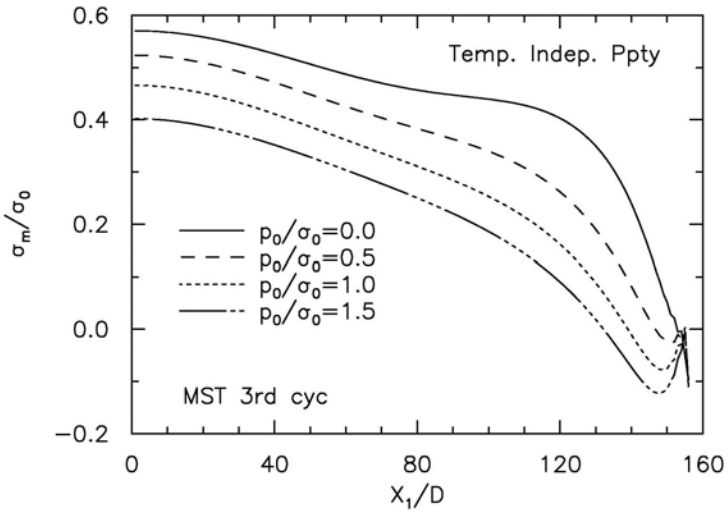

(b)

Figure 5.15 (a) Current void volume fraction f, and (b) mean stress σ_m/σ_0, along the die/die attach interface at the end of MST at various levels of p_0/σ_0, without f^*

However, as vapor pressure levels increased, the intense void activity zone further enlarge while shifting away from the corner and progressing towards the center of the

die attach – highlighting the possible formation of larger and multiple interface delamination sites. The mean stress declines toward the interface corner and more so with increased vapor pressure levels, reflecting the extent of damage by vapor pressure assisted void growth.

5.3.9 Crack initiation and propagation along the die/die attach interface

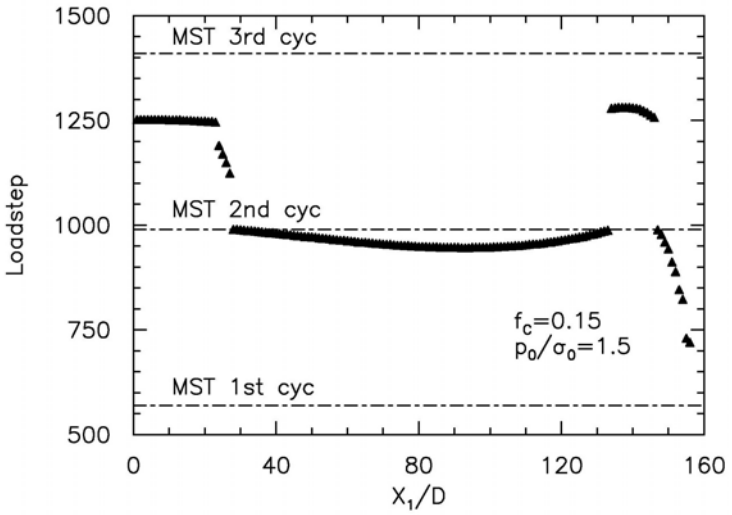

Figure 5.16History of crack initiation and propagation along the die/die attach interface with f_0 =0.05, p_0/σ_0 = 1.0 and f_C = 0.15.

To evaluate the crack initiation and propagation pattern, Fig. 5.16 presents the history of crack initiation and propagation along the die/die attach interface. Each cell element is assumed to have failed when the average void volume fraction over a cell reaches the critical value of 0.15. Crack initiates at the die/die attach interface corner (X_1/D = 156) towards the middle of the second cycle. In the early stages, the crack propagates gradually towards the interface center. However, near the end of the MST 2nd cycle, a second crack initiates at X_1/D = 93 and propagates rapidly in both directions towards the interface corner and interface center, resulting in a large delaminated zone. Towards

the end of the MST loading, the two cracks continue to propagate, causing the whole die/die attach interface to delaminate.

The deformed finite element mesh of the PBGA package with p_0/σ_0 = 1.0 and f_C =0.15 at the end of the MST loading is showed in Fig. 5.17. The whole die/die attach interface that had delaminated at the end of the MST loading is highlighted (Fig. 5.17b).

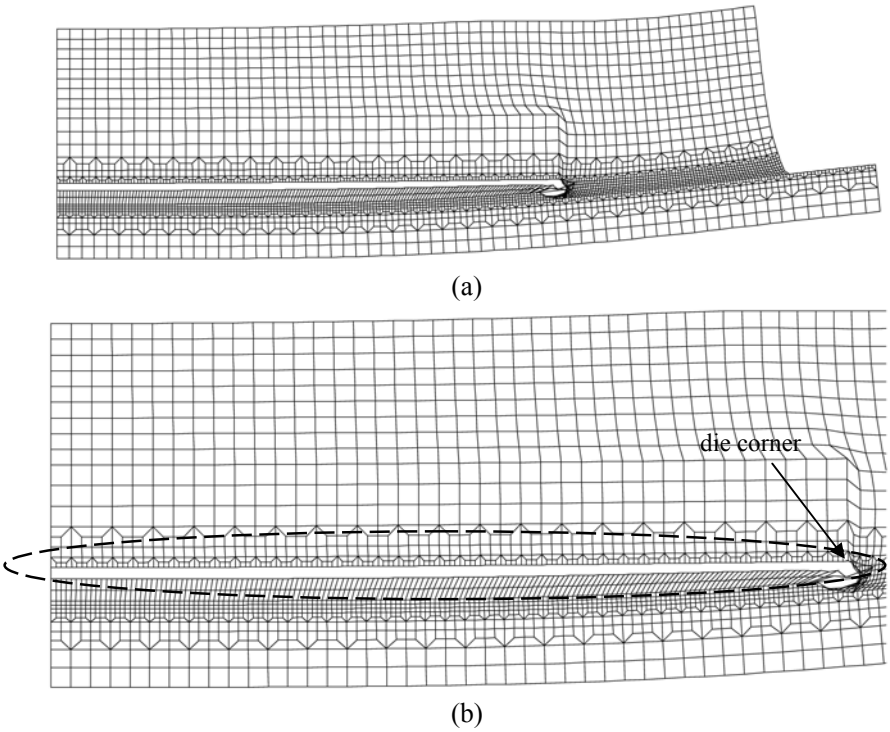

Figure 5.17 Deformed configuration of the PBGA package: (a) half the package, and (b) close up of the delamination site along the die/die attach interface.

5.3.10 Interface damage with temperature dependent material property

In the previous sections, the material properties of the PBGA components are assumed to be temperature independent, and serve to outline the most catastrophic cases of damages that can occur at reflow temperature. The die attach and overmold, however, are polymers which possess a temperature dependency in terms of their mechanical

response. Thus, for this section, analysis using temperature dependent material properties is carried out to provide a more complete illustration. The material properties, σ_0, E and α, of the die attach and overmold are assumed to be temperature dependent. All material properties, including other components, are showed in Table 5.1.

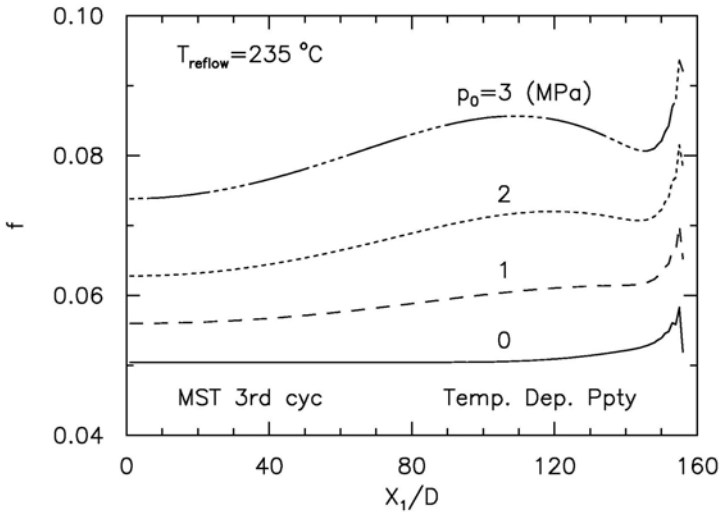

(a)

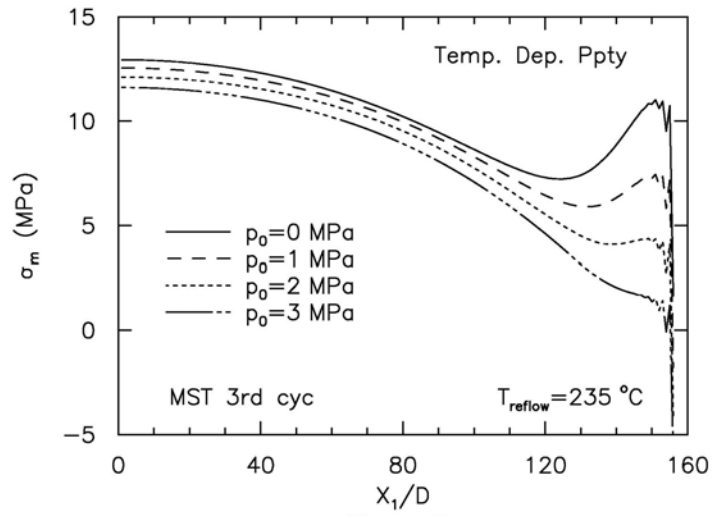

(b)

Figure 5.18 (a) Current void volume fraction f, and (b) mean stress σ_m, along the die/die attach interface at the end of MST at varying vapor pressures, p_0, with temperature dependent material properties.

Without additional vapor pressure (p_0 = 0) the void growth experienced along the die/die attach interface is limited, with only a slight increase from f_0 = 0.05 (Fig. 5.18a).

Nonetheless, the interface corner appears to undergo increased void damage, while the center of the die attach suffers insignificant or no damage. Under intense initial vapor pressure levels, similar damage trends are obtained, but with significantly less void activity as compared to the damage levels during analyses with temperature independent material properties. The mean stress remains high at the center and undergoes a decrease at the die attach corner with the increase in initial vapor pressure, as shown in Fig. 5.18b.

The present analysis with temperature dependent material properties does not fully explain the moisture-induced failures in the PBGA package because the current material data available is limited to the bulk, homogenous material only. The interface behavior, in particular the effect of absorbed moisture on the interface strength along with the changes in temperature, is not being taken into account in the cell model. Nevertheless, insight is provided on package failure due to thermal mismatch and vapor pressure effects on microvoids.

5.4 Results and Discussion – Full Field Analysis of Overmold

A full field analysis involves evaluating the PBGA package when the whole overmold is modeled by void-containing cell elements governed by the Gurson flow potential (3.8) as shown in Fig. 5.2c. The analysis will reveal the critical regions that undergo severe damage in the event of combined thermal mismatch stress and vapor pressure effects during the MST loading, indicating the likely paths of cracking during popcorn failure. The material properties of the components assume the values of the

corresponding investigations in the analysis on the die/die attach interface in section 5.3.3.

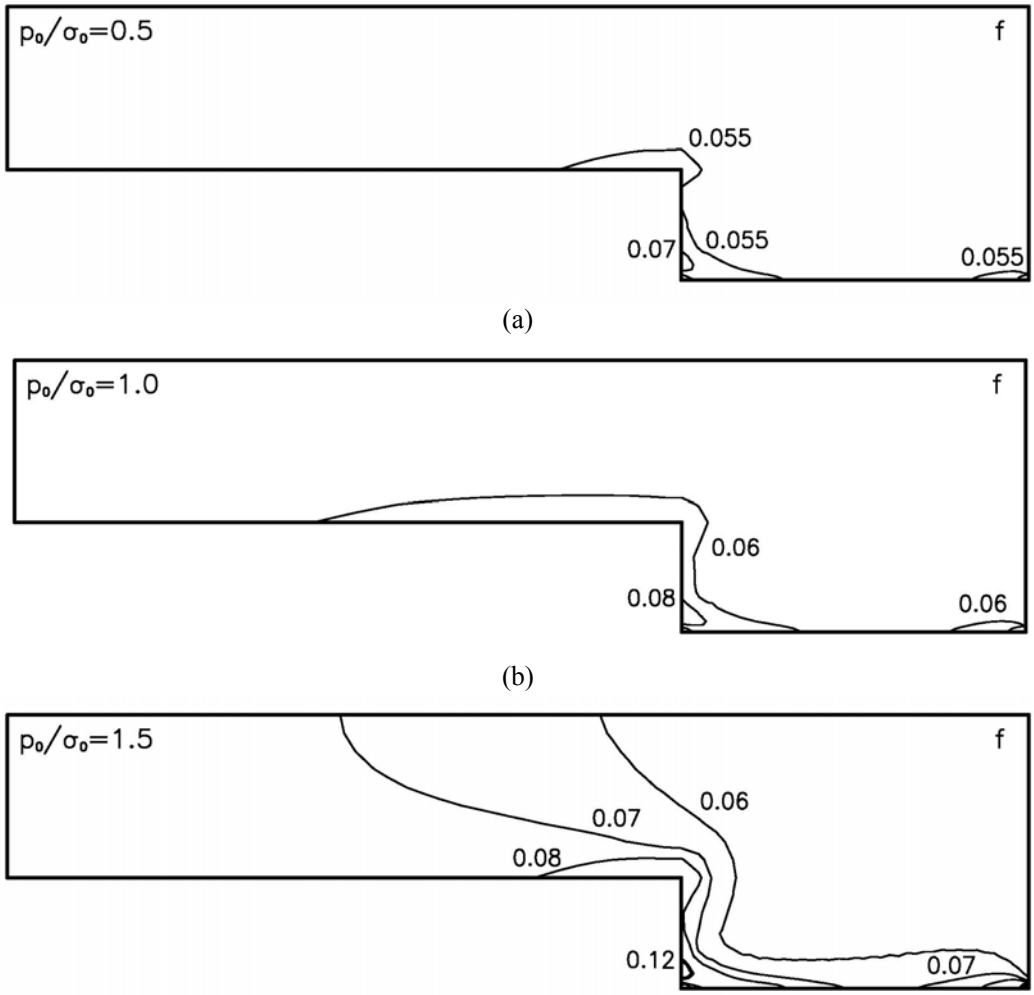

Figure 5.19 Full field analysis: contour plots of void volume fraction f at the end of 3rd MST cycle for (a) p_0/σ_0 = 0.5, (b) p_0/σ_0 = 1.0 and (c) p_0/σ_0 = 1.5, with f_0 = 0.05 and temperature independent material properties with T_{reflow} = 235 ^oC.

Figure 5.19 shows the void volume fraction contour plots at the end of 3rd MST cycle for p_0/σ_0 = 0.5, p_0/σ_0 = 1.0 and p_0/σ_0 = 1.5, with f_0 = 0.05. As the initial vapor pressure levels are increased, the level of void damage within the whole package increases drastically. On top of that, the regions near the die attach and the die corner show the

highest level of void activity and form the most possible sites for crack initiation and subsequent interface delamination (Fig. 5.19c).

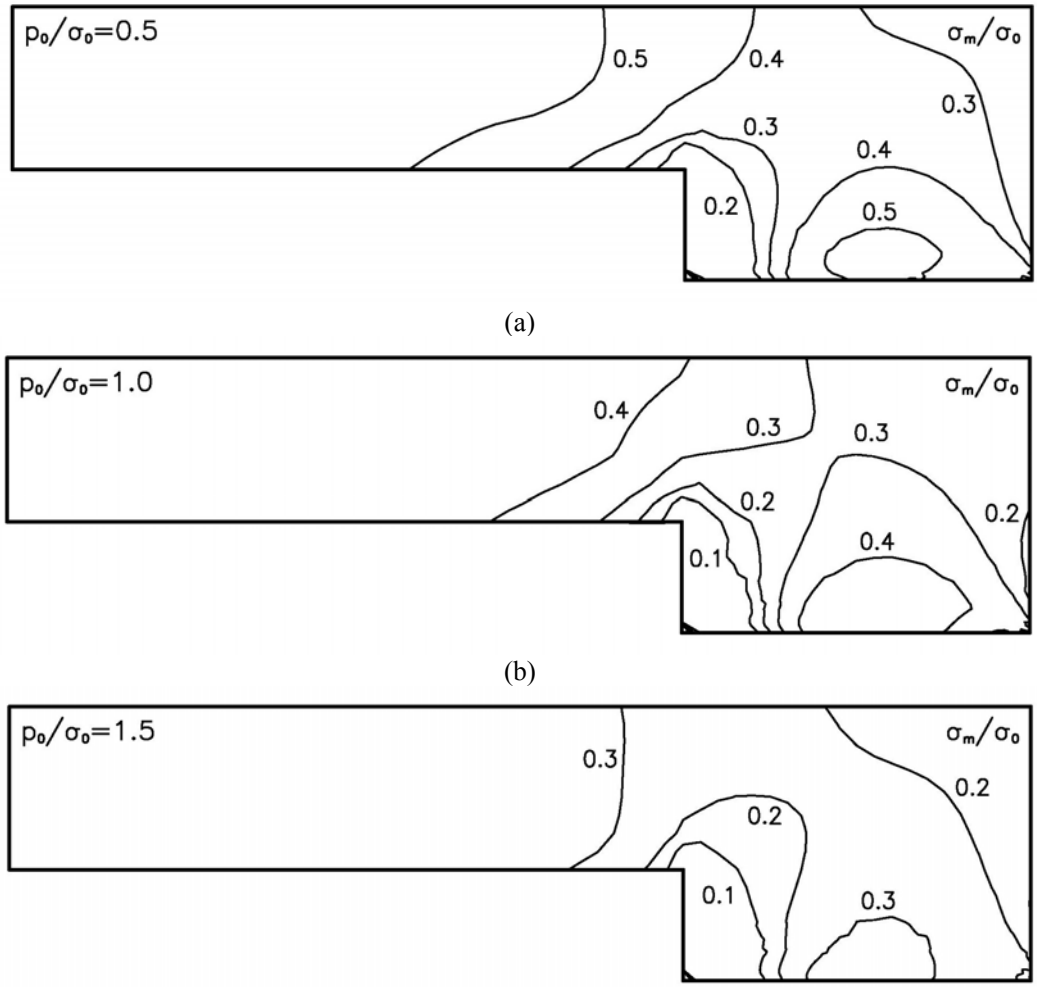

Figure 5.20 Full field analysis: contour plots of mean stress σ_m/σ_0 at the end of 3rd MST cycle for (a) p_0/σ_0 = 0.5, (b) p_0/σ_0 = 1.0 and (c) p_0/σ_0 = 1.5, with f_0 = 0.05 and temperature independent material properties with T_{reflow} = 235 ^oC

Figure 5.20 further indicates that with increased initial vapor pressure levels, the mean stress capacity that can be sustained by the package drops, especially at the critical interfaces highlighted earlier. Thus, this reinforces that the region close to the die attach is the most likely failure site.

From the full field analysis, void growth is observed to be insignificant in the bulk material, but rather occurs extensively at the interfaces. Although the moisture, and the moisture induced vapor pressure, exists throughout the overmold, the cracking of the bulk material prior to the interface delamination has not been observed. Interface delamination always causes the initiation of popcorn failure, where vapor pressure exerted on the delaminated interface causes crack branching into the bulk material. The current analysis affirms that despite vapor pressure in the whole overmold, the effect is insignificant on the void growth within the bulk material. In the event of the total delamination of the die/die attach interface, the critically damaged region in the overmold closest to the die attach will undergo cracking, and eventually lead to popcorn failure.

5.5 Chapter Conclusion

The cell element model has been applied to investigate moisture-induced interface delamination in PBGA packages. Analysis is focused on the die/die attach interface, modeled with three rows of uniformly sized cell elements. The full field analysis involves evaluating the PBGA package when all elements of the overmold are governed by the modified Gurson flow potential.

The current approach provides an in-depth mechanical analysis of popcorn cracking, especially in predicting the onset of delamination at the critical interfaces in an IC package, a precursor to popcorn failure. Both analyses of the die/die attach interface with temperature dependent and temperature independent material properties point

towards the interface region near the die corner as the most possible initiation site for interface delamination during moisture sensitivity tests. However, with increase in initial vapor pressure, another intense void damage zone deviates away from the die corner. Subsequent analysis reveals that cracks initiate at both intense void damage zone. The present phenomenon of having two competing sites of interface crack initiation clearly accounts for the fast and complete delamination of the whole die/die attach interface during the short time span of reflow soldering, and is further confirmed when considering effects of raising the reflow soldering temperature to Pb-free soldering temperature (260 ^{o}C).

For the package geometry and materials considered, the ensuing full field analysis predicts that the zone of intense void growth and damage occurs only at the interfaces, and the vapor pressure effect on void growth within the bulk material is limited. In the event of the total delamination of the die/die attach interface, the critically damaged region in the overmold closest to the die attach will undergo crack initiation, and lead to popcorn failure.

Chapter 6

Summary of Conclusions

The current thesis numerically simulates vapor pressure assisted void growth and coalescence in TQFP and PBGA, allowing investigations of the possible mechanisms of interface delamination and popcorn failure. In dealing with popcorn failure in IC packages, it is necessary to understand the entire cracking process: crack initiation, crack growth and final fracture. The ability to fully and accurately qualify the interface performance will be essential for future development. This chapter summarizes the conclusions drawn from the numerical findings. The studies offer new insights into the failure damage mechanism as well as the parameters that characterize it. A summary of major findings from Chapter 4 to Chapter 5 are presented as follows:

6.1 Vapor pressure assisted interface delamination and failure of thin quad flat pack (Chapter 4)

The combined effect of thermal mismatch stress and internal vapor pressure on a thin quad flat pack (TQFP) while undergoing the moisture sensitivity test (MST) is investigated. A mechanism based approach, the vapor pressure incorporated cell element model is adapted to model damage and predict the onset of delamination at the die pad/molding compound interface (Type I popcorn failure) and the die/die attach interface (Type II popcorn failure). Each interface is modeled by a row of cell elements. The effects of different die pad materials on damage across the interfaces are also investigated. Other factors, such as strain hardening exponent, initial void volume

fraction, the progress of each moisture sensitivity tests loading cycle, individual cell element behaviors, crack initiation and propagation are detailed. A study is made involving modeling the die/die attach interface with non uniform vapor pressure levels. The main findings include the following:

- In general, increased vapor pressure levels are detrimental to the interfaces as it brings about an overall increase in void growth and fall in stress carrying capacity across the interfaces.
- The analysis at the die pad/molding compound interface show that the region close to the die pad corner to be highly possible delamination sites, due to intense void growth brought about by increased vapor pressure levels, which is in line with experimental observations.
- High initial porosity and vapor pressure favor formation of a continuous damage zone along the die/die attach interface. The zone of intense void growth appears to be similarly close to the interface corner, but the region of void growth appears to be more wide spread.
- For each of the interfaces considered, crack initiates close to the interface corner and propagates in both directions towards the interface center and corner.
- By changing the die pad material properties from copper to alloy42, it affects the die pad/molding compound interface void growth behavior where the corners experience greater damage with the passing of each MST cycle. A different observation is made for the die/die attach interface where less void growth is experienced, suggesting that the failure of the constrained die attach is affected considerably by the substrates that it is sandwiched between. Using copper as the die pad material will increase the possibility to Type II popcorn failure (from the die/die

attach interface), while alloy42 promotes Type I popcorn failure (from the bottom of die pad/molding compound interface). Hence, in terms of mechanical performance, there is a trade off between the two die pad materials.

- Since the die attach is a very thin layer trapped between the die and die pad which are both moisture impermeable, the only path of moisture diffusion is at the die attach corner and most of the die attach not saturated with moisture. As such, a study is made involving modeling the die/die attach interface with non uniform vapor pressure levels. With the limited moisture penetration at the die attach corner, it is still possible to cause the interface corner to experience substantial void growth.

6.2 Thermo-mechanical analysis of Plastic Ball Grid Arrays with vapor pressure effects (Chapter 5)

A parametric study on the effects of vapor pressure and thermal mismatch stress on a plastic ball grid array (PBGA) package is performed. The cell element model, without assuming any pre-existing crack, is adapted to model void damage and crack initiation, a precursor to interface delamination and popcorn failure, at the die/die attach interface. The key difference with the previous simulations lies in the additional modeling of the coalescence effect through the complete loss of material stress carrying capacity at a realistic void volume fraction. The effects of porosity distribution and void vapor pressure on the integrity of the interface are discussed. The model is also extended to consider the effects of Pb-free reflow soldering. Analysis of the die/die attach interface using temperature dependent material properties is further discussed. A full field analysis is subsequently performed by evaluating the PBGA package when all elements of the overmold are governed by the Gurson flow potential. Similarly, other factors,

such as strain hardening exponent, the progress of each moisture sensitivity tests loading cycle, individual cell element behaviors, crack initiation and propagation are detailed. The findings are as follows:

- Both analyses of the die/die attach interface with temperature independent and temperature dependent material properties indicate the die corner as the most possible initiation site for interface delamination during moisture sensitivity tests. However, with increase in vapor pressure, another intense void damage zone deviates away from the die corner. The present phenomenon of having two competing sites of interface crack initiation clearly accounts for the fast and complete delamination of the whole die/die attach interface during the short time span of reflow soldering.
- Raising the reflow soldering temperature to Pb-free soldering temperature (260 ^{o}C) results in further void growth across the whole interface, and confirms the previous finding of having two competing sites of interface crack initiation.
- For the package geometry and materials considered, the ensuing full field analysis predicts that the zone of intense void growth and damage occurs only at the interfaces, and the vapor pressure effect on the void growth is limited within the bulk material. In the event of the total delamination of the die/die attach interface, the critically damaged region in the overmold closest to the die attach will undergo crack initiation, and lead to popcorn failure.

References

Ahn, S.-H. and Kwon, Y.-S., 1995, "Popcorn phenomena in a ball grid array package," IEEE Transactions on Components, Packaging, and Manufacturing Technology – Part B: Advanced Packaging, 18 (3), pp. 491-495.

Alpern, P., Dudek, R., Schmidt, R., Wicher, V. and Tilgner, R., 2002a, "On the Mode II Popcorn Effect in Thin Packages," IEEE Transactions on Components and Packaging Technologies, 25 (1), pp. 56-65.

Alpern, P., Lee, K. C., Dudek, R. and Tilgner, R., 2002b, "A simple model for the Mode I popcorn effect for IC packages with copper leadframe," IEEE Transactions on Components and Packaging Technologies, 25 (2), pp. 301-308.

Amagai, M., 1999, "Chip Scale Package (CSP) solder joint reliability and modeling," Microelectronics Reliability, 39, pp. 463-477.

Chai, T.C., Chan, K.C, Wong, E.H., Fan, X.J., Lim, T.B., 1999, "Achieving crack free package through elimination of type II failure," Proceedings on 49th Electronic Components and Technology Conference, pp. 702-707.

Chan, K.C., Chai, T.C., Wong, E.H., Lim, T.B., 1998, "The impact of die attach material on type II popcorn cracking," Proceedings on 2nd Electronics Packaging Technology Conference, pp. 331-337.

Chen, A. S., Schaefer, W. J., Lo, R. H. Y. and Weiler, P., 1994, "A Study of the Interactions of Molding Compound and Die Attach Adhesive, with regards to Package Cracking," Proceedings on 44th Electronic Components and Technology Conference, pp. 115-120.

Cheng, L. and Guo, T. F., 2003, "Vapor Pressure Assisted Void Growth and Cracking of Polymeric Films and Interfaces," Interface Science, 11, pp. 277-290.

Cheong, W. G., Guo, T. F. and Cheng, L., 2004, "Thermo-mechanical analysis of Plastic Ball Grid Arrays with vapor pressure effects," submitted for publication.

Chew, H. B., Guo, T. F. and Cheng, L., 2001, "Modeling interface delamination in plastic IC packages," Proceedings of APACK 2001 Conference on Advances in Packaging, ed. by Stephen Wong, John HL Pang, Z.P. Wang and Albert Lu, pp.381-388.

Chew, H. B., Guo, T. F. and Cheng, L., 2004a, "Vapor pressure and residual stress effects on the toughness of polymeric adhesive joints," Engineering Fracture Mechanics, 71, pp. 2435-2448.

Chew, H. B., Guo, T. F. and Cheng, L., 2004b, "Vapor Pressure and Residual Stress Effects on Failure of an Adhesive Film," submitted for publication.

Chong C. W., Guo, T. F. and Cheng, L., 2004, "Vapor pressure assisted crack growth at interfaces under mixed mode loading," Computational Material Science, accepted for publication.

Dudek, R., Sommer, P., Michel, P., Alpern, P., Birzer, C. and Tilgner, R., 1998, "Investigations on popcorn cracking of P-TQFP packages," Proceedings of 48th Electronic Components and Technology Conference, pp. 944-951.

Fan, X. J., 2000, "Modeling of Vapor Pressure during Reflow for Electronic Packages," Benefiting from Thermal and Mechanical Simulation in Micro-Electronics, ed. by G. Q. Zhang et al., Kluwer Academic Publishers, pp. 75-92.

Flinn, R. A. and Trojan, P. K., 1981, "Engineering Materials and Their Applications," 2nd Edition, Houghton Mifflin, pp. 137.

Fukazawa, I., Ishiguro, S., and Nanbu, S., 1985, "Moisture resistance degradation of plastic LSI's by reflow soldering," Proceedings on 23rd International Reliability Physics Symposium, pp. 192-197.

Gallo, A. A. and Munamarty, R., 1995, "Popcorning: A Failure Mechanism in Plastic – Encapsulated Microcircuits," IEEE Transactions on Reliability, 44, pp. 362-367.

Galloway, J.E. and Miles, B.M., 1997, "Moisture absorption and desorption predictions for plastic ball grid array packages," IEEE Transactions on Components, Packaging, and Manufacturing Technology – Part A, 20 (3), pp. 274-279.

Gibson, L. J. and Ashby, M. F., 1997, "Cellular Solids: Structure and Properties," 2nd Edition, Cambridge University Press, Cambridge.

Gibson, R. F., 1994, "Principles of composite material mechanics," McGraw Hill.

Groothuis, S.K., Stierman, R.J. and Heinen, K.G., 1995, "Mechanical characterization of epoxy resins used in IC packages," Application of Fracture Mechanics in Electronic Packaging and Materials, ASME, EEP, 11, pp. 211-222.

Gullerud, A. S., Koppenhoefer, K. C., Ruggieri, C. and Dodds Jr., R. H., 2000, "WARP3D – 3-D Dynamic Nonlinear Fracture Analysis of Solids Using Parallel Computers and Workstations," Civil Engineering Studies, Structural Research Series No. 607.

Guo, T. F. and Cheng, L., 2001, "Thermal and vapor pressure effects on cavitation and void growth," Journal of Materials Science, 36, pp. 5871-5879.

Guo, T. F. and Cheng, L., 2002, "Modeling Vapor Pressure Effects on Void Rupture and Crack Growth Resistance," Acta Materialia, 50, pp. 3487-3500.

Guo, T. F. and Cheng, L., 2003, "Vapor pressure and void size effects on failure of a constrained ductile adhesive," Journal of the Mechanics and Physics of Solids, 51, pp. 993-1014.

Gurson, A. L., 1977, "Continuum Theory of Ductile Rupture by Void Nucleation and Growth – Part I. Yield Criteria and Flow Rules for Porous Ductile Media," Journal of Engineering Materials and Technology, 99, pp. 2-15.

Huang, Y., Hu, K. X., Yeh, C. P., Li, N.-Y. and Hwang, K. C., 1996, "A Model Study of Thermal Stress-Induced Voiding in Electronic Packages," Journal of Electronic Packaging, 118, pp. 118-229.

Joint IPC/JEDEC Standard J-STD-020A, 1999, "Moisture/Reflow Sensitivity Classification for Non-Hermetic Solid State Surface Mount Devices", Joint Electron Device Engineering Council, http://www.jedec.org.

Kitano, M., Nishimura A. and Kawai S., 1988, "Analysis of packaging cracking during reflow soldering process," Proceedings on 26th International Reliability Physics Symposium, Electron Devices and Reliability Societies, New York, pp. 90-95.

Lam, T. F., 2000, "FEA simulation on moisture absorption in PBGA packages under various moisture pre-conditioning," Proceedings on 50th Electronic Components and Technology Conference, IEEE, Piscataway, N.J., pp. 1078-1082.

Lau, J., Chen, R., Chang, C., 1998, "Real-time popcorn analysis of plastic ball grid array packages during solder reflow," 23rd IEEE/CPMT International Electronics Manufacturing Technology Symposium, IEEE, Piscataway, N.J., pp. 455-463.

Lau, John H. and Lee, S. W. Ricky, 2000, "Temperature-Dependent Popcorning Analysis of Plastic Ball Grid Array Package During Solder Reflow With Fracture Mechanics Method," Journal of Electronic Packaging, 122 (1), pp. 34-41.

Lewis, G.L., Ganesan, G.S., Berg, H.M., 1994, "Role of materials evolution in VLSI plastic packages in improving reflow soldering performance," Proceedings on 44th Electronic Components and Technology Conference, pp. 177-185.

Liu, P., Cheng, L. and Zhang, Y. W., 2003, "Interface delamination in plastic IC packages induced by thermal loading and vapor pressure – a micromechanics model," IEEE Transactions on Advanced Packaging, 26 (1), pp. 1-9.

Liu, S. and Mei., Y., 1995, "Behavior of delaminated plastic IC packages subjected to encapsulation cooling, moisture absorption, and wave soldering," IEEE Transactions on Components, Packaging, and Manufacturing Technology – Part A, 18 (3), pp. 634-645.

Liu, W. and Shi, F. G., 2002, "Effect of the viscoelastic behavior of molding compounds on crack propagation in IC packages," Proceedings on 52nd Electronic Components and Technology Conference, IEEE, Piscataway, N.J., pp. 852-858.

Liu, Y., Irving, S., Rioux, M., Schoenberg, A. J. and Chong, D., 2002, "Die attach delamination characterization modeling for SOIC package," Proceedings on 52nd Electronic Components and Technology Conference, IEEE, Piscataway, N.J., pp. 839-846.

Morris, J. E. and Tummala, R. R., 2001, "The Role of Packaging in Microelectronics" Fundamental of microsystems packaging, ed. by Rao R. Tummala, McGraw-Hill, New York, pp. 44-79.

Ngyuyen, L. T., Chen, K. L., Schaefer, J., Kuo, A. Y. and Slenski, G., 1995, "A new criterion for package integrity under solder reflow conditions," Proceedings on 45th Electronic Components and Technology Conf, pp. 478-490.

Omi, S., Fujita, K., Tsuda, T. and Maeda, T., 1991, "Causes of cracks in SMD and type-specific remedies," IEEE Transaction on Components, Hybrids and Manufacturing Technology, 14 (4), pp. 818-823.

Park, Y. B. and Yu, J., 1997, "A fracture mechanics analysis of the popcorn cracking in the plastic IC packages," 21st IEEE/CPMT International Electronics Manufacturing Technology Symposium, pp. 12-19.

Pecht, M. G., 1999, "Moisture Sensitivity Characterization of Build-Up Ball Grid Array Substrates," IEEE Transactions on Advanced Packaging, 22 (3), pp. 515-523.

Proctor, P. and Solc, J., 1999, "Improved Thermal Conductivity in Microelectronics Encapsulants," Technical Paper, Dexter.

Shih, C. F. and Xia, L., 1995, "Modeling Crack Growth Resistance Using Computational Cells with Microstrcuturally-Based Length Scales," Constraint Effects in Fracture Theory and Applications: Second Volume, ASYM STP 1244, ed by Mark Kirk and Ad Bakker, ASME, Philadelphia, pp. 163-190.

Shook, R.L. and Sastry, V.S., 1997, "Influence of preheat and maximum temperature of the solder-reflow profile on moisture sensitive IC's," Proceedings on 47th Electronic Components and Technology Conference, IEEE, Piscataway, N.J., pp. 1041-1048.

Tan, G.-L., Hoo, C.-Y., Chew G., Low, J.-H., Tay, N.-B., Chakravorty, K.K. and Lim, T.-B., 1996, "Reliability assessment of BGA packages," Proceedings on 46th Electronic Components and Technology Conference, pp. 687 - 693

Tanaka, N. and Nishimura, A., 1995, "Measurement of IC molding compound adhesion strength and prediction of interface delamination within package," ASME Advances in Electronic Packagin, EEP-Vol. 10-2, pp. 765-773.

Tay, A.A.O. and Goh, K.Y., 2003, "A study of delamination growth in the die-attach layer of plastic IC packages under hygrothermal loading during solder reflow," IEEE Transactions on Device and Materials Reliability, 3 (4), pp. 144-151.

Tay, A. A. O. and Lin, T.Y., 1996a, "Effects of moisture and delamination on cracking of plastic IC packages during solder reflow," Proceedings on 46th Electronic Components and Technology Conference, pp. 777-782.

Tay, A. A. O. and Lin, T.Y., 1996b, "Moisture diffusion and heat transfer in plastic IC packages," IEEE Transactions on Components, Packaging, and Manufacturing Technology – Part A, 19 (2), pp.186-193.

Tay, A. A. O., Tan, G. L. and Lim, T.B., 1994, "Predicting delamination in plastic IC packages and determining suitable mold compound properties," IEEE Transactions on Components, Packaging and Manufacturing Technology – Part B: Advanced Packaging, 17 (2) , pp. 201-208.

Tvergaard, V., 1990, "Material Failure by Void Growth to Coalescence," Advances in Applied Mechanics, 27, pp. 83-151.

Tvergaard, V. and Hutchinson J. W., 1992, "The Relation Between Crack Growth Resistance and Fracture Process Parameters in Elastic-Plastic Solids," Journal of the Mechanics and Physics of Solids, 40, pp. 1377-1397.

Tvergaard, V. and Hutchinson, J. W., 1994, "Toughness of an Interface Along a Thin Ductile Layer Joining Elastic Solids," Philosophical Magazine A, 70, pp. 641-656.

Tvergaard, V. and Needleman, A., 1984, "Analysis of the cup-cone fracture in a round tensile bar," Acta Materialia, 32, pp. 157-169.

Wong, E. H., Koh, S. W., Lee, K. H. and Rajoo R., 2002a, "Advanced Moisture Diffusion Modeling and Characterisation for Electronic Packaging," Proceedings on 52nd Electronic Components and Technology Conference, pp.1297-1303.

Wong, E. H., Koh, S. W., Lee, K. H. and Rajoo R., 2002b, "Comprehensive treatment of moisture induced failure-recent advances," IEEE Transactions on Electronics Packaging Manufacturing, 25 (3), pp. 223-230.

Wong, E. H., Teo, Y. C. and Lim, T. B., 1998, "Moisture diffusion and vapor pressure modeling of IC packaging," Proceedings on 48th Electronic Components & Technology Conference, IEEE, Piscataway, N.J., pp. 1372-1378.

Xia, L. and Shih, C. F., 1995, "Ductile Crack Growth – I. A Numerical Study Using Computational Cells with Microstructurally-Based Length Scales," Journal of the Mechanics and Physics of Solids, 43, pp. 233-259.

Yip, L., Massingill, T., Naini, H., 1996, "Moisture sensitivity evaluation of ball grid array packages," Proceedings on 46th Electronic Components and Technology Conference, IEEE, New York, NY, pp. 829-835.